博士學位論文

Synthesis and Characterization of Dinuclear Copper-N_4O_2 Compartmental Macrocyclic Complexes Containing Auxiliary Ligands

Department of Chemistry

Graduate School

Cheju National University

Dae-Hun Mun

June, 2005

보조리간드을 포함한 이핵 Copper N_4O_2 칸막이형 거대고리를 갖는 착물들의 합성 및 특성

지도교수 : 변 종 철

문 대 훈

이 논문을 이학 박사학위 논문으로 제출함.

2005년 6월

문대훈의 이학 박사학위 논문을 인준함.

심사위원장 _____

위 원 _____

위 원 _____

위 원 _____

위 원 _____

제주대학교 대학원

2005년 6월

Synthesis and Characterization of Dinuclear Copper-N_4O_2 Compartmental Macrocyclic Complexes Containing Auxiliary Ligands

Dae-Hun Mun
(Supervised by professor Jong-Chul Byun)

A thesis submitted in partial fulfillment of the requirement for the degree of Doctor of Science.

2005. 6. .

This thesis has been examined and approved.

Date Approved :

Department of Chemistry
GRADUATE SCHOOL
CHEJU NATIONAL UNIVERSITY

Contents

List of Tables

List of Figures

Abstract

The reaction of 2,6-diformyl-*p*-cresol and trans-1,2-diaminocyclohexane in methanol in equimolar ratio using the high dilution technique affords a [3 + 3] Schiff-base macrocycle L_4 as yellow solid in high yield. The EA, IR, NMR and FAB mass spectral data of the product do not agree with the expected a [2 + 2] Schiff-base macrocycle ligand L_3 (= H_2[20]-DCHDC) but match with the composition of [3 + 3] Schiff-base macrocycle L_4. Binuclear Cu(II) complexe, $[Cu_2([20]\text{-DCHDC})Cl_2] \cdot H_2O$, with [2 + 2] symmetrical N_4O_2 compartmental macrocyclic ligand containing bridging phenolic oxygen atoms was synthesized by metal template condensation of 2,6-diformyl-*p*-cresol, trans-1,2-diaminocyclohexane, and $CuCl_2 \cdot 2H_2O$. The reaction of $[Cu_2([20]\text{-DCHDC})Cl_2] \cdot H_2O$ with auxiliary ligands (La ; Br^-, I^-, ClO_4^-, SCN^-, N_3^-, NO_2^-, NO_3^-, and $S_2O_3^{2-}$) in aqueous solution formed a new 8 complexes; $[Cu_2([20]\text{-DCHDC})Br_2] \cdot 0.5H_2O$, $[Cu_2([20]\text{-DCHDC})I_2]$, $[Cu_2([20]\text{-DCHDC})(\mu\text{-}O_2ClO_2)_2] \cdot H_2O$, $[Cu_2([20]\text{-DCHDC})(NCS)_2] \cdot H_2O$, $[Cu_2\text{-}([20]\text{-DCHDC})(N_3)_2] \cdot 6H_2O$, $[Cu_2([20]\text{-DCHDC})\text{-}(\mu\text{-}O_2N)]NO_2 \cdot 6H_2O$, $[Cu_2([20]\text{ -DCHDC})(\mu\text{-}O_2NO)]\text{-}NO_3 \cdot 0.5H_2O$, and $[Cu_2([20]\text{-DMTADO})(\mu\text{-}S_2O_3)]$, where [20]-DCHDC is the dianion of the binucleating macrocyclic ligand 14,29-dimethyl-3,10,18,25-tetraazapentacyclo-[25,3,1,$0^{4,9}$,$1^{12,16}$,$0^{19,24}$]ditriacontane-2,10,12,14,16(32),17,27(31),28,30-decane-31,32-diol. X-ray crystals and molecular structures of $[Cu_2([20]\text{-DCHDC})Cl_2] \cdot 6H_2O$ **(1)**, $[Cu_2([20]\text{-DCHDC})Br_2] \cdot 6H_2O$ **(2)**, $[Cu_2([20]\text{-DCHDC})(\mu\text{-}O_2ClO_2)_2] \cdot 1.6CH_3CN \cdot 0.4CH_3OH$ **(3)**, and $[Cu_2([20]\text{-DCHDC})(N_3)_2] \cdot 2CH_3OH$ **(4)** have been determined on a Bruker SMART-CCD diffractometer.

In **(1)** complex, a total 2047 reflections at the 2□(*I*) significance were used to give final discrepancy indices of R_1 = 0.0317 and wR_2 = 0.0841. The complex crystallizes in the orthorhombic space group *Cmca* in a cell having the dimensions *a* = 16.8306(7) Å, *b* = 7.9928(3) Å, and *c* = 24.5686(10) Å. The calculated density is 1.585 g/cm^3. Four formula units comprise the unit cell with quater of the binuclear complex in the asymmetric unit. The binuclear core structures are centrosymmetric with each copper(II) ion in the N(imine)$_2$O$_2$ sites being five-coordinate by square-pyramidal geometry of interactions with two nitrogen and two oxygen atoms of the binucleating ligand [20]-DCHDC and one chloride ligand at an apical site. The interatomic Cu···Cu separation is 2.9707(7) Å. The copper ions are 0.3625 Å displaced from the basal least-squares plane toward Cl^- ions. Two Cl^- ions attached to two central metal Cu are situated trans to each other with respect to the mean molecular plane.

In **(2)** complex, a total 2130 reflections at the 2□(*I*) significance were used to give final discrepancy indices of R_1 = 0.0305 and wR_2 = 0.0752. The complex crystallizes in the orthorhombic space group *Cmca* in a cell having the dimensions *a* = 116.8510(7) Å, *b* = 8.0835(3) Å, and *c* = 24.7963(11) Å. The calculated density is 1.726 g/cm^3. Four formula units comprise the unit cell with quater of the binuclear complex in the asymmetric unit. The binuclear core structures are centrosymmetric with each copper(II) ion in the N(imine)$_2$O$_2$ sites being five-coordinate by square-pyramidal geometry of interactions with two nitrogen and two oxygen atoms of the binucleating ligand [20]-DCHDC and one bromide ligand at an apical site. The interatomic Cu···Cu separation is 2.9549(8) Å. The copper ions are 0.3284

Å displaced from the basal least-squares plane toward Br^- ions. Two Br^- ions attached to two central metal Cu are situated trans to each other with respect to the mean molecular plane.

In **(3)** complex, a total 4383 reflections at the $2\sigma(I)$ significance were used to give final discrepancy indices of R_1 = 0.0495 and wR_2 = 0.1043. The complex crystallizes in the monoclinic space group $P2_1/c$ in a cell having the dimensions a = 8.0773(6) Å, b = 16.7494(13) Å, c = 14.0614(11) Å and β = 100.447(2)°. The calculated density is 1.575 g/cm^3. Four formula units comprise the unit cell with half of the binuclear complex in the asymmetric unit. The binuclear core structures are centrosymmetric with each copper(II) ion in the $N(imine)_2O_2$ sites being six-coordinate by octahedral geometry of interactions with two nitrogen and two oxygen atoms of the binucleating ligand [20]-DCHDC and two oxygen atoms each from the bridging perchlorate ligands at an apical site. The macrocyclic complex adopts an essentially flat structure with the two octahedral copper centers bridged by the two phenoxide oxygen atoms, with quite large Cu-O-Cu angles (98.54(10)°). The sum of angles at the phenoxide oxygens is almost exactly 360°, indicating no square oxygen distortion. The sum of angles at the copper basal planes (CuN_2O_2) is almost exactly 360°(360.28°), indicating no plane distortion. The interatomic Cu···Cu separation is 2.8786(9) Å.

In **(4)** complex, a total 3813 reflections at the $2\sigma(I)$ significance were used to give final discrepancy indices of R_1 = 0.0549 and wR_2 = 0.1217. The complex crystallizes in the monoclinic space group $P2_1/c$ in a cell having the dimensions a = 6.9849(5) Å, b = 19.6663(13) Å, c = 12.0317(8) Å, and β = 97.1770(10)°. The calculated density is 1.535 g/cm^3. Four formula units

comprise the unit cell with half of the binuclear complex in the asymmetric unit. The binuclear core structures are centrosymmetric with each copper(II) ion in the $N(imine)_2O_2$ sites being five-coordinate by square-pyramidal geometry of interactions with two nitrogen and two oxygen atoms of the binucleating ligand [20]-DCHDC and one nitrogen atom each from the azide ligands at an apical site. The copper ions are 0.3605 Å displaced from the basal least-squares plane toward N_3^- ions. Two N_3^- ions attached to two central metal Cu are situated trans to each other with respect to the mean molecular plane. The interatomic Cu···Cu separation is 2.9608(8) Å.

The one *d-d* band of title complexes observed at 17,271 ~ 18,868 cm^{-1} can be related to the spin-allowed transition, $^2E_g \rightarrow {}^2T_{2g}$. The two peak positions calculated at 16,778 - 17,793 and 18,349 - 20,408 cm^{-1} can be assigned to the $^2B_{1g} \rightarrow {}^2B_{2g}$ and $^2B_{1g} \rightarrow {}^2E_g$, respectively. The $^2B_{1g} \rightarrow {}^2A_{1g}$ transition bands have expected at much lower energy. The 21,368 - 24,752 cm^{-1} bands are clearly associated with ligand to metal charge transfer transitions.

I. Introduction

Interest in exploring metal ion complexes with macrocyclic ligands has been continually increasing owing to the recognition of their role played by these structures in metalloproteines. Schiff base macrocycles have been of great importance in macrocyclic chemistry. They were among the first artificial metal macrocyclic complexes to be synthesized. The metal complexes containing synthetic macrocyclic ligands have attracted a great deal of attention because they can be used as models for more intricate biological macrocyclic systems: metalloporphyrins (hemoglobin, myoglobin, cytochrome, chlorophyll), corrins (vitamin B_{12}) and antibiotics (valinomycin, nonactin). These discoveries have created supramolecular chemistry and its enormous diversity [1-5].

Over the past decade, many studies have been focused on the design, template synthesis and characterization of the new supramolecular polyaza and polyoxaaza Schiff base mono- and homo- or heterodinuclear macrocyclic complexes of metal ions of varying radii and electron configuration - in particular rare earth elements - and the factors which prove to be of importance in directing the synthetic pathway in these systems.

Selective recognition and incorporation of rare earth elements into organized architectures has been the subject of growing importance in supramolecular chemistry. The peculiar chemical, structural, spectroscopic and magnetic properties of the trivalent lanthanide ions associated with their $4f^n$ configuration make them suitable for development of novel supramolecular

photonic light-converting devices and sensors [6-21], contrast agents in magnetic resonance imaging [22-36], potential radiopharmaceuticals [24, 37-40], sensitizers for photodynamic therapy and biomedical diagnostics [41-48], and artificial nucleases for hydrolytic cleavage or transesterification of the DNA and RNA phosphate diester backbone [49-64]. Because ionic radii, coordination chemistry and binding behavior of lanthanide(III) cations and alkaline earth metal cations are similar, the lanthanides with their remarkable multitude of spectroscopic and magnetic properties, have been broadly used as presumed isomorphous replacement for calcium and, to a lesser degree, other biometals, and serve as informative spectroscopic probes of metal binding sites in biologically important macromolecules [65-70]. The latest suggestion that lanthanides can be applied as therapeutic agents in the treatment of inflammation, arthritis and atherosclerosis is based on the ability of lanthanide ions to antagonize calcium-dependent processes [6, 43, 44, 65, 68, 71]. Conjugation of macrocyclic complexes of yttrium and lanthanide radioisotopes to proteins in monoclonal antibody technology yields agents for radioimmunotherapy and other medical applications [10, 72-74]. In all these cases the metal complex must be sufficiently stable *in vivo* and inert to metal release under physiological conditions in order to prevent damaging of nontarget cells. The Schiff base macrocyclic complexes, which form neutral or cationic complexes with the metal of interest, fulfill these requirements, because they are extremely rigid and display kinetic inertness towards metal release, whereas exocyclic ligands are labile and easy to change.

Macrocyclic Schiff bases have been widely studied because they can selectively chelate certain metal ions depending on the number, type and

position of their donor atoms, the ionic radius of the metal center, and coordinating properties of counter ions.

1. Template synthesis of Schiff base macrocyclic complexes

Recognition of the importance of complexes containing macrocyclic ligands for supramolecular science, bioinorganic chemistry, biomedical applications, separation and encapsulation processes as well as formation of compounds with unusual properties and structures has led to considerable effort to develop methods for the synthesis of these compounds. The macrocyclic complex is formed by adding the required metal ion to a preformed macrocycle. However, the direct synthesis of macrocycles often results in very low yield of the desired product with the domination of competing linear polymerization or other side reactions.

Many synthetic routes to macrocyclic ligands involve the use of the metal ion template to orient the reacting groups of linear substrates in the desired conformation for the ring to close. The favorable enthalpy for the formation of metal-ligand bonds overcomes the unfavorable entropy of the ordering of the multidentate ligand around the metal ion and hence it promotes the cyclization reaction [1, 81, 82]. The effective method for the synthesis of Schiff base macrocyclic complexes which involves the condensation reaction between suitable dicarbonyl compounds and primary diamines carried out in the presence of appropriate metal ions which serve as templates in directing the steric course of the reaction. In this metal template effect the metal ion -

through coordination - organizes the linear substrates to facilitate the condensation process which may lead toward either [1 + 1] or [2 + 2] macrocyclic products.

Whether the cyclization proceeds through an intramolecular condensation to give a [1 + 1] macrocycle or through the bimolecular steps leading to a [2 + 2] macrocycle depends on the relative proportions of linear substrates, the nature of the cation and reactants (chain length, number and location of potential donor atoms), the ratio of the template ionic radius to the cavity size, conformation of acyclic intermediates and coordination properties of counter ions. Rare earth metal ions have found to be very efficient metal templates in the synthesis of the complexes of this type. The first example of such an action of these ions in the synthesis of polyaza Schiff base macrocyclic compounds was reported for scandium(III) ion [83]. Rare earth elements are known to have little or no stereochemical requirements and can be accommodated by the stereochemical constraints enforced by the template process. In some cases the mononuclear or dinuclear open-chain chelates with two terminal carbonyl groups or one terminal carbonyl group and one terminal amine group - considered as potential intermediates in the template process [1, 81, 82] - can be the final products of the Schiff base condensation [84-89]. The formation of these compounds instead of the expected macrocycles may be attributed to the unfavorable positioning of the terminal groups which decreases the probability of intermolecular linkage with next diamine molecule or a possibility of the nucleophilic attack of the amine nitrogen on the carbon atom of the carbonyl group and stabilizes the open-chain product once formed. The investigation of the mechanism of the

formation of Schiff base complexes demonstrates that the structure and coordination mode of potential intermediates is one of the key factors that determine the preferred pathway of the metal-ion templated condensation in the Schiff base systems and must be taken into account in the design and synthesis of desired products.

2. Hexadentate macrocycles derived from 2,6-diformylphenols

The incorporation of a phenol fragment into the macrocyclic core leads to the formation of ligands that are particularly suitable for coordination of two metal ions. The bridging hydroxyl groups protrude toward the center of the macrocycle, dividing it into two compartments that can accommodate metal ions. The first and most often studied macrocycle of this type is L_1 derived from propylenediamine, called the Robson ligand [90, 91].

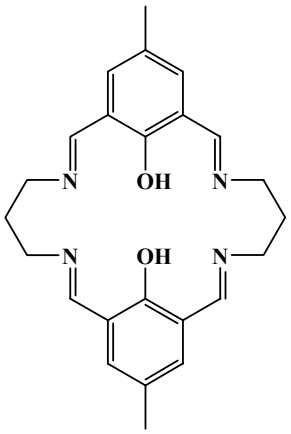

L_1

This ligand is able to form a variety of homodinuclear complexes with first row transition metal ions including Cu(II), Cu(I), Ni(II), Zn(II), Fe(II), Fe(III) [92-100], as well as second row transition metal ions Pd(II) and Ru(III) [101, 102]. Recently, the Robson ligand with a tert-butyl substituent has been prepared for the first time in its free form and used as a selective extractant for copper(II) ions [103]. Modification of one of the lateral propylene chains, e. g. by an ethylene bridge leads to formation of two compartments of different diameters preferring two different transition metal ions. The stepwise formation of such unsymmetrical N_4O_2 macrocycles can be exploited in the synthesis of heterodinuclear complexes [75, 104-108]. The heterodinuclear complexes are interesting as models for metalloenzymes possessing two different metal ions in their active site, such as cytochrome c oxidase, nitrogenase, nickel containing hydrogenase, superoxide dismutase, alkaline phosphatase or purple acid phosphatase.

The X-ray crystal structures of the dinuclear complexes of ligand L_1 usually exhibit almost flat conformation of the macrocycle core [92-94, 96, 98, 100-102], with two propylene chains pointing to opposite directions. Typically, the metal ion is five-coordinate and is positioned somewhat out of the N_4O_2 plane of the coordinating compartment. In the case of six-coordinate ions, the metal ion is located within the N_4O_2 plane. In contrast, the free ligand L_1 in its protonated form adopts highly bent conformation [101, 102]. In the mononuclear complex of L_1, $[NiH_2L_1](ClO_4)_2 \cdot 2CH_3OH$, macrocycle L_1 is also bent [109], although the angle between the two phenol rings is smaller than that in the free ligand. Similar conformation of the L_1 macrocycle is observed in the related Pb(II) complex [110]. The

$[NiH_2L_1](ClO_4)_2 \cdot 2CH_3OH$ complex is a convenient precursor for heterodinuclear complexes. Unlike the complexes of heterodinuclear complexes with unsymmetrical macrocycles mentioned above, heterodinuclear nickel(II) complexes $[NiML_1](ClO_4)_2 \cdot 2H_2O$, where M = Mn^{2+}, Fe^{2+}, Co^{2+}, Cu^{2+}, can be easily prepared from metal acetates and $[NiH_2L_1](ClO_4)_2 \cdot 2CH_3OH$ in one step [111]. Similarly, the mixed cobalt(II)-zinc(II) complex can be generated from the analogous mononuclear Co(II) complex of L_1. The purity and heterodinuclear nature of the complexes has been verified by mass spectrometry and NMR spectroscopy.

3. Chiral Schiff base macrocycles

The introduction of chiral diamines in the synthesis of hexaazamacrocycles leads to chiral macrocyclic lanthanide(III) complexes. These compounds are interesting from the perspective of a recent application of lanthanide(III) complexes of chiral crown ethers as enantioselective catalysts [112, 113].

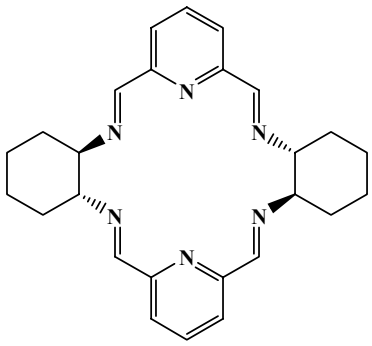

L_2

The first Schiff base complexes of this type were obtained for the ligand L_2, both as racemates [114] and in the enantiopure form [115, 116]. The latter complexes have been shown to exhibit circularly polarized luminescence and their photophysical properties have been studied in detail [116].

This work performs synthesis, crystal X-ray diffraction studies and physicochemical characterization of dinuclear Cu(II) complexes, $[Cu_2([20]\text{-DCHDC})(L_a)_n]^{(2-n)+}$, with [2+2] symmetrical N_4O_2 compartmental macrocyclic ligand {H_2[20]-DCHDC ; 14,29-dimethyl-3,10,18,25-tetraazapentacyclo-[25,3,1, $0^{4,9}$,$1^{12,16}$,$0^{19,24}$]ditriacontane-2,10,12,14,16(32),17,27(31),28,30-decane-31,32-diol} by condensation of 2,6-diformyl-*p*-cresol and *trans*-1,2-diaminocyclohexane containing auxiliary ligands (La ; Cl^-, Br^-, I^-, ClO_4^-, SCN^-, N_3^-, NO_2^-, NO_3^-, and $S_2O_3^{2-}$).

II. Experimental section

1. Chemicals and Physical Measurements

All chemicals were commercial analytical reagents and were used without further purification. For the spectroscopic and physical measurements, organic solvents were dried and purified according to the literature methods [117]. Nanopure quality water was used throughout this work. Microanalyses of C, H, and N were carried out using LECO CHN-900 analyzer. NMR spectra were obtained with a JNM-LA400 FT-NMR (JEOL) Spectrophotometer. Conductance measurements of the complexes were performed at 25±1℃ using an ORION 162 conductivity temperature meter. IR spectra were recorded with a Bruker FSS66 FT-IR spectrometer in the range 4000-370 cm^{-1} using KBr pellets. Electronic absorption spectra were measured at 25℃ on a UV-3150 UV-VIS-NIR Spectrophotometer (SHIMADZU). FAB-mass spectra were obtained on a JEOL JMS-700 Mass Spectrometer using argon (6 kV, 10 mA) as the FAB gas. The accelerating voltage was 10 kV andglycerol was used as the matrix. The mass spectrometer was operated in positive ion mode and mass spectrum was calibrated by Alkali-CsI positive.

2. Synthesis of Ligand and Complexes

1) Preparation of 2, 6-diformyl-*p*-cresol.

The synthesis of 2, 6-diformyl-*p*-cresol was prepared according to the methods previously reported [118, 119].

2) Preparation of the macrocyclic ligand with 2,6-diformyl-*p*-cresol and *trans*-1,2-diaminocyclohexane

To a solution of trans-1,2-diaminocyclohexane (0.48 mL, 4 mmol) in 50 mL of methanol was added dropwise a hot solution of 2,6-diformyl-*p*-cresol (0.656 g, 4 mmol) in 50 mL of methanol and the resulting red solution was refluxed for 3 h, after which time a yellow compound separated out. The solution was cooled to room temperature and the yellow product was filtered, thoroughly washed with ice-cold methanol, and dried *in vacuo*.

Yield 0.8843 g (89%).

Anal. Calc. (%) for : $(C_{45}H_{54}N_6O_3)(H_2O)$:

C, 72.55 ; H, 7.58 ; N, 11.28.

Found (%) : C, 72.75 ; H, 7.03 ; N, 11.33.

Solubility : DMF, acetone, chloroform, THF.

UV-Vis (DMF) [λ_{max} (nm) (ε ($M^{-1}cm^{-1}$))] : 450 br (474)

Λ_M (DMF) : 0.32 $ohm^{-1}cm^2mol^{-1}$.

FAB-mass : Calc. for $C_{45}H_{54}N_6O_3$ m/z 727. Found 727.4 (M^+).

^{1}H-NMR ($CDCl_3$, ppm) : 8.670 (s, HC=N), 8.210 (s, HC=N), 7.576 (s, Ar-H), 6.898 (s, Ar-H), 3.383 (m, N-CH, cyclohexane), 2.079 (s, Ar-CH_3), 1.845-1.469 (m, CH_2CH_2, cyclohexane).

^{13}C-NMR ($CDCl_3$, ppm) : 19.98, 24.40, 33.15, 33.45, 73.29, 75.36, 118.77, 122.959, 126.84, 129.62, 134.21, 156.18, 159.46, 163.46.

FT-IR (KBr, cm^{-1}) : 3439 (br), 3018, 2926, 2856, 1638(ν(C=N)), 1601, 1447, 1390, 1371, 1312, 1258, 868, 827, 761.

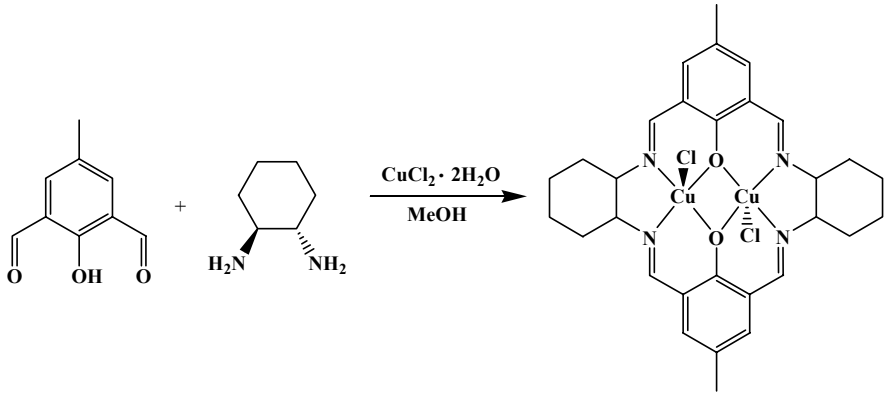

$[Cu_2([20]\text{-DCHDC})Cl_2]\cdot H_2O$

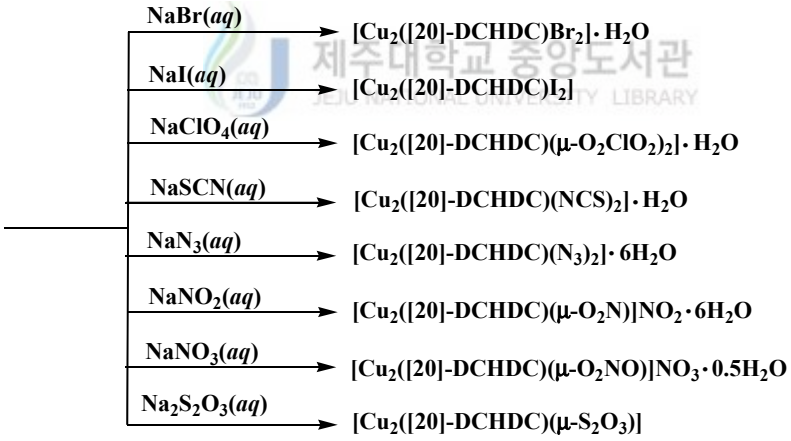

Scheme 1. Synthesis of the dinuclear Cu(II) complexes of phenol-based macrocyclic ligand ([20]-DCHDC).

3) Preparation of binuclear Cu(II) complexes.

The dinuclear Cu(II) complexes with [2+2] symmetrical N_4O_2 compartmental macrocyclic ligand {([20]-DCHDC)$^{2-}$} containing bridging phenolic oxygen atoms was synthesized by condensation, in the Cu(II) ions, of 2,6-diformyl-*p*-cresol and trans-1,2-diaminocyclohexane (Scheme 1).

(1) $[Cu_2([20]\text{-DCHDC})Cl_2] \cdot H_2O$

A solution of 2, 6-diformyl-*p*-cresol (3.280 g, 20 mmol) in the boiling methanol (50 mL) was added to the pale blue suspension formed by mixing trans-1,2-diaminocyclohexane (2.400 g, 20 mmol) with a solution of cupric chloride dihydrate (3.410 g, 20 mmol) in methanol (30 mL). The mixture was heated under reflux whereupon the initial pale green suspended solid first turned dark blue and then eventually dissolved. Methanol was removed by boiling at atmospheric pressure until precipitation had just commenced and the dark blue mixture was poured into ten times its volume of tetrahydrofuran. The resulting pale green precipitate was filtered, thoroughly washed twice with water, yielding crystal as dark blue platelets which were dried over anhydrouse calcium chloride at room temperature and atmospheric pressure. Prolonged heating in vacuum at 150℃ was required for removal of the water.

Yield 4.4909 g (64%).

Anal. Calc. (%) for $Cu_2(C_{30}H_{34}N_4O_2)(Cl)_2(H_2O)$:

C, 51.58 ; H, 5.19 ; N, 8.02.

Found (%) : C, 51.62 ; H, 5.01 ; N, 8.15.

Solubility : water, methanol, hot ethanol, hot DMSO, hot DMF

Λ_M (methanol) : 64.9 $ohm^{-1}cm^2mol^{-1}$.

Crystals of $[Cu_2([20]\text{-DCHDC})Cl_2] \cdot 6H_2O$ suitable for X-ray diffratration study were obtained by slow evaporation of water : methanol (1 : 1) solutions of the complex.

(2) $[Cu_2([20]\text{-DCHDC})Br_2] \cdot 0.5H_2O$

To a hot aqueous solution (150 mL) of $[Cu_2([20]\text{-DCHDC})Cl_2] \cdot H_2O$ (0.6986 g, 1 mmol) was added dropwise a solution of NaBr (0.5145 g, 5 mmol) in water (20 mL) with stirring and refluxed for 2 h. The resulting pale green precipitates were filter, thoroughly washed twice with water, and dried *in vacuo*.

Yield 0.6145 g (80 %).

Anal. Calc. (%) for $Cu_2(C_{30}H_{34}N_4O_2)(Br)_2(H_2O)_{0.5}$:

C, 46.28 ; H, 4.53 ; N, 7.20.

Found (%) : C, 46.25 ; H, 4.31 ; N, 7.16.

Solubility : hot methanol, hot DMSO.

Λ_M (DMSO) : 48.7 $ohm^{-1}cm^2mol^{-1}$.

Crystals of $[Cu_2([20]\text{-DCHDC})Br_2] \cdot 6H_2O$ suitable for X-ray diffratration

study were obtained by slow evaporation of methanol solutions of the complex.

(3) [Cu_2([20]-DCHDC)I_2]

To a hot aqueous solution (150 mL) of [Cu_2([20]-DCHDC)Cl_2]・H_2O (0.6986 g, 1mmol) was added dropwise a solution of NaI (0.7496 g, 5 mmol) in water (20 mL) with stirring and refluxed for 2 h. The resulting dark green precipitates were filter, thoroughly washed twice with water, and dried *in vacuo*.

Yield 0.7607 g (89%).

Anal. Calc. (%) for $Cu_2(C_{30}H_{34}N_4O_2)(I)_2$:

C, 41.73 ; H, 3.97 ; N, 6.49.

Found (%) : C, 42.31 ; H, 3.87 ; N, 6.57.

Solubility : hot DMF, hot DMSO.

Λ_M (DMSO) : 68.1 $ohm^{-1}cm^2mol^{-1}$.

(4) [Cu_2([20]-DCHDC)(μ-O_2ClO_2)$_2$]・H_2O

To a hot aqueous solution (150 mL) of [Cu_2([20]-DCHDC)Cl_2]・H_2O (0.6986 g, 1 mmol) was added dropwise a saturated aqueous $NaClO_4$ solution (15 mL) with stirring and refluxed for 2 h. The resulting pale green precipitates were filter, thoroughly washed twice with water, and dried *in vacuo*.

Yield 0.5960g (72 %).

Anal. Calc. (%) for $Cu_2(C_{30}H_{34}N_4O_2)(ClO_4)_2(H_2O)$:

C, 43.59 ; H, 4.39 ; N, 6.78.

Found (%) : C, 43.42 ; H, 4.18 ; N, 7.01.

Solubility : acetonitrile, DMSO, hot DMF, hot methanol, hot acetone.

Λ_M (methanol) : 108 $ohm^{-1}cm^2mol^{-1}$.

Crystals of $[Cu_2([20]\text{-DCHDC})(\mu\text{-}O_2ClO_2)_2] \cdot 1.6CH_3CN \cdot 0.4CH_3OH$ with x-ray quality were obtained by slow evaporation of acetonitrile : methanol (1 : 1) solutions of $[Cu_2([20]\text{-DCHDC})(ClO_4)_2]$ complex at atmospheric pressure.

(5) $[Cu_2([20]\text{-DCHDC})(NCS)_2] \cdot H_2O$

To a hot aqueous solution (150 mL) of $[Cu_2([20]\text{-DCHDC})Cl_2] \cdot H_2O$ (0.6986 g, 1 mmol) was added dropwise a solution of NaSCN (0.4054 g, 5 mmol) in water (20 mL) with stirring and refluxed for 2 h. The resulting pale green precipitates were filter, thoroughly washed twice with water, and dried *in vacuo*.

Yield 0.6428g (86 %).

Anal. Calc. (%) for $Cu_2(C_{3.0}H_{34}N_4O_2)(NCS)_2(H_2O)$:

C, 51.67 ; H, 4.88 ; N, 11.30.

Found (%) : C, 51.19 ; H, 4.23 ; N, 11.41

Solubility : hot DMSO

Λ_M (DMSO) : 30.6 $ohm^{-1}cm^2mol^{-1}$.

(6) $[Cu_2([20]\text{-}DCHDC)(N_3)_2]\cdot 6H_2O$.

To a hot aqueous solution (150 mL) of $[Cu_2([20]\text{-}DCHDC)Cl_2]\cdot H_2O$ (0.6986 g, 1 mmol) was added dropwise a solution of NaN_3 (0.3250 g, 5 mmol) in water (20 mL) with stirring and refluxed for 2 h. The resulting dark green precipitates were filter, thoroughly washed twice with water, and dried *in vacuo*.

Yield 0.6720 g (84 %).

Anal. Calc. (%) for $Cu_2(C_{30}H_{34}N_4O_2)(N_3)_2(H_2O)_6$:

C, 44.94 ; H, 5.78 ; N, 17.47

Found (%) : C, 44.95 ; H, 5.07 ; N, 17.53

Solubility : DMSO, chloroform, hot methanol, hot ethanol

Λ_M (methanol) : 33.4 $ohm^{-1}cm^2mol^{-1}$.

Crystals of $[Cu_2([20]\text{-}DCHDC)(N_3)_2]\cdot 2CH_3OH$ suitable for X-ray diffratration study were obtained by slow evaporation of methanol solutions of the complex.

(7) $[Cu_2([20]\text{-}DCHDC)(\mu\text{-}O_2N)]NO_2\cdot 6H_2O$

To a hot aqueous solution (150 mL) of $[Cu_2([20]\text{-}DCHDC)Cl_2]\cdot H_2O$ (0.6986 g, 1 mmol) was added dropwise a solution of $NaNO_2$ (0.3450 g, 5 mmol) in water (20 mL) with stirring and refluxed for 2 h. The resulting green precipitates were filter, thoroughly washed twice with water, and dried

in vacuo.

Yield 0.6760 g (83 %).

Anal. Calc. (%) for $Cu_2(C_{28}H_{34}N_4O_2)(NO_2)_2(H_2O)_6$:

C, 44.50 ; H, 5.73 ; N, 10.38.

Found (%) : C, 44.18 ; H, 5.46 ; N, 9.44.

Solubility : methanol, hot water, hot DMSO, hot chloroform

Λ_M (methanol) : 65.8 $ohm^{-1}cm^2mol^{-1}$.

(8) $[Cu_2([20]\text{-DCHDC})(\mu\text{-}O_2NO)]NO_3 \cdot 0.5H_2O$

To a hot aqueous solution (150 mL) of $[Cu_2([20]\text{-DCHDC})Cl_2] \cdot H_2O$ (0.6986 g, 1 mmol) was added dropwise a solution of $NaNO_3$ (0.4250 g, 5 mmol) in water (20 mL) with stirring and refluxed for 2 h. The resulting dark brown precipitates were filter, thoroughly washed twice with water, and dried *in vacuo*.

Yield 0.5723 g (77 %).

Anal. Calc. (%) for $Cu_2(C_{30}H_{34}N_4O_2)(NO_3)_2(H_2O)_{0.5}$:

C, 48.51 ; H, 4.75 ; N, 11.32.

Found (%) : C, 48.47 ; H, 5.22 ; N, 11.31.

Solubility : hot methanol, hot DMSO,

Λ_M (methanol) : 64.3 $ohm^{-1}cm^2mol^{-1}$.

(9) $[Cu_2([20]\text{-DMTADO})(\mu\text{-}S_2O_3)]$

To a hot aqueous solution (150 mL) of $[Cu_2([20]\text{-}DCHDC)Cl_2] \cdot H_2O$ (0.6986 g, 1 mmol) was added dropwise a solution of $Na_2S_2O_3 \cdot 5H_2O$(1.2409 g, 5 mmol) in water (20 mL) with stirring and refluxed for 2 h. The resulting dark green precipitates were filter, thoroughly washed twice with water, and dried *in vacuo*.

Yield 0.5130 g (71 %).

Anal. Calc. (%) for $Cu_2(C_{30}H_{34}N_4O_2)(S_2O_3)$:

C, 49.92 ; H, 5.03 ; N, 7.76

Found (%) : C, 50.50 ; H, 4.64 ; N, 6.58

Solubility : hot DMSO

Λ_M (DMSO) : 50 $ohm^{-1}cm^2mol^{-1}$.

3. X-ray Diffraction Measurements

1) $[Cu_2([20]\text{-}DCHDC)Cl_2] \cdot 6H_2O$

Suitable crystals of $[Cu_2([20]\text{-}DCHDC)Cl_2] \cdot 6H_2O$ were obtained by slow evaporation of water : methanol (1 : 1) solutions of $[Cu_2([20]\text{-}DCHDC)Cl_2] \cdot H_2O$ complex at atmospheric pressure. The dark green crystal of $[Cu_2([20]\text{-}DCHDC)Cl_2] \cdot 6H_2O$ was attached to glass fibers and mounted on a Bruker SMART diffractometer equipped with a graphite monochromated Mo Kα (λ = 0.71073 Å) radiation, operating at 50 kV and 30 mA and a CCD detector ; 45 frames of two-dimensional diffraction images were collected and processed to obtain the cell parameters and orientation matrix. The crystallographic data, conditions for the collection of intensity data, and some features of the structure refinements are listed in Table 1, and atomic coordinates were given in Table 2. The intensity data were corrected for Lorentz and polarization effects. Absorption correction was not made during processing. Of the 10041 unique reflections measured, 2047 reflections in the range $2.42° \leq \theta \leq 28.29°$ were considered to be observed($I>2\sigma(I)$) and were used in subsequent structure analysis. The program SAINTPLUS [121] was used for integration of the diffraction profiles. The structures were solved by direct methods using the XS program of the SHELXTL package [122] and refined by full matrix least squares against F^2 for all data using XL program of the SHELXTL package. All non-H atoms were refined with anisotropic displacement parameters (Table 3). Hydrogen atoms were placed

in idealized positions [U_{iso} = 1.2U_{eq} (parent atom)]. Hydrogen coordinates and isotropic displacement parameters were given in Table 4.

Table 1. Crystal data and structure refinement for $[Cu_2([20]\text{-DCHDC})Cl_2] \cdot 6H_2O$

Empirical formula	$C_{30}H_{46}Cl_2Cu_2N_4O_8$ $[Cu_2(C_{30}H_{34}N_2O_2)Cl_2]\cdot 6H_2O$	
Formula weight	788.69	
Temperature	173(2) K	
Wavelength	0.71073 Å	
Crystal system	Orthorhombic	
Space group	*Cmca*	
Unit cell dimensions	a = 16.8306(7) Å	α = 90°.
	b = 7.9928(3) Å	β = 90°.
	c = 24.5686(10) Å	γ = 90°.
Volume	3305.1(2) Å^3	
Z	4	
Density (calculated)	1.585 g/cm^3	
Absorption coefficient	1.504 mm^{-1}	
F(000)	1640	
Crystal size	0.45 x 0.30 x 0.30 mm^3	
Theta range for data collection	2.42 to 28.27°.	
Index ranges	-22<=h<=19, -10<=k<=10, -32<=l<=30	
Reflections collected	10041	
Independent reflections	2047 [R(int) = 0.0594]	
Completeness to theta = 28.27°	96.3 %	
Absorption correction	None	
Refinement method	Full-matrix least-squares on F^2	
Data / restraints / parameters	2047 / 0 / 128	
Goodness-of-fit on F^2	1.088	
Final R indices [I>2sigma(I)]	R_1 = 0.0317, wR_2 = 0.0841	
R indices (all data)	R_1 = 0.0392, wR_2 = 0.0882	
Largest diff. peak and hole	0.551 and -0.522 e.Å^{-3}	

$R = \sum \| F_0 | - | F_c \| / \sum | F_0 |$, $R_w = \left[\sum w(F_0^2 - F_c^2)^2 / \sum w(F_0^2)^2 \right]^{1/2}$

$w = 1/[\sigma^2(F_o^2)+(0.0382P)^2+7.0524P]$ where $P = (F_o^2+2F_c^2)/3$.

Table 2. Atomic coordinates ($x10^4$) and equivalent isotropic displacement parameters ($Å^2 \times 10^3$) for $[Cu_2([20]\text{-}DCHDC)Cl_2] \cdot 6H_2O$

atom	*x*	*y*	*z*	*U*(eq)
Cu(1)	5000	502(1)	5582(1)	16(1)
Cl(1)	5000	-2106(1)	6160(1)	34(1)
O(1)	5722(1)	0	5000	22(1)
N(1)	5796(1)	1695(2)	5980(1)	20(1)
C(1)	6504(2)	0	5000	16(1)
C(2)	6928(1)	769(2)	5435(1)	16(1)
C(3)	7760(1)	753(3)	5419(1)	19(1)
C(4)	8184(2)	0	5000	20(1)
C(5)	6547(1)	1658(3)	5887(1)	20(1)
C(61)	5420(3)	2997(6)	6336(2)	17(1)
C(81)	5436(4)	4716(7)	7179(2)	23(1)
C(62)	5396(3)	2271(7)	6499(2)	17(1)
C(82)	5390(4)	4089(8)	7321(2)	23(1)
C(7)	5887(1)	3517(3)	6827(1)	21(1)
C(9)	9078(2)	0	5000	25(1)
O(1W)	7500	5556(3)	7500	38(1)
O(2W)	6832(1)	3008(2)	8227(1)	41(1)

U(eq) is defined as one third of the trace of the orthogonalized U^{ij} tensor.

Table 3. Anisotropic displacement parameters ($Å^2 \times 10^3$) for [Cu_2([20]-DCHDC)Cl_2]・6H_2O

atom	U^{11}	U^{22}	U^{33}	U^{23}	U^{13}	U^{12}
Cu(1)	11(1)	24(1)	14(1)	-6(1)	0	0
Cl(1)	52(1)	23(1)	27(1)	4(1)	0	0
O(1)	10(1)	38(1)	18(1)	-11(1)	0	0
N(1)	16(1)	27(1)	18(1)	-9(1)	-2(1)	3(1)
C(1)	12(1)	19(1)	17(1)	1(1)	0	0
C(2)	13(1)	19(1)	18(1)	1(1)	-1(1)	0(1)
C(3)	14(1)	21(1)	21(1)	0(1)	-4(1)	-2(1)
C(4)	13(1)	22(1)	25(1)	2(1)	0	0
C(5)	15(1)	25(1)	20(1)	-6(1)	-4(1)	0(1)
C(61)	17(2)	18(2)	16(2)	-4(2)	-1(2)	0(2)
C(81)	28(3)	19(3)	22(3)	-5(2)	-4(2)	-2(2)
C(62)	18(2)	17(2)	15(2)	-3(2)	-3(2)	3(2)
C(82)	28(2)	26(3)	14(3)	-7(2)	-4(2)	2(3)
C(7)	21(1)	23(1)	20(1)	-5(1)	-3(1)	-2(1)
C(9)	10(1)	36(2)	29(2)	-1(1)	0	0
O(1W)	40(1)	31(1)	45(2)	0	-6(1)	0
O(2W)	39(1)	44(1)	39(1)	5(1)	0(1)	2(1)

The anisotropic displacement factor exponent takes the form: $-2\pi^2[h^2 a^{*2}U^{11} + ... + 2 hka^{*}b^{*}U^{12}]$.

Table 4. Hydrogen coordinates (x 10^4) and isotropic displacement parameters ($Å^2 \times 10^3$) for $[Cu_2([20]\text{-DCHDC})Cl_2] \cdot 6H_2O$

atom	*x*	*y*	*z*	*U*(eq)
H(3)	8046	1276	5706	23
H(5)	6883	2254	6130	24
H(61)	5513	4002	6102	20
H(81A)	5610	4525	7559	28
H(81B)	5610	5858	7078	28
H(62)	5487	1252	6727	20
H(82A)	5558	3388	7633	27
H(82B)	5558	5247	7406	27
H(7A)	6026	2513	7042	26
H(7B)	6389	4050	6707	26
H(7C)	6026	4493	6597	26
H(7D)	6386	2984	6952	26
H(9A)	9272	583	5325	30
H(9B)	9272	573	4673	30
H(9C)	9272	-1156	5002	30
H(1WA)	7177	6109	7297	46
H(1WB)	7803	4962	7297	46
H(2WA)	6394	3095	8389	49
H(2WB)	6950	3857	8045	49

2) $[Cu_2([20]\text{-DCHDC})Br_2] \cdot 6H_2O$

Suitable crystals of $[Cu_2([20]\text{-DCHDC})Br_2] \cdot 6H_2O$ were obtained by slow evaporation of methanol solutions of $[Cu_2([20]\text{-DCHDC})Br_2] \cdot 0.5H_2O$ complex at atmospheric pressure. The dark green crystal of $[Cu_2([20]\text{-DCHDC})Br_2] \cdot 6H_2O$ was attached to glass fibers and mounted on a Bruker SMART diffractometer equipped with a graphite monochromated Mo Kα (λ = 0.71073 Å) radiation, operating at 50 kV and 30 mA and a CCD detector ; 45 frames of two-dimensional diffraction images were collected and processed to obtain the cell parameters and orientation matrix. The crystallographic data, conditions for the collection of intensity data, and some features of the structure refinements are listed in Table 5, and atomic coordinates were given in Table 6. The intensity data were corrected for Lorentz and polarization effects. Empirical Absorption correction was applied using the program SADABS[120]. Of the 10390 unique reflections measured, 2130 reflections in the range $2.42° \leq \theta \leq 28.31°$ were considered to be observed($I>2\sigma(I)$) and were used in subsequent structure analysis. The program SAINTPLUS [121] was used for integration of the diffraction profiles. The structures were solved by direct methods using the XS program of the SHELXTL package [122] and refined by full matrix least squares against F^2 for all data using XL. All non-H atoms were refined with anisotropic displacement parameters (Table 7). Hydrogen atoms were placed in idealized positions [U_{iso} = $1.2U_{eq}$ (parent atom)]. Hydrogen coordinates and isotropic displacement parameters were given in Table 8.

Table 5. Crystal data and structure refinement for $[Cu_2([20]\text{-DCHDC})Br_2] \cdot 6H_2O$

Empirical formula	$C_{30}H_{46}Br_2Cu_2N_4O_8$	
	$[Cu_2(C_{30}H_{34}N_4O_2)Br_2]\cdot 6H_2O$	
Formula weight	877.61	
Temperature	173(2) K	
Wavelength	0.71073 Å	
Crystal system	Orthorhombic	
Space group	*Cmca*	
Unit cell dimensions	a = 16.8510(7) Å	α = 90°.
	b = 8.0835(3) Å	β = 90°.
	c = 24.7963(11) Å	γ = 90°.
Volume	3377.6(2) $Å^3$	
Z	4	
Density (calculated)	1.726 g/cm^3	
Absorption coefficient	3.680 mm^{-1}	
F(000)	1784	
Crystal size	0.30 x 0.25 x 0.10 mm^3	
Theta range for data collection	2.42 to 28.31°.	
Index ranges	-20<=h<=22, -9<=k<=10, -31<=l<=32	
Reflections collected	10390	
Independent reflections	2130 [R(int) = 0.0320]	
Completeness to theta = 28.31°	97.6 %	
Absorption correction	Empirical(SADABS)	
Refinement method	Full-matrix least-squares on F^2	
Data / restraints / parameters	2130 / 0 / 128	
Goodness-of-fit on F^2	1.100	
Final R indices [I>2sigma(I)]	R_1 = 0.0305, wR_2 = 0.0752	
R indices (all data)	R_1 = 0.0431, wR_2 = 0.0829	
Largest diff. peak and hole	0.487 and -0.562 e.$Å^{-3}$	

$R = \sum \| F_0 | - | F_c \| / \sum | F_0 |$, $R_w = [\sum w(F_0^2 - F_c^2)^2 / \sum w(F_0^2)^2]^{1/2}$

$w = 1/[\sigma^2(F_o^2)+(0.0404P)^2+7.2146P]$ where $P = (F_o^2+2F_c^2)/3$.

Table 6. Atomic coordinates ($x10^4$) and equivalent isotropic displacement parameters ($Å^2 \times 10^3$) for $[Cu_2([20]\text{-}DCHDC)Br_2] \cdot 6H_2O$

atom	x	y	z	U(eq)
Cu(1)	5000	542(1)	5569(1)	16(1)
Br(2)	5000	-2219(1)	6169(1)	30(1)
O(1)	4278(1)	0	5000	20(1)
N(1)	4206(1)	1675(3)	5972(1)	18(1)
C(1)	3500(2)	0	5000	15(1)
C(2)	3075(1)	761(3)	5430(1)	15(1)
C(3)	2244(1)	736(3)	5416(1)	18(1)
C(4)	1821(2)	0	5000	19(1)
C(5)	927(2)	0	5000	25(1)
C(6)	3457(1)	1624(3)	5881(1)	19(1)
C(7)	4581(3)	2929(8)	6336(2)	15(1)
C(7')	4595(3)	2213(8)	6493(2)	15(1)
C(8)	4117(2)	3395(3)	6829(1)	22(1)
C(9)	4561(5)	4511(9)	7197(3)	20(2)
C(9')	4609(5)	3912(10)	7319(3)	23(2)
O(2W)	3121(1)	2088(3)	3215(1)	39(1)
O(3W)	2500	425(4)	7500	37(1)

U(eq) is defined as one third of the trace of the orthogonalized U^{ij} tensor.

Table 7. Anisotropic displacement parameters ($Å^2 \times 10^3$) for [Cu_2([20]-DCHDC)Br_2]・6H_2O

atom	U^{11}	U^{22}	U^{33}	U^{23}	U^{13}	U^{12}
Cu(1)	10(1)	26(1)	12(1)	-7(1)	0	0
Br(2)	44(1)	22(1)	23(1)	2(1)	0	0
O(1)	8(1)	39(2)	13(1)	-11(1)	0	0
N(1)	15(1)	25(1)	14(1)	-7(1)	1(1)	-2(1)
C(1)	12(1)	20(2)	13(2)	1(1)	0	0
C(2)	11(1)	20(1)	14(1)	1(1)	1(1)	-1(1)
C(3)	13(1)	23(1)	18(1)	-1(1)	3(1)	3(1)
C(4)	11(1)	22(2)	23(2)	1(1)	0	0
C(5)	12(2)	40(2)	24(2)	-4(2)	0	0
C(6)	15(1)	25(1)	16(1)	-4(1)	4(1)	1(1)
C(7)	13(2)	20(3)	11(3)	-4(2)	0(2)	2(2)
C(7')	18(2)	19(3)	8(2)	-2(2)	-1(2)	-2(2)
C(8)	19(1)	28(1)	18(1)	-8(1)	3(1)	3(1)
C(9)	23(3)	20(4)	18(4)	-10(3)	0(3)	10(3)
C(9')	28(3)	26(4)	16(4)	-8(3)	-1(3)	6(3)
O(2W)	35(1)	44(1)	37(1)	0(1)	2(1)	1(1)
O(3W)	40(2)	31(2)	40(2)	0	-6(1)	0

The anisotropic displacement factor exponent takes the form: $-2\pi^2[h^2 a^{*2}U^{11} + ... + 2 hka^{*}b^{*}U^{12}]$.

Table 8. Hydrogen coordinates (x 10^4) and isotropic displacement parameters ($Å^2 \times 10^3$) for $[Cu_2([20]\text{-}DCHDC)Br_2] \cdot 6H_2O$

atom	x	y	z	U(eq)
H(3A)	1960	1243	5702	22
H(5A)	734	572	5323	30
H(5B)	734	-1143	5000	30
H(5C)	734	571	4677	30
H(6A)	3121	2194	6127	22
H(7A)	4487	3944	6115	18
H(7'A)	4505	1184	6708	18
H(8A)	3620	3948	6716	26
H(8B)	3971	2376	7027	26
H(8A)	3621	2854	6949	26
H(8B)	3975	4381	6612	26
H(9A)	4387	5656	7119	24
H(9B)	4387	4256	7569	24
H(9'A)	4441	5050	7413	28
H(9'E)	4441	3193	7621	28
H(2WA)	3587	1972	3330	46
H(2WB)	3150	2672	2931	46
H(3WA)	2316	1161	7292	44
H(3WB)	2275	-161	7739	44

3) $[Cu_2([20]\text{-}DCHDC)(\mu\text{-}O_2ClO_2)_2] \cdot 1.6CH_3CN \cdot 0.4CH_3OH$

Suitable crystals of $[Cu_2([20]\text{-}DCHDC)(\mu\text{-}O_2ClO_2)_2] \cdot 1.6CH_3CN \cdot 0.4CH_3OH$ were obtained by slow evaporation of acetonitrile : methanol (1 : 1) solutions of $[Cu_2([20]\text{-}DCHDC)(ClO_4)_2] \cdot H_2O$ complex at atmospheric pressure. The pale green crystal of $[Cu_2([20]\text{-}DCHDC)(\mu\text{-}O_2ClO_2)_2] \cdot 1.6CH_3CN \cdot 0.4CH_3OH$ was attached to glass fibers and mounted on a Bruker SMART diffractometer equipped with a graphite monochromated Mo Kα (λ = 0.71073 Å) radiation, operating at 50 kV and 30 mA and a CCD detector ; 45 frames of two-dimensional diffraction images were collected and processed to obtain the cell parameters and orientation matrix. The crystallographic data, conditions for the collection of intensity data, and some features of the structure refinements are listed in Table 9, and atomic coordinates were given in Table 10. The intensity data were corrected for Lorentz and polarization effects. Absorption correction was not made during processing. Of the 11833 unique reflections measured, 4383 reflections in the range $1.91° \leq \theta \leq 28.29°$ were considered to be observed($I>2\sigma(I)$) and were used in subsequent structure analysis. The program SAINTPLUS [121] was used for integration of the diffraction profiles. The structures were solved by direct methods using the XS program of the SHELXTL package [122] and refined by full matrix least squares against F^2 for all data using XL. All non-H atoms were refined with anisotropic displacement parameters (Table 11). Hydrogen atoms were placed in idealized positions [U_{iso} = $1.2U_{eq}$ (parent atom)]. Hydrogen coordinates and isotropic displacement parameters were given in Table 12.

Table 9. Crystal data and structure refinement for $[Cu_2([20]\text{-}DCHDC)\text{-}(\mu\text{-}O_2ClO_2)_2] \cdot 1.6CH_3CN \cdot 0.4CH_3OH$

Empirical formula	$C_{33.60}H_{40.40}Cl_2Cu_2N_{5.60}O_{10.40}$	
	$[Cu_2(C_{30}H_{34}N_4O_2)(ClO_4)_2]\cdot 1.6(CH_3CN)\cdot 0.4(CH_3OH)$	
Formula weight	887.1	
Temperature	173(2) K	
Wavelength	0.71073 Å	
Crystal system	Monoclinic	
Space group	$P2_1/c$	
Unit cell dimensions	a = 8.0773(6) Å	α = 90°.
	b = 16.7494(13) Å	β = 100.447(2)°.
	c = 14.0614(11) Å	γ = 90°.
Volume	1870.8(2) $Å^3$	
Z	2	
Density (calculated)	1.575 g/cm^3	
Absorption coefficient	1.344 mm^{-1}	
F(000)	913	
Crystal size	0.40 x 0.30 x 0.12 mm^3	
Theta range for data collection	1.91 to 28.29°.	
Index ranges	-10<=h<=10, -22<=k<=21, -18<=l<=14	
Reflections collected	11833	
Independent reflections	4383 [R(int) = 0.0760]	
Completeness to theta = 28.29°	94.4 %	
Absorption correction	None	
Refinement method	Full-matrix least-squares on F^2	
Data / restraints / parameters	4383 / 6 / 298	
Goodness-of-fit on F^2	1.028	
Final R indices [I>2sigma(I)]	R_1 = 0.0495, wR_2 = 0.1043	
R indices (all data)	R_1 = 0.1014, wR_2 = 0.1223	
Largest diff. peak and hole	0.470 and -0.526 e.$Å^{-3}$	

$R = \sum \| |F_0| - |F_c| \| / \sum |F_0|$, $R_w = [\sum w(F_0^2 - F_c^2)^2 / \sum w(F_0^2)^2]^{1/2}$

$w = 1/[\sigma^2(F_o^2)+(0.0457P)^2+1.0708P]$ where $P = (F_o^2+2F_c^2)/3$.

Table 10. Atomic coordinates ($x10^4$) and equivalent isotropic displacement parameters ($Å^2 \times 10^3$) for $[Cu_2([20]\text{-}DCHDC)(\mu\text{-}O_2ClO_2)_2] \cdot 1.6CH_3CN \cdot 0.4CH_3OH$

atom	*x*	*y*	*z*	*U*(eq)
Cu(1)	1368(1)	5188(1)	775(1)	27(1)
O(1)	921(3)	4529(1)	-342(2)	29(1)
N(1)	3573(4)	4792(2)	1179(2)	30(1)
N(2)	1701(4)	5922(2)	1810(2)	28(1)
C(1)	1735(4)	3889(2)	-560(3)	24(1)
C(2)	1024(4)	3408(2)	-1347(2)	24(1)
C(3)	1963(5)	2752(2)	-1569(3)	28(1)
C(4)	3548(5)	2569(2)	-1054(3)	31(1)
C(5)	4193(5)	3042(2)	-269(3)	28(1)
C(6)	3340(4)	3707(2)	-1(3)	24(1)
C(7)	4186(5)	4175(2)	831(3)	31(1)
C(8)	4167(13)	5130(6)	2193(7)	34(2)
C(8')	4562(10)	5394(5)	1876(6)	17(2)
C(9)	6107(5)	5067(2)	2502(3)	31(1)
C(10)	6600(20)	5474(11)	3475(14)	47(4)
C(11)	5858(19)	6281(8)	3571(10)	46(3)
C(10')	6930(20)	5706(10)	3224(12)	29(3)
C(11')	5659(18)	5968(7)	3855(9)	38(3)
C(12)	4024(5)	6321(2)	3210(3)	36(1)
C(13)	3486(13)	5932(6)	2240(8)	27(2)
C(13')	3262(13)	5654(6)	2534(7)	21(2)
C(14)	638(5)	6466(2)	1941(3)	31(1)
C(15)	4543(5)	1866(2)	-1342(3)	45(1)
Cl(1)	-961(1)	3387(1)	1270(1)	35(1)
O(2)	-1926(4)	3677(2)	374(2)	59(1)
O(3)	215(4)	3977(2)	1690(2)	69(1)

O(4)	-90(5)	2678(2)	1095(2)	71(1)
O(5)	-2084(4)	3203(2)	1922(2)	46(1)
N(3)	11583(8)	4733(4)	4136(4)	74(2)
C(16)	10586(8)	4265(4)	4213(4)	49(2)
C(17)	9409(11)	3705(4)	4310(5)	48(2)
O(6)	9040(30)	3930(30)	4820(20)	190(20)
C(18)	8190(30)	4507(16)	5490(20)	53(7)

U(eq) is defined as one third of the trace of the orthogonalized U^{ij} tensor.

Table 11. Anisotropic displacement parameters ($Å^2 \times 10^3$) for $[Cu_2([20]\text{-DCHDC})(\mu\text{-}O_2ClO_2)_2] \cdot 1.6CH_3CN \cdot 0.4CH_3OH$

atom	U^{11}	U^{22}	U^{33}	U^{23}	U^{13}	U^{12}
Cu(1)	23(1)	26(1)	29(1)	-11(1)	-6(1)	7(1)
O(1)	23(1)	27(1)	32(1)	-12(1)	-5(1)	9(1)
N(1)	27(2)	30(2)	31(2)	-10(1)	-6(1)	5(1)
N(2)	24(2)	30(2)	26(2)	-9(1)	-1(1)	4(1)
C(1)	25(2)	20(2)	28(2)	-2(2)	9(2)	1(2)
C(2)	26(2)	19(2)	27(2)	-5(2)	4(2)	0(2)
C(3)	29(2)	25(2)	31(2)	-8(2)	5(2)	0(2)
C(4)	35(2)	21(2)	37(2)	-5(2)	9(2)	4(2)
C(5)	22(2)	26(2)	36(2)	0(2)	3(2)	3(2)
C(6)	23(2)	21(2)	27(2)	-1(2)	4(2)	3(2)
C(7)	27(2)	30(2)	32(2)	-4(2)	-6(2)	9(2)
C(8)	33(6)	34(6)	32(6)	-2(4)	-2(4)	5(4)
C(8')	19(4)	21(5)	12(4)	-2(3)	2(3)	-7(3)
C(9)	27(2)	28(2)	34(2)	-4(2)	-3(2)	1(2)
C(10)	36(9)	52(12)	47(11)	-11(7)	-14(7)	7(7)
C(11)	55(7)	41(9)	33(8)	-10(5)	-14(6)	15(7)

C(10')	16(6)	37(8)	31(8)	-3(5)	-7(5)	-1(5)
C(11')	38(6)	35(8)	33(7)	-1(5)	-18(5)	11(6)
C(12)	38(2)	35(2)	30(2)	-10(2)	-7(2)	6(2)
C(13)	21(5)	31(6)	28(6)	-13(4)	-1(4)	2(4)
C(13')	20(5)	24(6)	19(5)	7(4)	5(3)	-1(4)
C(14)	29(2)	31(2)	33(2)	-13(2)	2(2)	-2(2)
C(15)	37(3)	39(3)	57(3)	-20(2)	2(2)	10(2)
Cl(1)	37(1)	35(1)	31(1)	9(1)	-2(1)	-4(1)
O(2)	53(2)	67(2)	44(2)	33(2)	-25(2)	-26(2)
O(3)	76(3)	70(2)	47(2)	15(2)	-24(2)	-44(2)
O(4)	82(3)	77(3)	56(2)	-4(2)	17(2)	31(2)
O(5)	43(2)	49(2)	49(2)	11(1)	13(2)	6(1)
N(3)	68(4)	101(5)	54(4)	8(3)	13(3)	-12(4)
C(16)	47(4)	62(4)	36(3)	6(3)	3(3)	10(3)
C(17)	71(5)	37(3)	42(4)	-1(3)	22(4)	4(3)
O(6)	57(18)	310(50)	160(30)	200(30)	-72(19)	-120(20)
C(18)	45(16)	55(16)	67(18)	-16(14)	33(13)	-16(12)

The anisotropic displacement factor exponent takes the form: $-2\pi^2[h^2 a^{*2}U^{11} + ... + 2 hka^{*}b^{*}U^{12}]$.

Table 12. Hydrogen coordinates (x 10^4) and isotropic displacement parameters ($Å^2 \times 10^3$) for $[Cu_2([20]\text{-DCHDC})(\mu\text{-}O_2ClO_2)_2] \cdot 1.6CH_3CN \cdot 0.4CH_3OH$

atom	x	y	z	U(eq)
H(3)	1493	2419	-2096	34
H(5)	5259	2909	104	34
H(7A)	5277	4007	1135	38
H(8A)	3659	4790	2650	41
H(8'A)	4865	5866	1507	21

H(9A)	6455	4500	2550	37
H(9B)	6670	5331	2016	37
H(9C)	6918	4894	2093	37
H(9D)	5806	4596	2859	37
H(10A)	6276	5121	3975	57
H(10B)	7843	5525	3617	57
H(11A)	6086	6438	4261	55
H(11B)	6425	6672	3211	55
H(10A)	7950	5485	3637	35
H(10B)	7267	6172	2869	35
H(11A)	6180	6377	4323	46
H(11B)	5355	5504	4224	46
H(12A)	3673	6888	3163	43
H(12B)	3434	6058	3684	43
H(12C)	3217	6498	3619	43
H(12D)	4310	6784	2833	43
H(13A)	4032	6256	1784	32
H(13A)	2975	5187	2918	25
H(14)	963	6816	2473	38
H(15A)	3888	1602	-1910	54
H(15B)	4771	1485	-805	54
H(15C)	5610	2058	-1496	54
H(17A)	9933	3278	4738	58
H(17B)	8940	3481	3675	58
H(17C)	8506	3953	4589	58

4) $[Cu_2([20]\text{-}DCHDC)(N_3)_2] \cdot 2CH_3OH$

Suitable crystals of $[Cu_2([20]\text{-}DCHDC)(N_3)_2] \cdot 2CH_3OH$ were obtained by slow evaporation of methanol solutions of $[Cu_2([20]\text{-}DCHDC)(N_3)_2] \cdot 6H_2O$ complex at atmospheric pressure. The dark green crystal of $[Cu_2([20]\text{-}DCHDC)(N_3)_2] \cdot 2CH_3OH$ was attached to glass fibers and mounted on a Bruker SMART diffractometer equipped with a graphite monochromated Mo Kα (λ = 0.71073 Å) radiation, operating at 50 kV and 30 mA and a CCD detector ; 45 frames of two-dimensional diffraction images were collected and processed to obtain the cell parameters and orientation matrix. The crystallographic data, conditions for the collection of intensity data, and some features of the structure refinements are listed in Table 13, and atomic coordinates were given in Table 14. The intensity data were corrected for Lorentz and polarization effects. Absorption correction was not made during processing. Of the 10318 unique reflections measured, 3813 reflections in the range 2.00° ≤ θ ≤ 28.30° were considered to be observed(I>2□(I)) and were used in subsequent structure analysis. The program SAINTPLUS [121] was used for integration of the diffraction profiles. The structures were solved by direct methods using the XS program of the SHELXTL package [122] and refined by full matrix least squares against F^2 for all data using XL. All non-H atoms were refined with anisotropic displacement parameters (Table 15). Hydrogen atoms were placed in idealized positions [U_{iso} = 1.2U_{eq} (parent atom)]. Hydrogen coordinates and isotropic displacement parameters were given in Table 16.

Table 13. Crystal data and structure refinement for $[Cu_2([20]\text{-}DCHDC)(N_3)_2]\cdot 2CH_3OH$

Empirical formula	$C_{32}H_{42}Cu_2N_{10}O_4$	
	$[Cu_2(C_{30}H_{34}N_4O_2)(N_3)_2]\cdot 2CH_3OH$	
Formula weight	757.84	
Temperature	173(2) K	
Wavelength	0.71073 Å	
Crystal system	Monoclinic	
Space group	$P2_1/c$	
Unit cell dimensions	a = 6.9849(5) Å	α = 90°.
	b = 19.6663(13) Å	β = 97.1770(10)°.
	c = 12.0317(8) Å	γ = 90°.
Volume	1639.81(19) $Å^3$	
Z	2	
Density (calculated)	1.535 g/cm^3	
Absorption coefficient	1.351 mm^{-1}	
F(000)	788	
Crystal size	0.40 x 0.15 x 0.08 mm^3	
Theta range for data collection	2.00 to 28.30°.	
Index ranges	$-9<=h<=9$, $-23<=k<=25$, $-12<=l<=15$	
Reflections collected	10318	
Independent reflections	3813 [R(int) = 0.0740]	
Completeness to theta = 28.30°	93.5 %	
Absorption correction	None	
Refinement method	Full-matrix least-squares on F^2	
Data / restraints / parameters	3813 / 0 / 217	
Goodness-of-fit on F^2	1.169	
Final R indices [I>2sigma(I)]	R_1 = 0.0549, wR_2 = 0.1217	
R indices (all data)	R_1 = 0.0677, wR_2 = 0.1273	
Largest diff. peak and hole	0.905 and -0.717 e.$Å^{-3}$	

$R = \sum \| F_0 | - | F_c \| / \sum | F_0 |$, $R_w = \left[\sum w(F_0^2 - F_c^2)^2 / \sum w(F_0^2)^2 \right]^{1/2}$

$w = 1/[\sigma^2(F_o^2)+(0.0341P)^2+3.2103P]$ where $P = (F_o^2+2F_c^2)/3$.

Table 14. Atomic coordinates ($x10^4$) and equivalent isotropic displacement parameters ($Å^2 \times 10^3$) for $[Cu_2([20]\text{-DCHDC})(N_3)_2] \cdot 2CH_3OH$

atom	*x*	*y*	*z*	*U*(eq)
Cu(1)	4155(1)	4309(1)	4923(1)	20(1)
O(1)	3902(3)	5162(1)	5671(2)	26(1)
N(1)	1673(4)	4005(1)	5242(2)	19(1)
N(2)	4000(4)	3669(1)	3719(2)	20(1)
N(3)	5956(5)	3761(2)	6336(3)	33(1)
N(4)	5818(5)	3158(2)	6285(3)	31(1)
N(5)	5712(6)	2569(2)	6215(3)	45(1)
C(1)	2917(4)	5285(2)	6517(3)	17(1)
C(2)	3410(5)	5848(2)	7231(3)	18(1)
C(3)	2301(5)	5971(2)	8106(3)	21(1)
C(4)	705(5)	5570(2)	8271(3)	22(1)
C(5)	248(5)	5028(2)	7556(3)	20(1)
C(6)	1326(4)	4862(2)	6685(3)	18(1)
C(7)	693(5)	4278(2)	5969(3)	19(1)
C(8)	912(6)	3474(2)	4430(3)	33(1)
C(9)	-473(5)	2972(2)	4814(3)	27(1)
C(10)	-1121(6)	2441(2)	3924(4)	40(1)
C(11)	473(6)	2142(2)	3359(4)	38(1)
C(12)	1884(6)	2658(2)	2994(3)	27(1)
C(13)	2542(6)	3150(2)	3913(3)	35(1)
C(14)	5008(5)	3674(2)	2900(3)	20(1)
C(15)	-512(6)	5750(2)	9195(3)	30(1)
O(2)	6391(5)	4293(2)	8569(3)	64(1)
C(16)	4808(7)	4124(3)	9090(4)	52(1)

U(eq) is defined as one third of the trace of the orthogonalized U^{ij} tensor.

Table 15. Anisotropic displacement parameters ($Å^2 \times 10^3$) for $[Cu_2([20]\text{-DCHDC})(N_3)_2] \cdot 2CH_3OH$

	U^{11}	U^{22}	U^{33}	U^{23}	U^{13}	U^{12}
Cu(1)	19(1)	19(1)	23(1)	-8(1)	11(1)	-6(1)
O(1)	28(1)	22(1)	33(1)	-10(1)	22(1)	-11(1)
N(1)	19(1)	18(1)	20(1)	-1(1)	7(1)	-4(1)
N(2)	19(1)	20(1)	21(1)	-7(1)	6(1)	-3(1)
N(3)	26(2)	44(2)	29(2)	1(2)	4(1)	1(2)
N(4)	22(2)	48(2)	24(2)	14(2)	6(1)	0(2)
N(5)	46(2)	41(2)	49(2)	24(2)	10(2)	-1(2)
C(1)	16(2)	17(2)	20(2)	1(1)	8(1)	1(1)
C(2)	17(2)	21(2)	16(1)	0(1)	4(1)	1(1)
C(3)	22(2)	25(2)	16(1)	-2(1)	4(1)	2(1)
C(4)	25(2)	22(2)	21(2)	3(1)	9(1)	4(1)
C(5)	21(2)	22(2)	20(2)	3(1)	8(1)	0(1)
C(6)	16(2)	18(2)	19(2)	1(1)	5(1)	3(1)
C(7)	18(2)	18(2)	22(2)	4(1)	6(1)	-3(1)
C(8)	33(2)	27(2)	41(2)	-13(2)	19(2)	-11(2)
C(9)	25(2)	28(2)	30(2)	-6(2)	10(1)	-8(2)
C(10)	41(2)	33(2)	51(3)	-13(2)	19(2)	-18(2)
C(11)	40(2)	32(2)	45(2)	-16(2)	16(2)	-14(2)
C(12)	32(2)	23(2)	29(2)	-6(2)	11(2)	-4(2)
C(13)	38(2)	36(2)	34(2)	-17(2)	18(2)	-17(2)
C(14)	20(2)	21(2)	19(2)	-7(1)	4(1)	-1(1)
C(15)	35(2)	33(2)	26(2)	-2(2)	18(2)	-1(2)
O(2)	47(2)	97(3)	50(2)	-18(2)	11(2)	-33(2)
C(16)	37(2)	77(4)	44(3)	11(2)	8(2)	5(3)

The anisotropic displacement factor exponent takes the form: $-2\pi^2[h^2 a^{*2}U^{11} + ... + 2 hka^* b^* U^{12}]$.

Table 16. Hydrogen coordinates (x 10^4) and isotropic displacement parameters ($Å^2 \times 10^3$) for $[Cu_2([20]\text{-}DCHDC)(N_3)_2] \cdot 2CH_3OH$

	x	*y*	*z*	*U*(eq)
H(3)	2646	6339	8603	25
H(5)	-841	4757	7659	24
H(7)	-531	4085	6047	23
H(8A)	150	3727	3804	39
H(9A)	-1619	3217	5014	32
H(9B)	146	2740	5496	32
H(10A)	-1784	2068	4277	49
H(10B)	-2072	2652	3347	49
H(11A)	-102	1885	2692	46
H(11B)	1195	1814	3878	46
H(12A)	3018	2416	2768	33
H(12B)	1260	2910	2335	33
H(13)	3209	2859	4525	42
H(14)	4712	3342	2330	24
H(15A)	-1565	5420	9194	36
H(15B)	-1052	6207	9063	36
H(15C)	296	5738	9922	36
H(2)	6023	4429	7916	77
H(16A)	4949	3658	9376	63
H(16B)	3638	4157	8551	63
H(16C)	4710	4438	9713	63

III. Results and Discussion

1. Synthesis and characterization of the macrocyclic ligand with 2,6-diformyl -*p*-cresol and *trans*-1,2-diaminocyclohexane

Synthesis and study of new ligands with phenolic groups is an area of active research interest because of their use as models for biological metal-binding sites, their ability to form metal complexes with interesting magnetic exchange, redox and catalytic properties. 2,6-Diformyl-*p*-cresol is a useful source to synthesise such ligands and oxo-bridged macrocyclic complexes with diamines in the presence of template metal salts. Preformed ligands are required to investigate host-guest interactions, to synthesise complexes of metals inert to template reactions and complexes of heteronuclear metals.

The reaction of 2,6-diformyl-*p*-cresol and trans-1,2-diaminocyclohexane in methanol in equimolar ratio using the high dilution technique affords a [3 + 3] Schiff-base macrocycle L_4 as yellow solid in high yield. The EA, IR, NMR and FAB mass spectral data of the product do not agree with the expected a [2 + 2] Schiff-base macrocycle ligand L_3 but match with the composition of [3 + 3] Schiff-base macrocycle L_4 (Scheme 2).

The molecular ion peak at m/z 727 in the FAB mass spectra of L_4 indicates the condensation of three units of 2,6-diformyl-*p*-cresol and three units of trans-1,2-diaminocyclohexane (Fig. 1).

The 400 MHz ($CDCl_3$) ^1H NMR spectrum of the ligand, depicted in Fig.

2, consists of a singlet at 8.670, 8.210, 7.576, and 6.898 ppm due to the azomethine N=CH- and cresol aromatic protons, respectively. The singlet at 2.08 ppm is due to the Ar-CH_3 protons. The multilet at 3.3 and 1.86 -1.46 ppm are due to the N-CH and CH_2CH_2 protons of cyclohexane, respectively. The 100 MHz ($CDCl_3$) ^{13}C NMR spectrum of the ligand, depicted in Fig. 3, consists of 14 peaks (19.98, 24.40, 33.15, 33.45, 73.29, 75.36, 118.77, 122.959, 126.84, 129.62, 134.21, 156.18, 159.46, 163.46).

Infrared spectra (Fig. 4) of the ligand show *v*(C=N) stretching vibration bands at around 1638 cm^{-1} and the absence of any carbonyl bands associated with the diformyl-phenol starting materials or nonmarcrocyclic intermediates. The IR spectra displayed three C-H stretching vibrations from 3018 to 2856 cm^{-1}. A strong bands at near ~1600 cm^{-1} region associated with the aromatic ring C=C vibrations. The sharp absorption bands occurring at ~1258 cm^{-1} are attributed to phenolic C-O stretching vibration. The present complexes exhibited four C-H deformation bands at 1447, 1390, 1371 and 1312 cm^{-1} regions and three out-of-plan vibration bands at 868, 827 and 761 cm^{-1} regions. The broad band occurring in the IR spectra of the complexes in the ~3439 cm^{-1} regions may probably be due to the *v*(OH) vibration of the phenol and lattice water.

The electronic absorption spectrum of the free ligand H_2[20]-DCHDC in DMF was represented in Fig. 5. The absorption band at 450 nm (ε = 3,130 $M^{-1}cm^{-1}$) is associated with π-π^* transitions of conjugated [3 + 3] macrocyclic ligand.

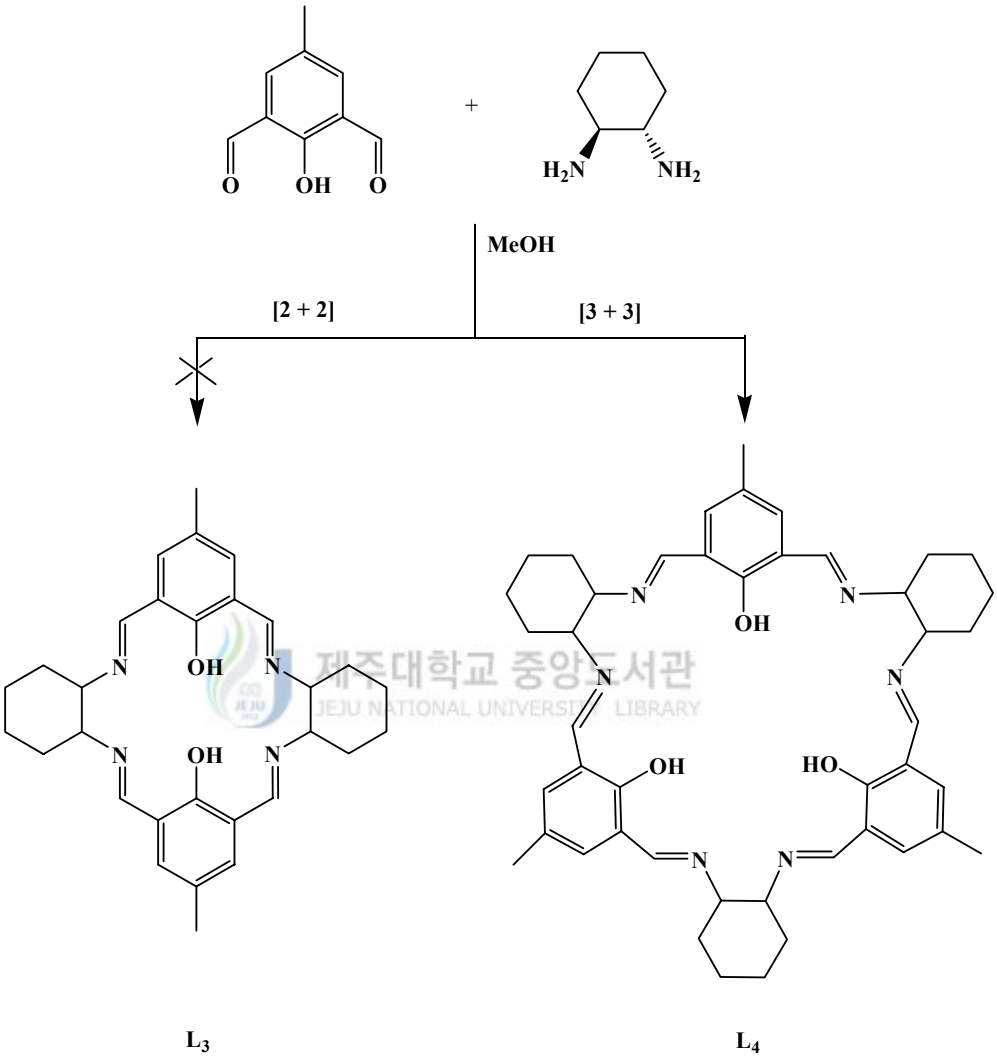

L_3 L_4

Scheme 2. Product formation pattern of macrocyclic ligand with 2,6-diformyl -*p*-cresol and *trans*-1,2-diaminocyclohexane.

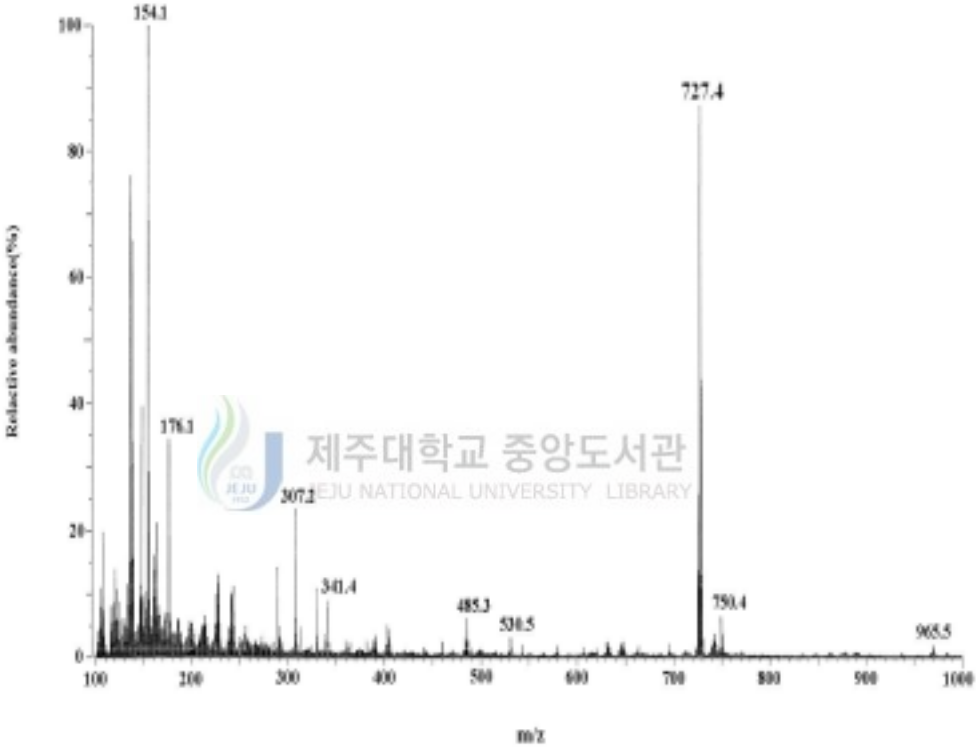

Fig. 1. FAB-mass spectrum of the [3 + 3] Schiff-base macrocycle L_4 ligand.

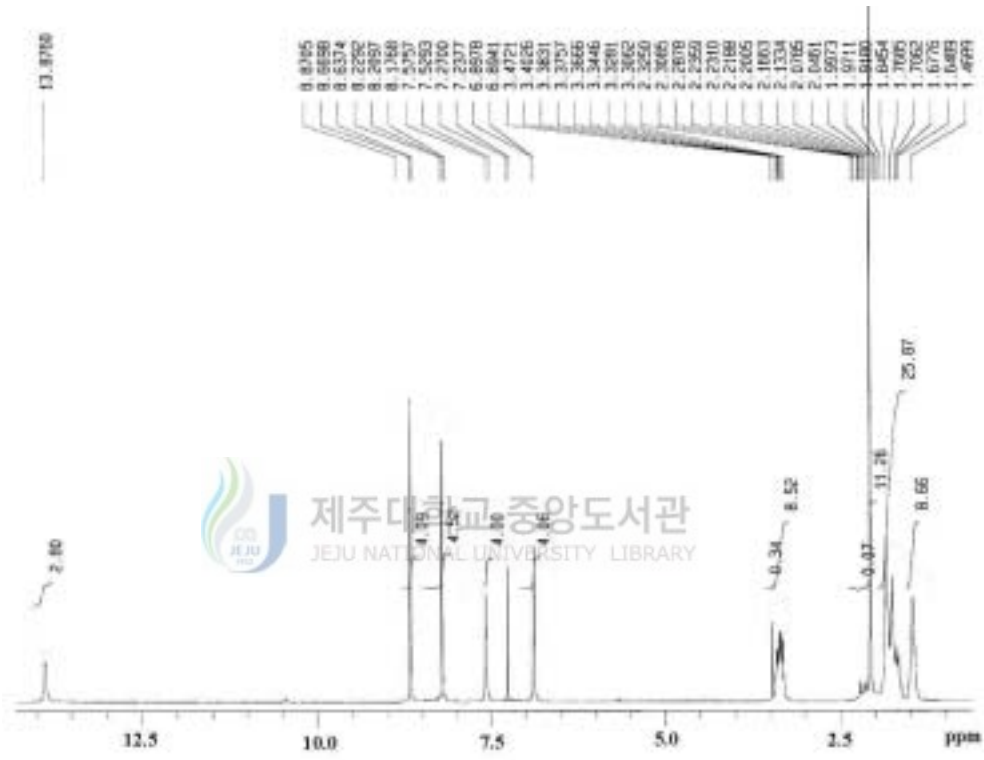

Fig. 2. ^{1}H-NMR spectrum of the [3 + 3] Schiff-base macrocycle L_4 ligand (solvent : $CDCl_3$).

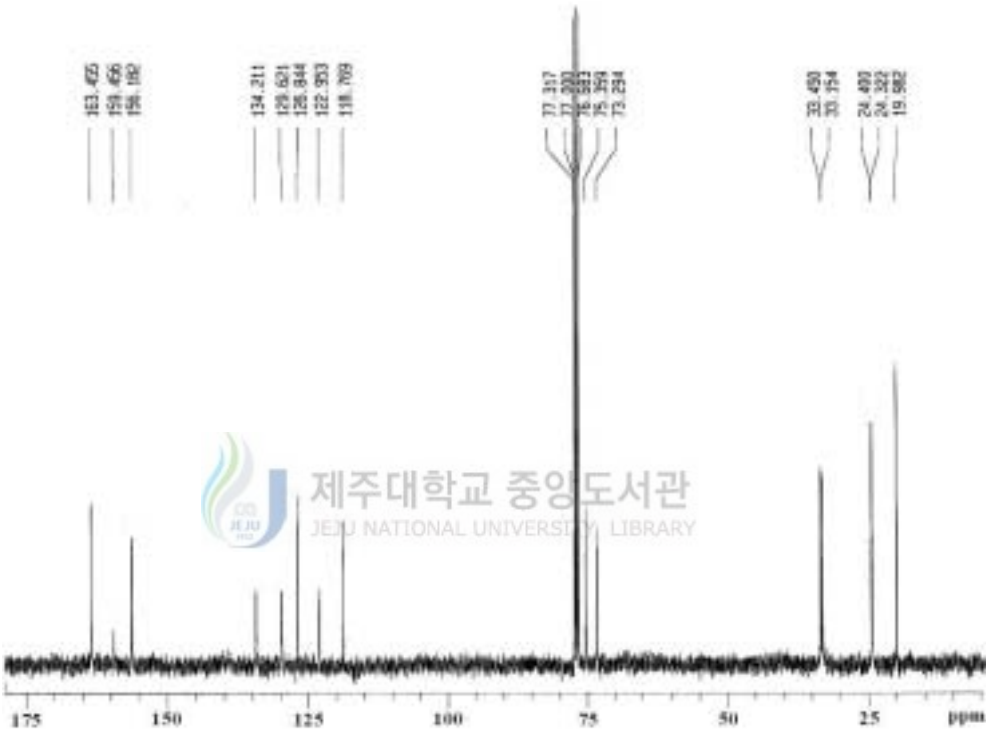

Fig. 3. ^{13}C-NMR spectrum of the [3 + 3] Schiff-base macrocycle L_4 ligand (solvent : $CDCl_3$).

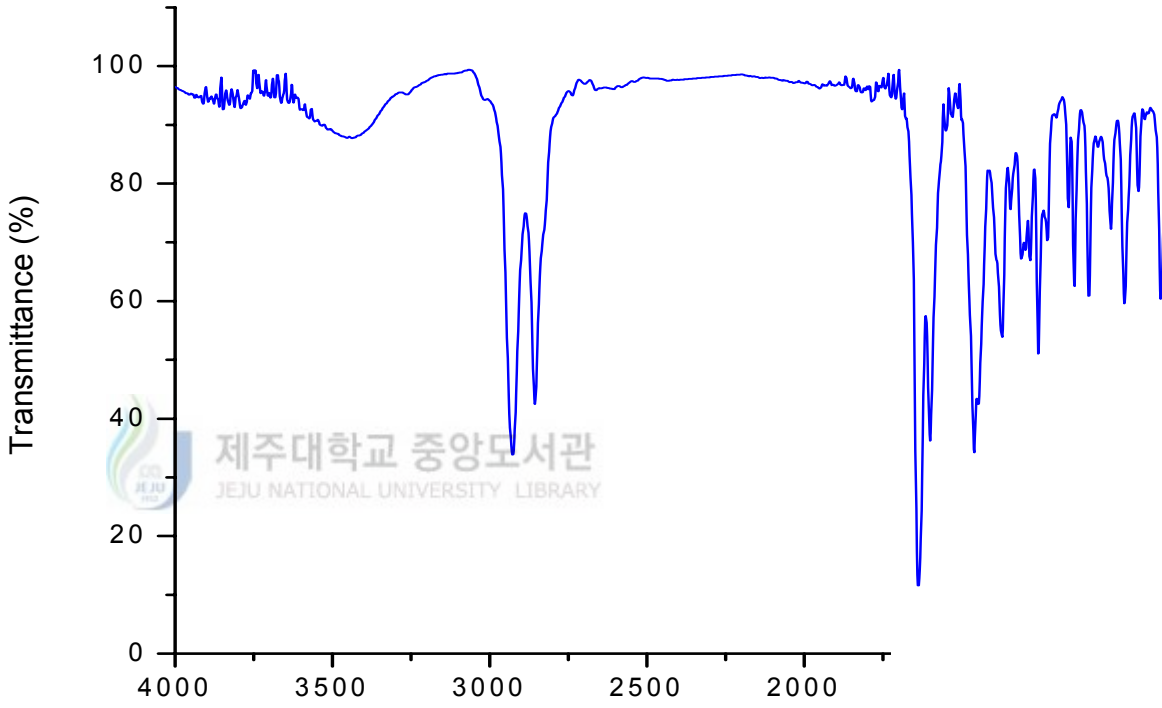

Fig. 4. IR spectrum of the [3 + 3] Schiff-base macrocycle L_4 ligand.

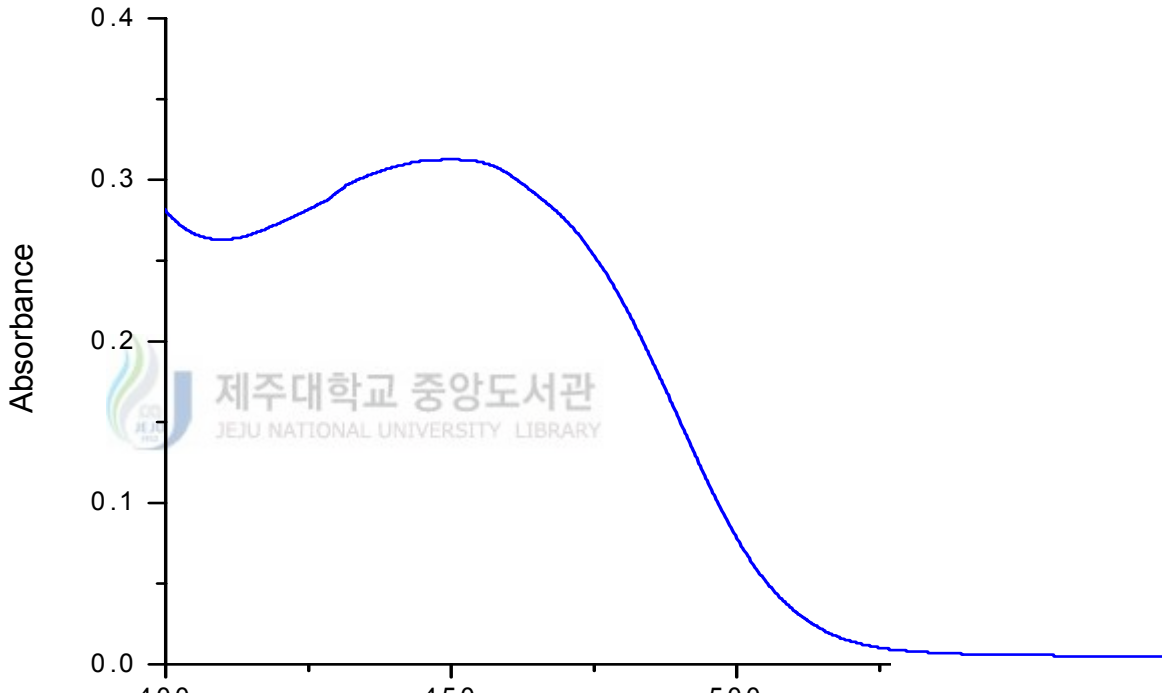

Fig. 5. Electronic absorption spectrum of [3 + 3] Schiff-base macrocycle L_4 ligand in DMF.

2. IR spectra of the complexes

IR spectra of the copper complexes were presented in Fig. 6 ~ 14. The characteristics of the complexes were listed in Table 17 and 18. The strong and sharp absorption bands occurring at 1624～1633 cm^{-1} are attributed to *ν*(C=N) of the coordinated [20]-DCHDC ligand [123, 124], and the absence of any carbonyl bands associated with the diformylphenol starting materials or nonmarcrocyclic intermediates. The IR spectra displayed three C-H stretching vibrations from 3000 to 2800 cm^{-1}. A strong bands at near ～1550 cm^{-1} region associated with the aromatic ring C=C vibrations. The sharp absorption bands occurring at ～1230 cm^{-1} regions are attributed to phenolic C-O stretching vibration. The present complexes exhibited four C-H deformation bands at 1450, 1380, 1350 and 1320 cm^{-1} regions and three out-of-plan vibration bands at 860, 820 and 770 cm^{-1} regions. The bands occurring in the IR spectra of the complexes in the 3500～3300 cm^{-1} regions may probably be due to the *ν*(OH) vibration of the lattice water. A weak bands at near 503 cm^{-1} region associated with the Cu-N(macrocycle) vibration.

The perchlorate ion may be coordinated to a metal atom as a unidentate ligand(Ⅰ), as a chelating bidentate ligand(Ⅱ) or as a bridging bidentate ligand(Ⅲ).

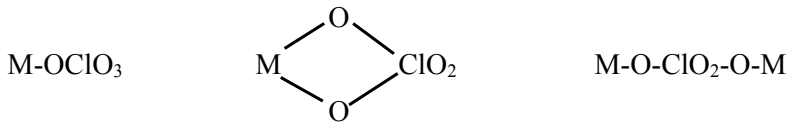

(Ⅰ) (Ⅱ) (Ⅲ)

Free ClO_4^- ion with tetrahedral symmetry, T_d, have four fundamental vibrations, only two of which are infrared active (one stretching mode and bending mode). For unidentate coordination (M-$OClO_3$), the symmetry is reduced to C_{3v}, each of the bands for the free ion being split into two bands with, in addition, the two previously only Raman active vibrations now becoming infrared active. Therefore, three bands due to stretching vibrations and three due to bending vibrations are expected. For bidentate coordination (M-O_2ClO_2 and M-O-ClO_2-O-M), the symmetry is reduced to C_{2v} and each of the bands due to the two modes of vibration of the free ion is now split into three, so that, taking into account the bands which were inactive for the free ion, four bands due to stretching vibrations and four due to bending vibrations are observed [125]. The strong four bands at 1148, 1121, 1109, and 1085 cm^{-1} in $[Cu_2([20]\text{-DCHDC})(\mu\text{-}O_2ClO_2)_2]\cdot H_2O$ are attributed to a bridging bidentate ligand Cu-O-ClO_2-O-Cu. The complex exhibited two ClO_4^- deformation bands at 636 and 627 cm^{-1} regions.

The thiocyanate ion may act as an ambidentate ligand, bonding may occur either through the nitrogen or the sulphur atom. The bonding mode may easily be distinguished by examining the band due to the C-S stretching vibration which occurs at 730-690 cm^{-1} when the bonding occurs through the sulphur atom and at 860-780 cm^{-1} when it is through the nitrogen atom [126]. The C≡N stretching vibration of thiocyanato-complexes (sulphur-bound, i.e. M-SCN) gives rise to a sharp band at about 2100 cm^{-1} and Ga-NCS (i.e. nitrogen bound), the resulting band is often broad and occurs near and below 2050 cm^{-1}. The absorption vibrations due to the N-coordinated bonded NCS^- in $[Cu_2([20]\text{-DCHDC})(NCS)_2]\cdot H_2O$ appear 2067 and 894 cm^{-1}.

In general, for azides the band due to the asymmetric N_3 stretching vibration is strong and occurs in the region 2195-2030 cm^{-1}, while that due to the symmetric vibration is much weaker and occurs in the region 1375-1175 cm^{-1} and the band due to the deformation vibration is also weak and occurs at 680-410 cm^{-1} [127]. The absorption peak at 2034 cm^{-1} in the $[Cu_2([20]\text{-DCHDC})(N_3)_2] \cdot 6H_2O$ is assigned to the asymmetric stretching mode of coordinated azide. The symmetric stretching frequency of coordinated azide is observed at 1321 cm^{-1}.

Linkage isomerism is possible in the case of metal complexes containing the unit NO_2. Coordination to the metal atom may occur through the nitrogen atom, resulting in a nitro-complex, or through an oxygen atom, resulting in a nitrito-complex. Nitro-complexes exhibit bands due to asymmetric and symmetric -NO_2 stretching vibration and, in addition, one due to a NO_2 deformation vibration [126]. The nitrito-complexes exhibit bands due to asymmetric and symmetric -ONO stretching vibrations which are well separated and occur at 1485-1400 cm^{-1} and 1110-1050 cm^{-1}, respectively. Nitro-groups in metal coordination complexes may exist as bridging or as end groups. Terminal nitro-groups absorb at 1485-1370 cm^{-1} and 1340-1315 cm^{-1} due to the asymmetric and symmetric stretching vibrations of the NO_2 group, respectively [126]. Nitrito-complexes do not have a band near 620cm^{-1} which is present for all nitro-complexes. Nitro- groups acting as bridging units (M-ONO-M) between two metal atoms absorb at 1485-1470 cm^{-1} and at about 1200 cm^{-1}, these bands being broader than those for terminal nitro-groups [126, 128].

The strong absorption peaks at 1446 and 1205 cm^{-1} in the

$[Cu_2([20]\text{-}DCHDC)(\mu\text{-}ONO)]NO_2 \cdot H_2O$ are assigned to a bridging bidentate ligand Cu-ONO-Cu. And stretching bands of NO_2 counter ion are observed at 1327 and 1272 cm^{-1}.

The nitrate ion may form complexes as a unidentate or bidentate ligand. The free ion , which has D_{3h} symmetry, has one stretching and one in-plane deformation vibration which are infrared active, the bands each being split into two in the case of both unidentate or bidentate coordination. In addition, a band due to the symmetry stretching vibration, which previously appeared only in the Raman spectrum, appears in the infrared spectrum, this vibration now being infrared active. Unidentate coordination may be distinguished from bidentate coordination since the separation of the bands due to stretching vibration is larger for the latter [125].

The absorption bands of bidentate coordinate nitrate occurring in the IR spectra of $[Cu_2([20]\text{-}DCHDC)(\mu\text{-}O_2NO)]NO_3 \cdot 0.5H_2O$ in the 1454, 1339 and 1043 cm^{-1} regions are assignable to the $\nu(N{=}O)$ (ν_1), $\nu_a(NO_2)$ (ν_5) and $\nu_s(NO_2)$ (ν_2) vibrations, respectively. The very strong absorption band at 1385 cm^{-1} is characteristic of ionic nitrate present in the outer-coordination sphere [124, 129].

The absorption peaks at 1236-1198 and 1022-1005 cm^{-1} in the $[Cu_2([20]\text{-}DCHDC)(\mu\text{-}S_2O_3)]$ are assigned to the asymmetric and symmetric stretching mode of bridging coordinate $S_2O_3^{2-}$, respectively. And deformation bands of coordinate $S_2O_3^{2-}$ are observed at 629, 598, and 532 cm^{-1} regions.

Table 17. Characteristic IR absorptions (cm^{-1}) of macrocyclic ligand (H_2[20]-DCHDC) for the binuclear Cu(II) complexes

Compounds	Assignments					
	Macrocycle					
	ν(CH)			ν(C=N)	ν(C=C)	ν(C-O)
[H_2[20]-DCHDC]・0.5H_2O	3018	2926	2856	1638	1601	1258
[Cu_2([20]-DCHDC)Cl_2]・H_2O	3022	2929	2858	1627	1548	1240
[Cu_2([20]-DCHDC)Br_2]・0.5H_2O	3001	2933	2860	1627	1544	1236
[Cu_2([20]-DCHDC)I_2]	3018	2935	2858	1624	1542	1234
[Cu_2([20]-DCHDC)(μ-O_2ClO_2)$_2$]・H_2O	3024	2929	2862	1627	1546	1238
[Cu_2([20]-DCHDC)(NCS)$_2$]・H_2O	3041	2937	2858	1625	1546	1234
[Cu_2([20]-DCHDC)(N_3)$_2$]・6H_2O	3030	2947	2860	1624	1548	1236
[Cu_2([20]-DCHDC)(μ-O_2N)]NO_2・6H_2O	3018	2931	2860	1627	1548	1238
[Cu_2([20]-DCHDC)(μ-O_2NO)]NO_3・0.5H_2O	3031	2939	2862	1625	1550	1238
[Cu_2([20]-DCHDC)(μ-S_2O_3)]	3014	2941	2858	1633	1542	1236

Table 17. *continued*

Compounds	Assignments						
	Macrocycle						
	δ(CH)				δ_{oop}(CH)		
$[H_2[20]\text{-DCHDC}] \cdot 0.5H_2O$	1447	1390	1371	1312	868	827	761
$[Cu_2([20]\text{-DCHDC})Cl_2] \cdot H_2O$	1448	1382	1348	1311	862	819	769
$[Cu_2([20]\text{-DCHDC})Br_2] \cdot 0.5H_2O$	1444	1382	1346	1301	864	817	769
$[Cu_2([20]\text{-DCHDC})I_2]$	1442	1380	1342	1325	862	819	767
$[Cu_2([20]\text{-DCHDC})(\mu\text{-}O_2ClO_2)_2] \cdot H_2O$	1448	1382	1348	1309	864	819	769
$[Cu_2([20]\text{-DCHDC})(NCS)_2] \cdot H_2O$	1444	1382	1344	1323	860	819	767
$[Cu_2([20]\text{-DCHDC})(N_3)_2] \cdot 6H_2O$	1444	1382	1350	1321	867	821	767
$[Cu_2([20]\text{-DCHDC})(\mu\text{-}O_2N)]NO_2 \cdot 6H_2O$	1446	1382	1348	1325	862	819	771
$[Cu_2([20]\text{-DCHDC})(\mu\text{-}O_2NO)]NO_3 \cdot 0.5H_2O$	1444	1384	1350	1323	864	821	767
$[Cu_2([20]\text{-DCHDC})(\mu\text{-}S_2O_3)]$	1448	1384	1350	1326	866	829	767

Table 18. Characteristic IR absorptions (cm^{-1}) of exocycle molecules for the binuclear Cu(II) complexes

Compounds	Assignments
$[H_2[20]\text{-DCHDC}] \cdot 0.5H_2O$	3439(br); ν(OH) lattice H_2O
$[Cu_2([20]\text{-DCHDC})Cl_2] \cdot H_2O$	3454(br); ν(OH) lattice H_2O 503(w); Cu-N(macrocycle)
$[Cu_2([20]\text{-DCHDC})Br_2] \cdot 0.5H_2O$	3429(br); ν(OH) lattice H_2O 503(w); Cu-N(macrocycle)
$[Cu_2([20]\text{-DCHDC})I_2]$	503(w); Cu-N(macrocycle)
$[Cu_2([20]\text{-DCHDC})(\mu\text{-}O_2ClO_2)_2] \cdot H_2O$	3313(br); ν(OH) lattice H_2O 1148(s), 1121(vs), 1109(s), 1085(s); bridging ClO_4^- Cu-O-ClO_2-O-Cu 636(m), 627(sh); coord. ClO_4^- 503(w); Cu-N(macrocycle)
$[Cu_2([20]\text{-DCHDC})(NCS)_2] \cdot H_2O$	3464(br); ν(OH) lattice H_2O 2067(vs); ν(CN) N-bonded NCS^- 894(w); ν(CS) N-bonded NCS^- 503(w); Cu-N(macrocycle)
$[Cu_2([20]\text{-DCHDC})(N_3)_2] \cdot 6H_2O$	3462(sh), 3342(m); ν(OH) lattice H_2O 2034(vs); ν_{as}(NNN) coord. N_3^- 1321(m); ν_s(NNN) coord. N_3^- 503(w); Cu-N(macrocycle)
$[Cu_2([20]\text{-DCHDC})(\mu\text{-}O_2N)]NO_2 \cdot 6H_2O$	3398 (br); ν(OH) lattice H_2O 1446(s), 1205(m); bridging NO_2, Cu-ONO-Cu 1327(s), 1272(m); ionic NO_2 503(w); Cu-N(macrocycle)
$[Cu_2([20]\text{-DCHDC})(\mu\text{-}O_2NO)]NO_3 \cdot 0.5H_2O$	3442(br); ν(OH) lattice H_2O 1454 (m) ν(N=O), 1339(s) $\nu_{as}(NO_2)$, 1043(m) $\nu_s(NO_2)$; monodentate NO_3^- 1385 (sp, vs) ; ionic NO_3^- 503(w); Cu-N(macrocycle)
$[Cu_2([20]\text{-DCHDC})(\mu\text{-}S_2O_3)]$	1236(s), 1198(s); $\nu_{as}(SO_3)$ coord. $S_2O_3^{2-}$ 1022(s), 1005(s); $\nu_{as}(SO_3)$ coord. $S_2O_3^{2-}$ 629(m), 598(s), 532(s); $\delta(SO_3)$ coord. $S_2O_3^{2-}$ 503(w); Cu-N(macrocycle)

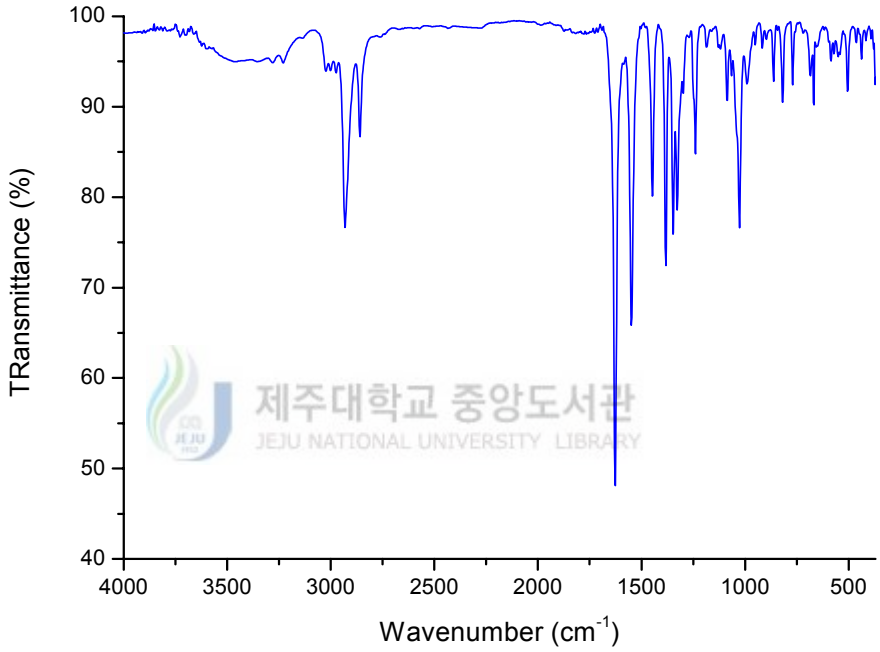

Fig. 6. FT-IR spectrum of $[Cu_2([20]\text{-DCHDC})Cl_2] \cdot H_2O$.

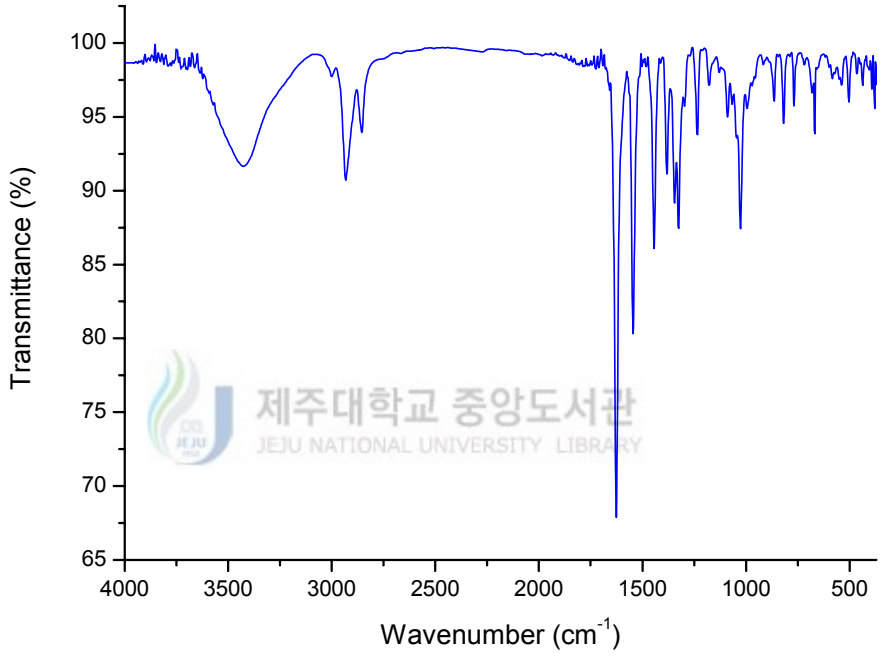

Fig. 7. FT-IR spectrum of $[Cu_2([20]\text{-DCHDC})Br_2] \cdot 0.5H_2O$.

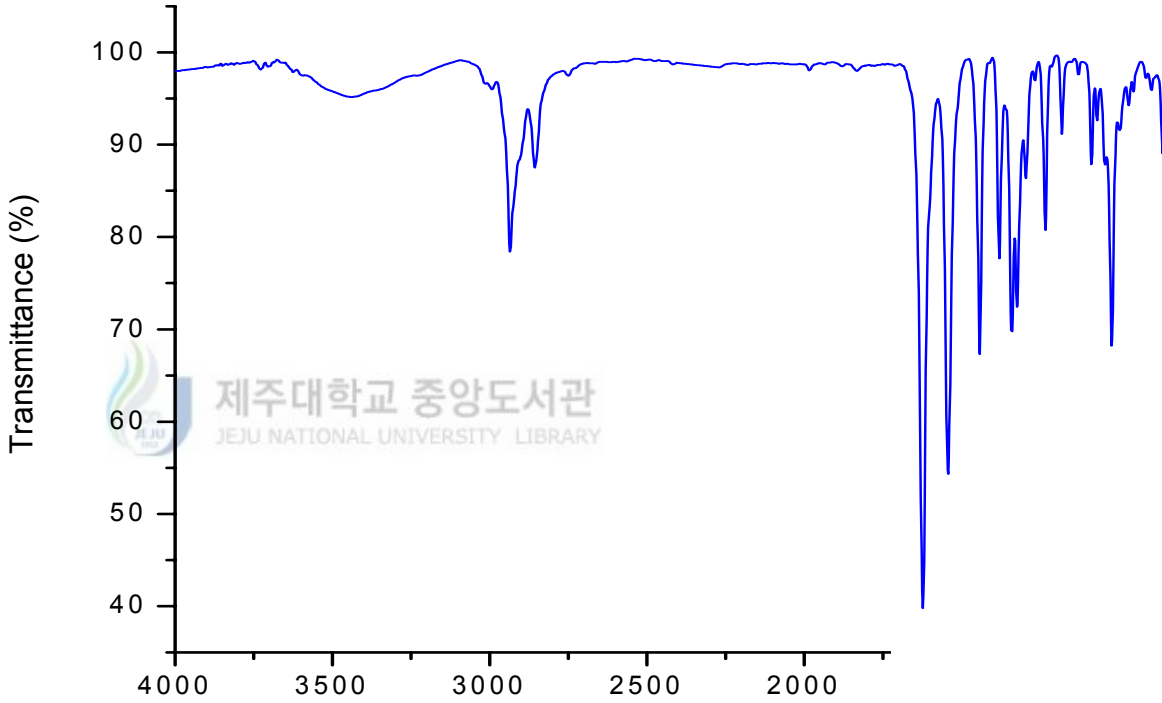

Fig. 8. FT-IR spectrum of $[Cu_2([20]\text{-DCHDC})I_2]$.

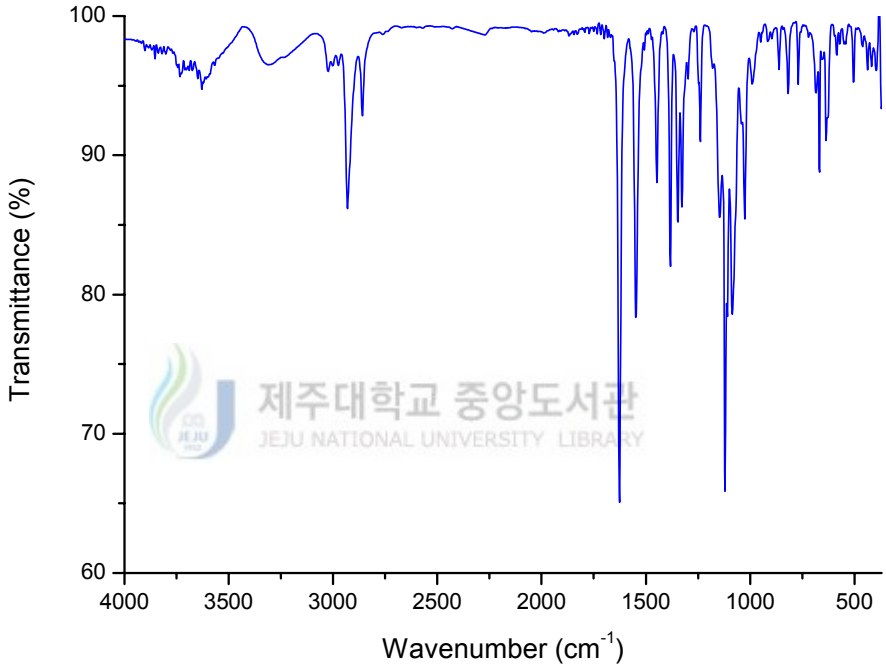

Fig. 9. FT-IR spectrum of $[Cu_2([20]\text{-}DCHDC)(\mu\text{-}O_2ClO_2)_2] \cdot H_2O$.

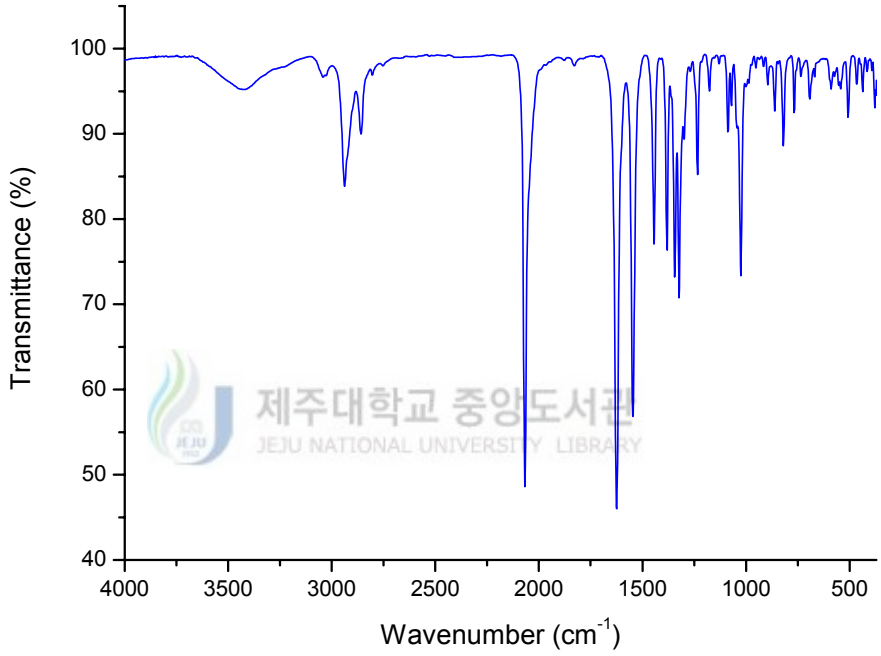

Fig. 10. FT-IR spectrum of $[Cu_2([20]\text{-}DCHDC)(NCS)_2] \cdot H_2O$.

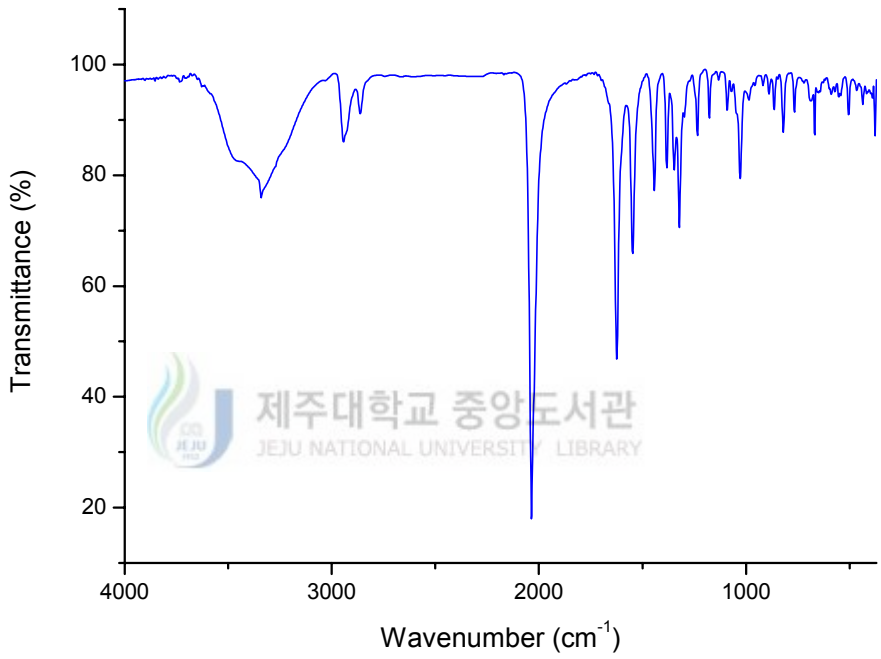

Fig. 11. FT-IR spectrum of $[Cu_2([20]\text{-DCHDC})(N_3)_2] \cdot 6H_2O$.

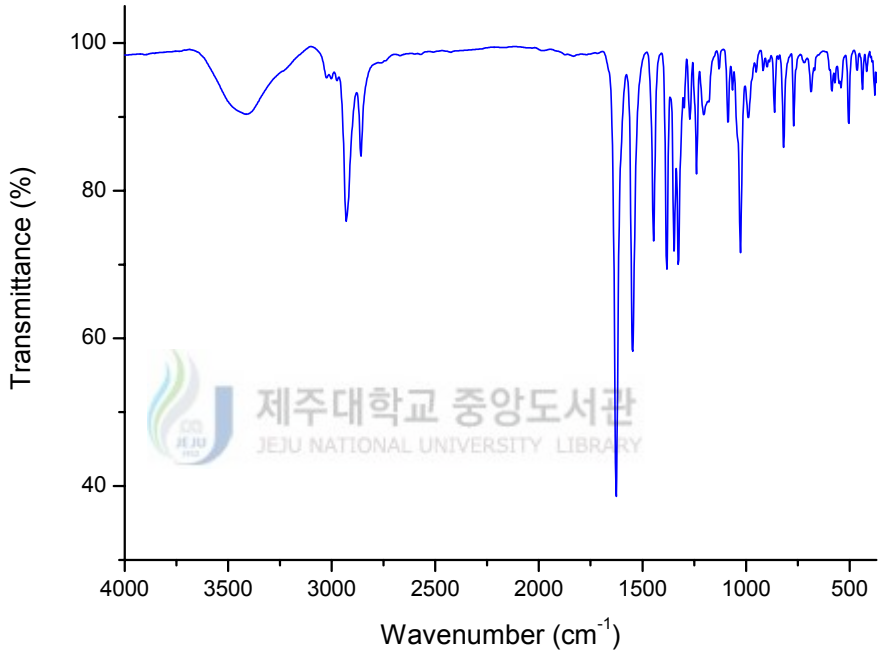

Fig. 12. FT-IR spectrum of $[Cu_2([20]\text{-}DCHDC)(\mu\text{-}O_2N)]NO_2 \cdot 6H_2O$.

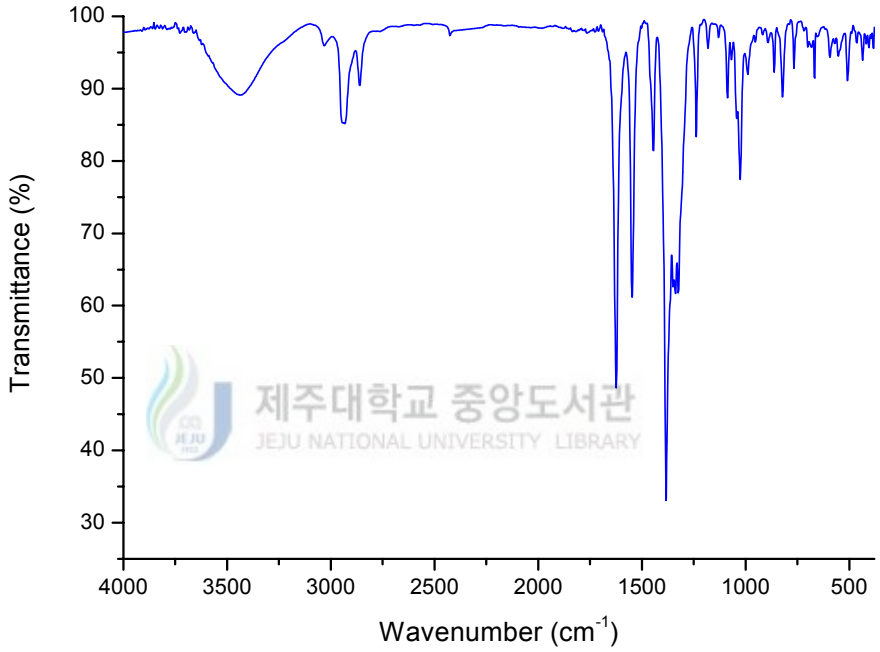

Fig. 13. FT-IR spectrum of $[Cu_2([20]\text{-}DCHDC)(\mu\text{-}O_2NO)]NO_3 \cdot 0.5H_2O$.

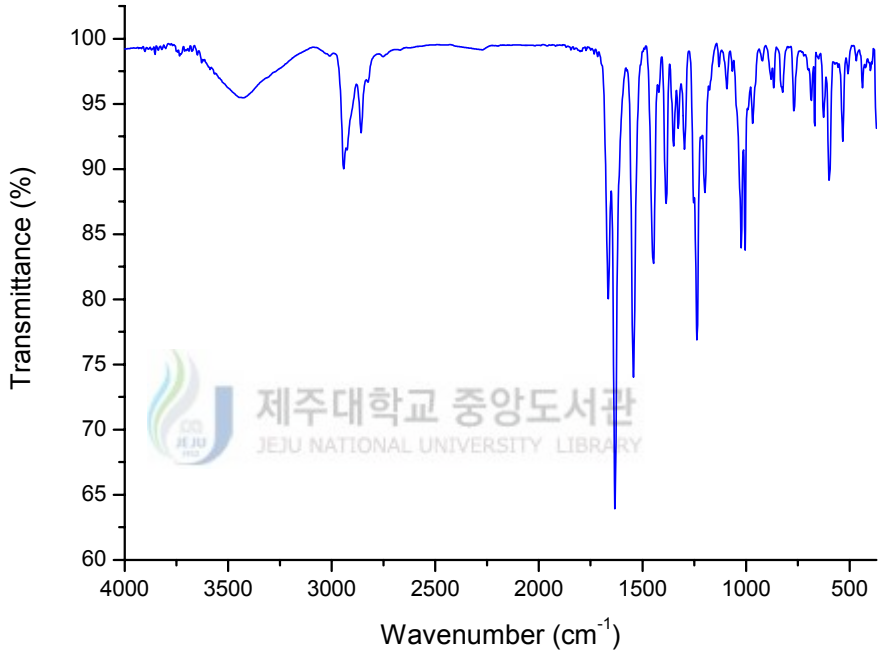

Fig. 14. FT-IR spectrum of [Cu_2([20]-DCHDC)(μ-S_2O_3)].

3. FAB-mass spectra of the complexes

The FAB mass spectra of the Cu(Ⅱ) complexes were shown in Fig. 15～23, and summarized at Table 19. The molecular ion loses the exocyclic ligands resulting in the formation of the fragment $[Cu_2([20]\text{-DCHDC})]^+$. All these species are well observed in the FAB mass spectra at m/z 608 region. α-cleavage peaks of one cyclohexane from the $[Cu_2([20]\text{-DCHDC})]^+$ ion in the formation of the fragment $[Cu_2(L_{ac})]^+$ are observed at m/z 526 region.

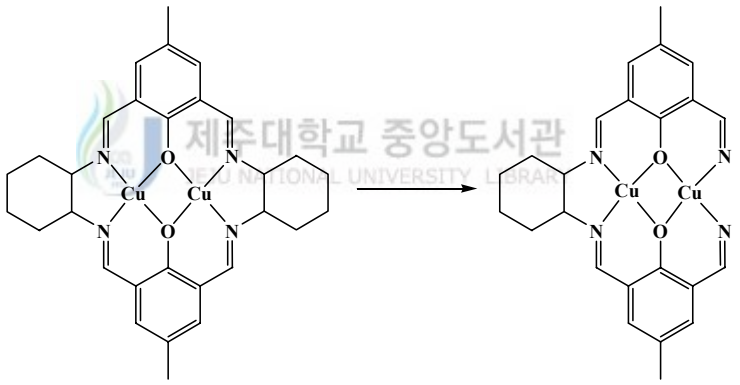

$[Cu_2([20]\text{-DCHDC})]^+$ (m/z 608) $[Cu_2(L_{ac})]^+$ (m/z 526)

Removal peaks of one copper ion from the $[Cu_2([20]\text{-DCHDC})]^+$ ion in the formation of the fragment $[Cu([20]\text{-DCHDC})]^+$ is observed at m/z 545. The FAB mass spectra of all the complexes contain peaks corresponding to the $[(H_2[20]\text{-DCHDC})]^+$ fragment ion at m/z 489 region. This indicates that the species $[Cu_2([20]\text{-DCHDC})]^+$ undergoes demetallation to give the tetraazadioxa macrocycle $H_2[20]$-DCHDC under FAB conditions. These peaks are associated

with peaks of mass one or two greater or less, which are attributed to protonated /deprotonated forms. This also accounts for the slight ambiguities in making assignments.

The week molecular ion peaks corresponding to the $[Cu_2([20]\text{-DCHDC})(\mu\text{-}O_2N)]^+$ and $[Cu_2([20]\text{-DCHDC})(\mu\text{-}O_2NO)]^+$ are observed at m/z 655.3, and 671.5, respectively. Removal peaks of one exocyclic ligand resulting in the formation of the fragment $[Cu_2(H_2[20]\text{-DCHDC})(L_a)]^+$ (L_a = Cl^-, Br^-, I^-, ClO_4^-, NCS^- and N_3^-) are observed at m/z 644.5, 688.4, 735.0, 708.2, 667.5 and 651.5, respectively.

In the mass spectrum of $[Cu_2([20]\text{-DCHDC})(\mu\text{-}S_2O_3)]$ the peak observed at m/z 703.5 is due to the molecular ion $[Cu_2([20]\text{-HMTADO})SO_4]^+$, that is, sulfate ion may coordinate to the copper atom. The rearrangement reactions and oxidation by Fe^{3+} and O_2 from thiosulfate to sulfate has been described by Drushel et al. (see Scheme 3) [130]. In the FAB-mass spectrum, this complex is not appeared to vibration bands by thiosulfate ion, but appeared to vibration bands by coordinated sulfate.

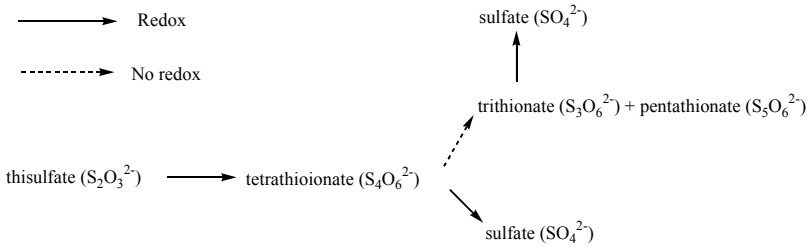

Scheme. 3. The rearrangement reactions and oxidation from thiosulfate to sulfate.

Table 19. FAB-mass spectra for the binuclear Cu(II) complexes of phenol-based macrcocyclic ligand (H_2[20]-DCHDC)

complex	m/z	Assignments	
$[Cu_2([20]\text{-DCHDC})Cl_2] \cdot H_2O$	525.3	$[Cu_2(L_{ac})]^+$	526.0
	545.5	$[Cu([20]\text{-DCHDC})]^+$	545.2
	607.5	$[Cu_2([20]\text{-DCHDC})]^+$	608.1
	644.5	$[Cu_2([20]\text{-DCHDC})(Cl)]^+$	643.1
$[Cu_2([20]\text{-DCHDC})Br_2] \cdot 0.5H_2O$	525.3	$[Cu_2(L_{ac})]^+$	526.0
	545.4	$[Cu([20]\text{-DCHDC})]^+$	545.2
	607.5	$[Cu_2([20]\text{-DCHDC})]^+$	608.1
	688.4	$[Cu_2([20]\text{-DCHDC})(Br)]^+$	687.1
$[Cu_2([20]\text{-DCHDC})I_2]$	525.3	$[Cu_2(L_{ac})]^+$	526.0
	545.4	$[Cu([20]\text{-DCHDC})]^+$	545.2
	607.5	$[Cu_2([20]\text{-DCHDC})]^+$	608.1
	735.0	$[Cu_2([20]\text{-DCHDC})\ I]^+$	735.0
$[Cu_2([20]\text{-DCHDC})(\mu\text{-}O_2ClO_2)_2] \cdot H_2O$	525.3	$[Cu_2(L_{ac})]^+$	526.0
	545.4	$[Cu([20]\text{-DCHDC})]^+$	545.2
	607.4	$[Cu_2([20]\text{-DCHDC})]^+$	608.1
	708.2	$[Cu_2([20]\text{-DCHDC})(ClO_4)]^+$	707.1
$[Cu_2([20]\text{-DCHDC})(NCS)_2] \cdot H_2O$	525.3	$[Cu_2(L_{ac})]^+$	526.0
	545.3	$[Cu([20]\text{-DCHDC})]^+$	545.1
	607.3	$[Cu_2([20]\text{-DCHDC})]^+$	608.1
	667.5	$[Cu_2([20]\text{-DCHDC})(NCS)]^+$	666.1
$[Cu_2([20]\text{-DCHDC})(N_3)_2] \cdot 6H_2O$	525.3	$[Cu_2(L_{ac})]^+$	526.0
	545.3	$[Cu([20]\text{-DCHDC})]^+$	545.1
	607.3	$[Cu_2([20]\text{-DCHDC})]^+$	608.1
	651.5	$[Cu_2([20]\text{-DCHDC})(N_3)]^+$	650.2

$[Cu_2([20]\text{-}DCHDC)(\mu\text{-}O_2N)]NO_2 \cdot 6H_2O$	525.3	$[Cu_2(L_{ac})]^+$	526.0
	545.3	$[Cu([20]\text{-}DCHDC)]^+$	545.1
	607.3	$[Cu_2([20]\text{-}DCHDC)]^+$	608.1
	655.3	$[Cu_2([20]\text{-}DCHDC)(NO_2)]^+$	654.1
$[Cu_2([20]\text{-}DCHDC)(\mu\text{-}O_2NO)]NO_3 \cdot 0.5H_2O$	525.3	$[Cu_2(L_{ac})]^+$	526.0
	545.3	$[Cu([20]\text{-}DCHDC)]^+$	545.1
	607.4	$[Cu_2([20]\text{-}DCHDC)]^+$	608.1
	671.5	$[Cu_2([20]\text{-}DCHDC)(NO_3)]^+$	670.1
$[Cu_2([20]\text{-}DCHDC)(\mu\text{-}S_2O_3)]$	525.3	$[Cu_2(L_{ac})]^+$	526.0
	545.3	$[Cu([20]\text{-}DCHDC)]^+$	545.1
	607.4	$[Cu_2([20]\text{-}DCHDC)]^+$	608.1
	703.5	$[Cu_2([20]\text{-}DCHDC)(SO_4)]^+$	704.0

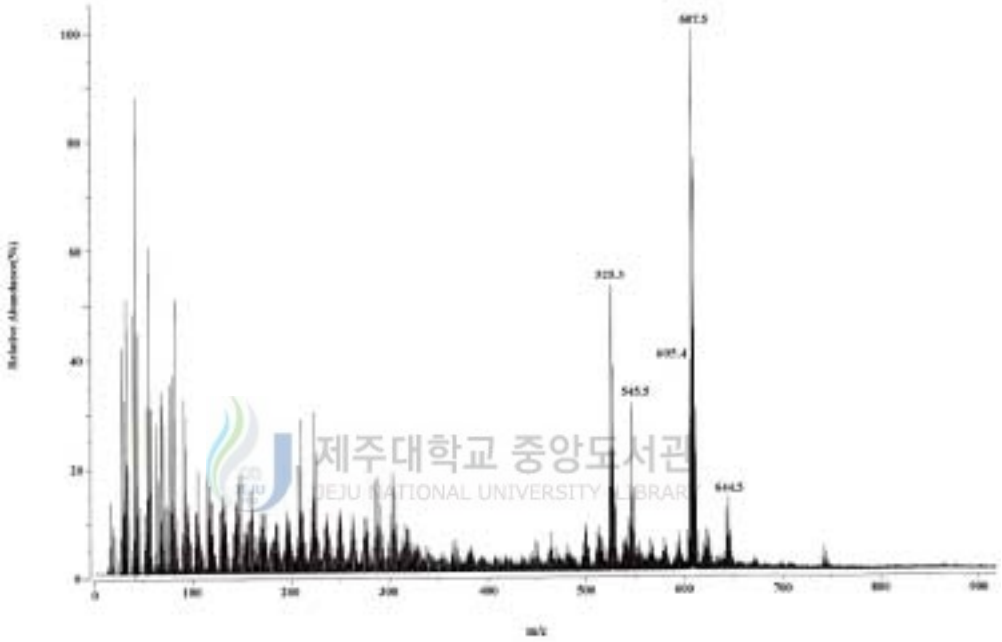

Fig. 15. FAB mass spectrum of the $[Cu_2([20]\text{-DCHDC})Cl_2] \cdot H_2O$

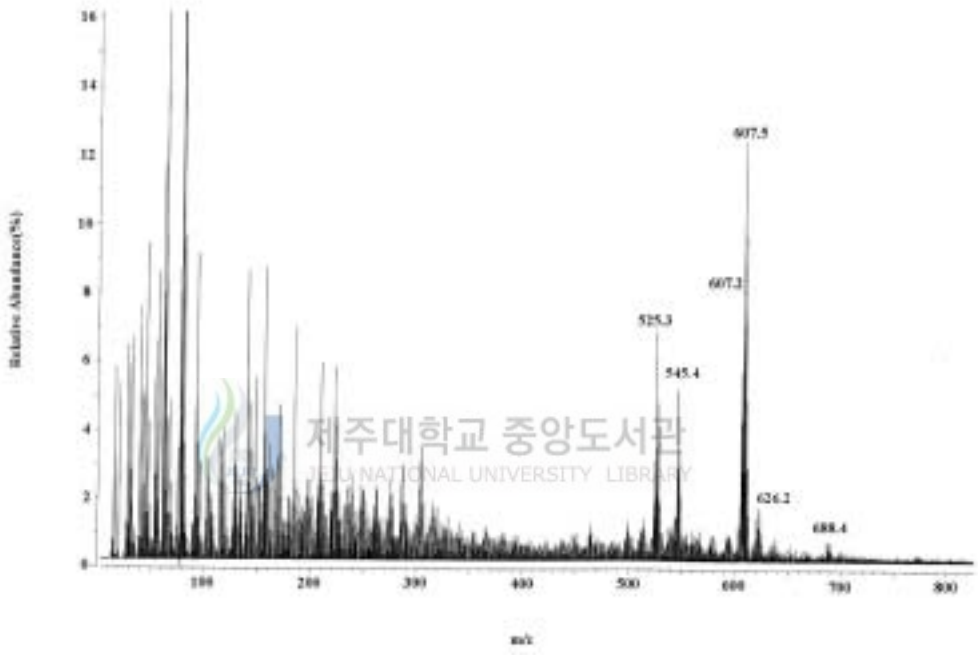

Fig. 16. FAB mass spectrum of the $[Cu_2([20]\text{-DCHDC})Br_2] \cdot 0.5H_2O$

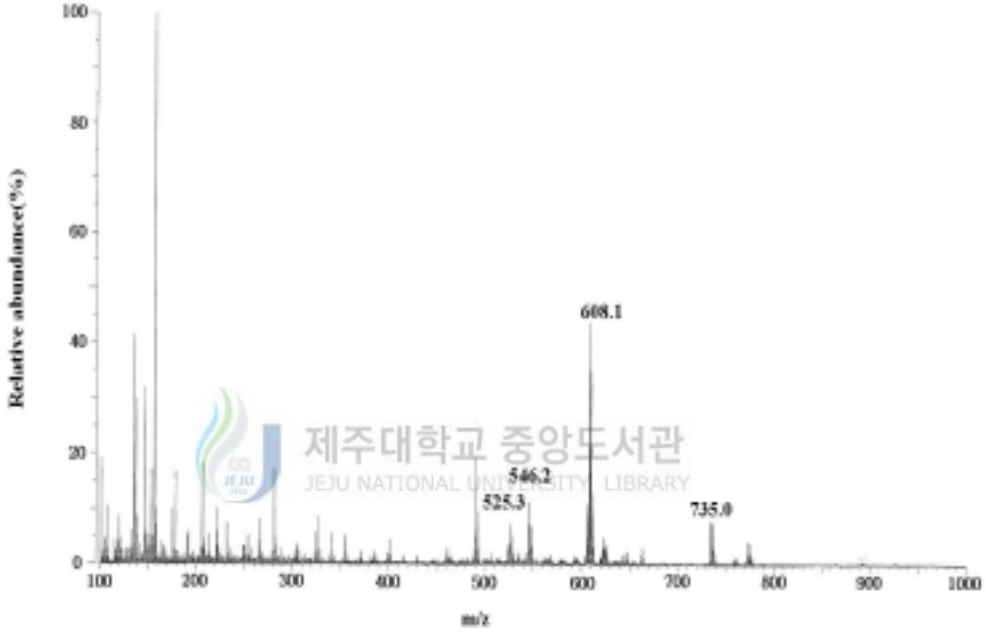

Fig. 17. FAB mass spectrum of the $[Cu_2([20]\text{-DCHDC})I_2]$

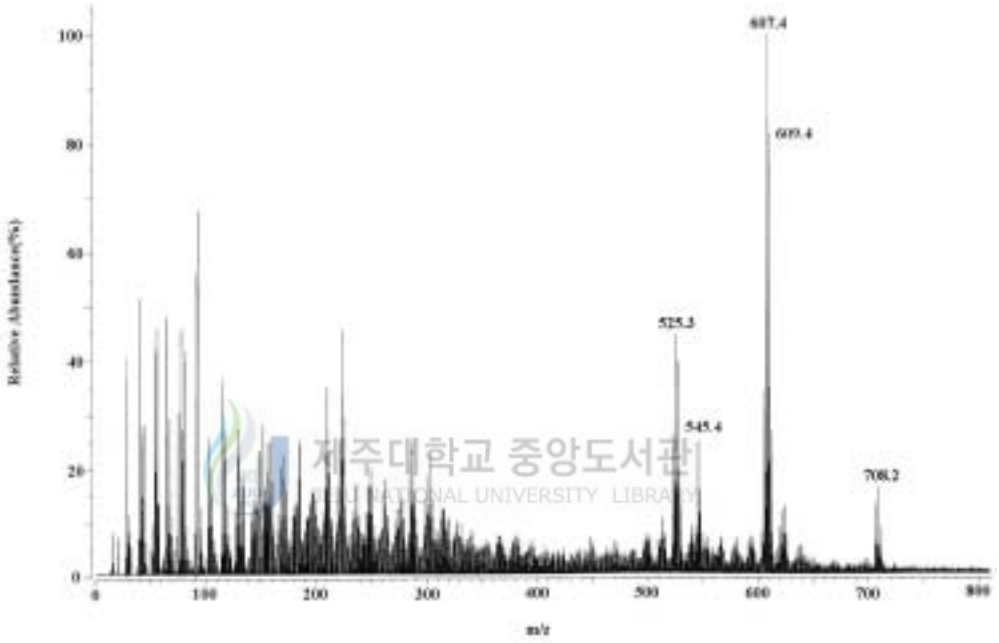

Fig. 18. FAB mass spectrum of the $[Cu_2([20]\text{-DCHDC})(\mu\text{-}O_2ClO_2)_2] \cdot H_2O$

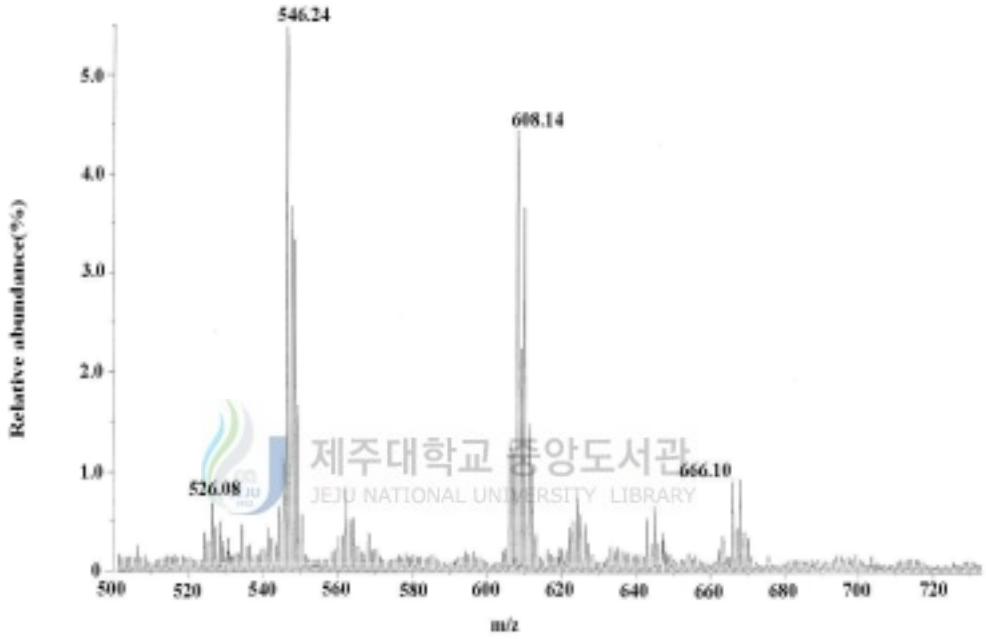

Fig. 19. FAB mass spectrum of the $[Cu_2([20]\text{-DCHDC})(NCS)_2] \cdot H_2O$

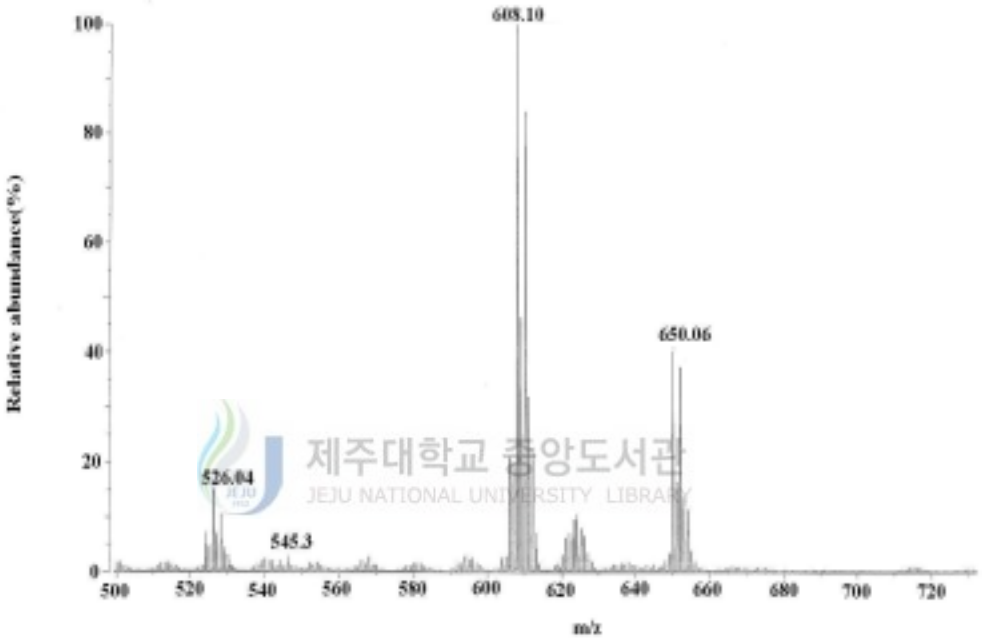

Fig. 20. FAB mass spectrum of the $[Cu_2([20]\text{-}DCHDC)(N_3)_2] \cdot H_2O$

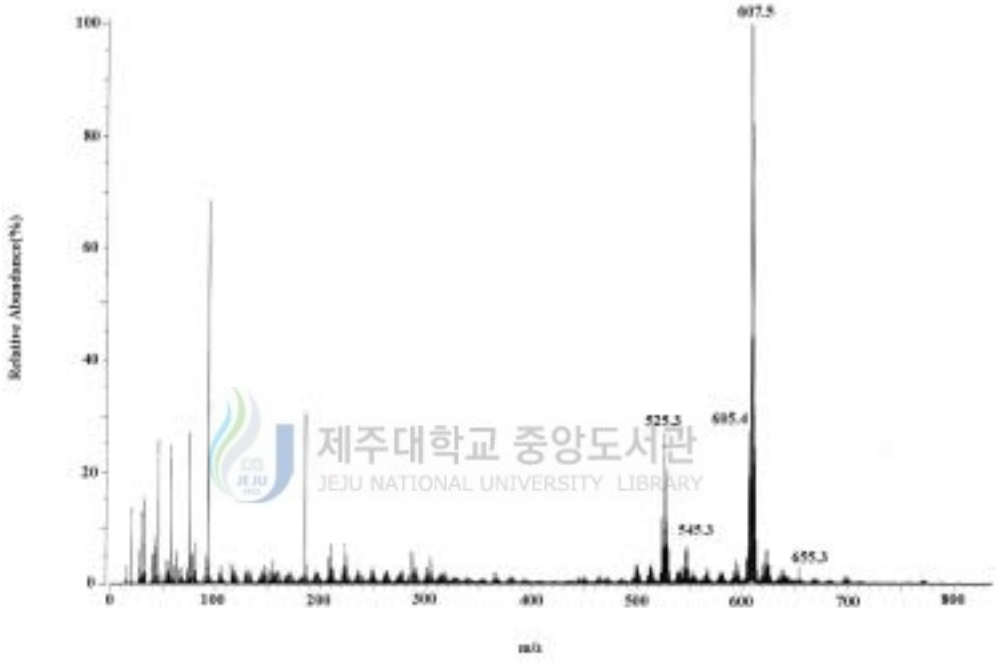

Fig. 21. FAB mass spectrum of the $[Cu_2([20]\text{-DCHDC})(\mu\text{-}O_2N)]NO_2 \cdot 6H_2O$

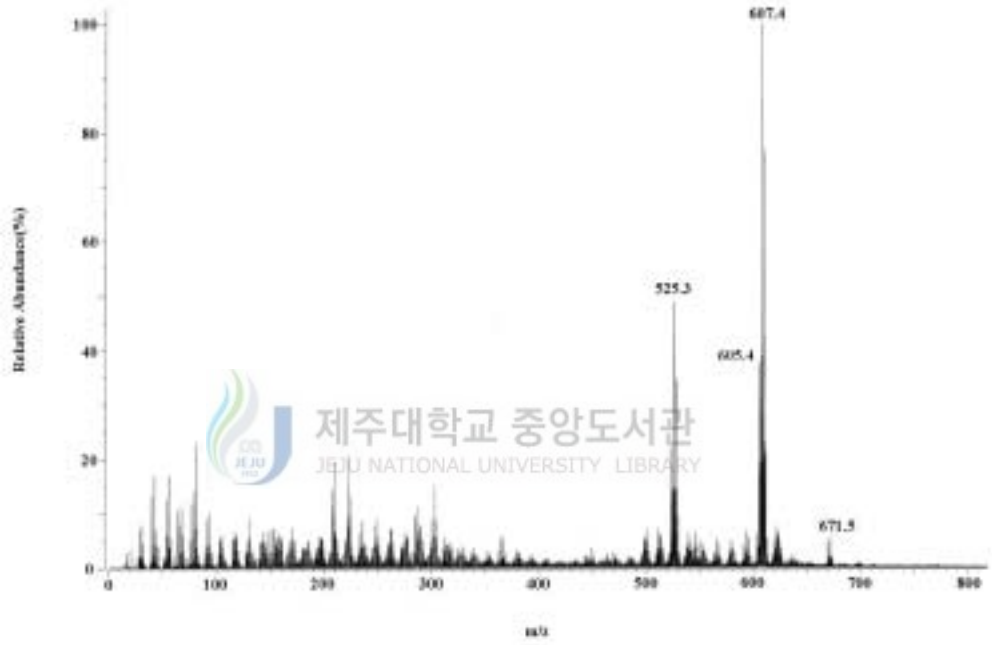

Fig. 22. FAB mass spectrum of the $[Cu_2([20]\text{-}DCHDC)(\mu\text{-}O_2NO)]NO_3 \cdot 0.5H_2O$

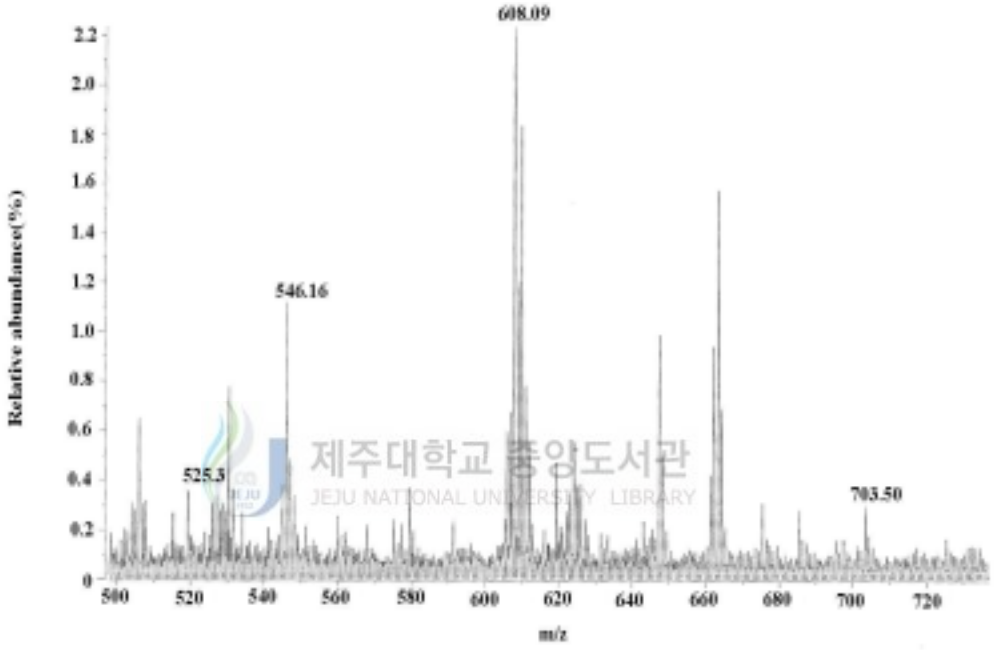

Fig. 23. FAB mass spectrum of the [Cu_2([20]-DCHDC)(μ-S_2O_3)]

4. Electronic absorption spectrum of the complexes

The electronic absorption spectra of Cu(II) complexes at room temperature were represented in Fig. 24～32 and summarized Table 20. As shown these spectra exhibited one band at 530～579 nm due to the $^2E_g \rightarrow {}^2T_{2g}$ (O_h) transitions. The symmetry of the octahedron, elongated or squashed along one axis, is D_{4h}, exactly that of the square plane. For tetragonal Cu^{2+} (d^9) complexes the octahedral doublet ^2E_g and $^2T_{2g}$ are seen to split as

$$^2E_g \rightarrow {}^2A_{1g} + {}^2B_{1g}$$
$$^2T_{2g} \rightarrow {}^2E_g + {}^2B_{2g}$$

The relative energies of the tetragonal components depend upon whether the octahedron is elongated or squashed, for ground state of elongated form is $^2B_{1g}$ [130]. Instead of the single $^2E_g \rightarrow {}^2T_{2g}$ transition which occurs for the regular octahedron, the tetragonally distorted molecule will exhibit two transitions $^2B_{1g} \rightarrow {}^2B_{2g}$ and $^2B_{1g} \rightarrow {}^2E_g$ at about the octahedral frequency. A further band at much lower energy is expected from $^2B_{1g} \rightarrow {}^2A_{1g}$ transition [131].

The one *d-d* band of title complexes observed at 17,271 ~ 18,868 cm^{-1} can be related to the spin-allowed transition, $^2E_g \rightarrow {}^2T_{2g}$. Copper complexes in tetragonal symmetry are expected to have three absorption bands in *d-d* region, but title spectra apparently have one major component. Thus, we fitted the spectrum roughly with Gaussian functions first and then added a

minor component to reproduce the more suitable shape of the spectrum in the region of interest. Finally, we performed least-squares fitting procedures, and the dotted lines in Fig. 24 ~ 32 are Gaussian bands representing the approximate deconvolution of the spectrum yielded by the calculations. The two peak positions calculated at 16,778 - 17,793 and 18,349 - 20,408 cm^{-1} can be assigned to the $^2B_{1g} \rightarrow {}^2B_{2g}$ and $^2B_{1g} \rightarrow {}^2E_g$, respectively. The $^2B_{1g} \rightarrow {}^2A_{1g}$ transition bands have expected at much lower energy. The 21,368 - 24,752 cm^{-1} bands are clearly associated with ligand to metal charge transfer transitions.

Table 20. Electronic spectral data for the Cu(II) complexes

Complexes	medium	λ_{max}, nm (ε, M^{-1} cm^{-1})	Spin-allowed transition, cm^{-1} (ε, M^{-1} cm^{-1})		
			$^2B_{1g} \rightarrow {}^2B_{2g}$	$^2B_{1g} \rightarrow {}^2E_g$	MLCT
$[Cu_2([20]\text{-DCHDC})Cl_2] \cdot H_2O$	MeOH	539 (89)	17,730 (63)	18,939 (22)	23,753 (181)
	solid	395, 452sh, 650	13,812	16,779	21,692
$[Cu_2([20]\text{-DCHDC})Br_2] \cdot 0.5H_2O$	DMSO	572 (183)	17,793 (127)		22,523 (159)
	solid	386, 651	15,221	17,606	23,641
$[Cu_2([20]\text{-DCHDC})I_2]$	DMSO	550 (119)	16,949 (84)	18,349 (41)	24,272 (241)
	solid	404, 624	14,628	16,920	22,321
$[Cu_2([20]\text{-DCHDC})(\mu\text{-}O_2ClO_2)_2] \cdot H_2O$	DMSO	546 (124)	16,778 (78)	18,553 (58)	24,752 (285)
	solid	379, 534	17,544	18,975	25,575
$[Cu_2([20]\text{-DCHDC})(NCS)_2] \cdot H_2O$	DMSO	551 (124)	17,212 (72)	18,553 (36)	22,472 (88)
	solid	387, 562	16,949	18,282	25,381
$[Cu_2([20]\text{-DCHDC})(N_3)_2] \cdot 6H_2O$	DMSO	550sh (132)	18,553 (87)	20,408 (41)	22,883 (246)
	solid	418, 586	16,949	18,281	25,381
$[Cu_2([20]\text{-DCHDC})(\mu\text{-}O_2N)]NO_2 \cdot 6H_2O$	MeOH	530 (122)	18,315 (82)	19,011 (27)	24,038 (253)
	solid	403, 662	13,369	15,528	21,598
$[Cu_2([20]\text{-DCHDC})(\mu\text{-}O_2NO)]NO_3 \cdot 0.5H_2O$	MeOH	531 (96)	18,215 (63)	19,084 (28)	23,981 (214)
	solid	397, 581	17,241	20,790	24,814
$[Cu_2([20]\text{-DCHDC})(\mu\text{-}S_2O_3)]$	DMSO	579 (251)	17,637 (173)	19,455 (40)	21,368 (210)
	solid	405, 552	16,920	18,939	23,364

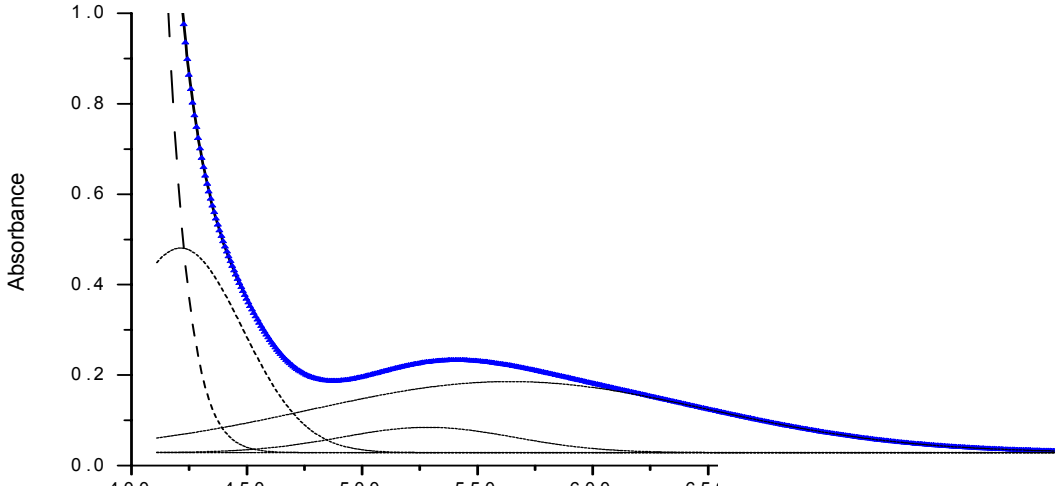

(a)

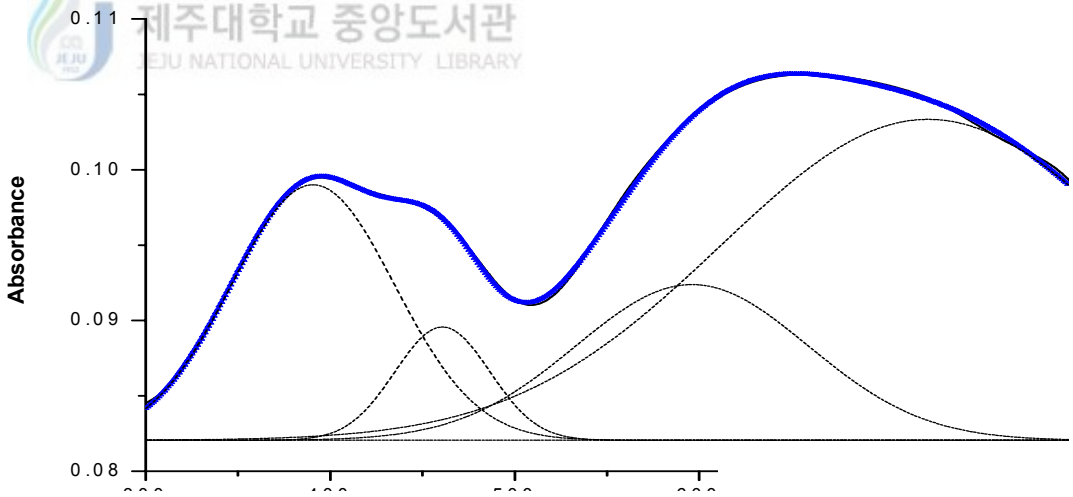

(b)

Fig. 24. Electronic absorption spectrum of $[Cu_2([20]\text{-}DCHDC)Cl_2] \cdot H_2O$ in (a) methanol (2.5×10^{-3}M) and (b) solid ($BaSO_4$).

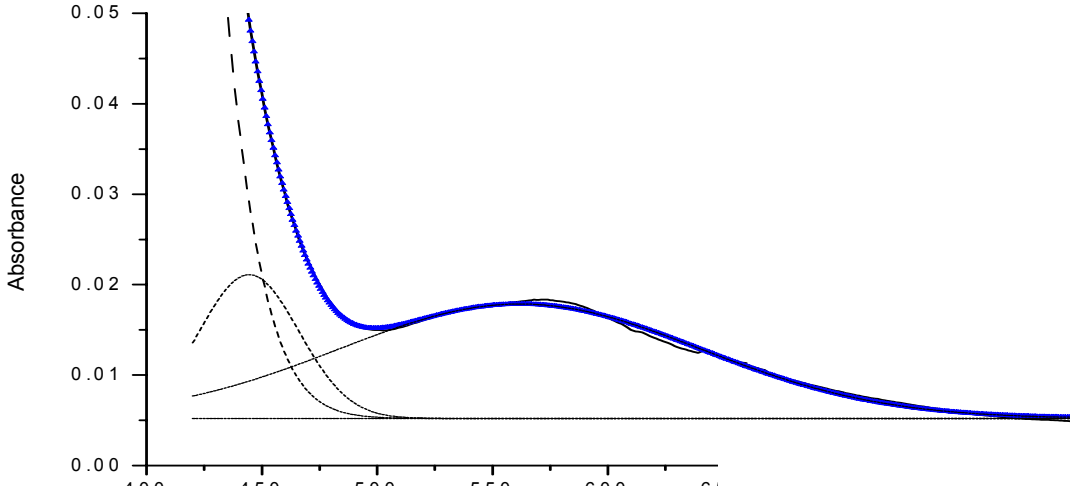

(a)

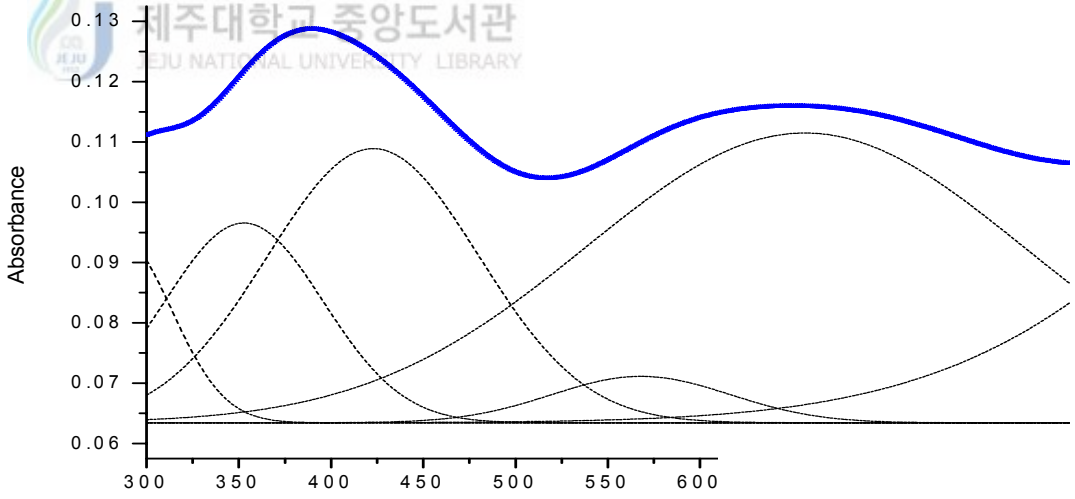

(b)

Fig. 25. Electronic absorption spectrum of $[Cu_2([20]\text{-DCHDC})Br_2] \cdot 0.5H_2O$ in (a) DMSO (1.0×10^{-4}M) and (b) solid ($BaSO_4$).

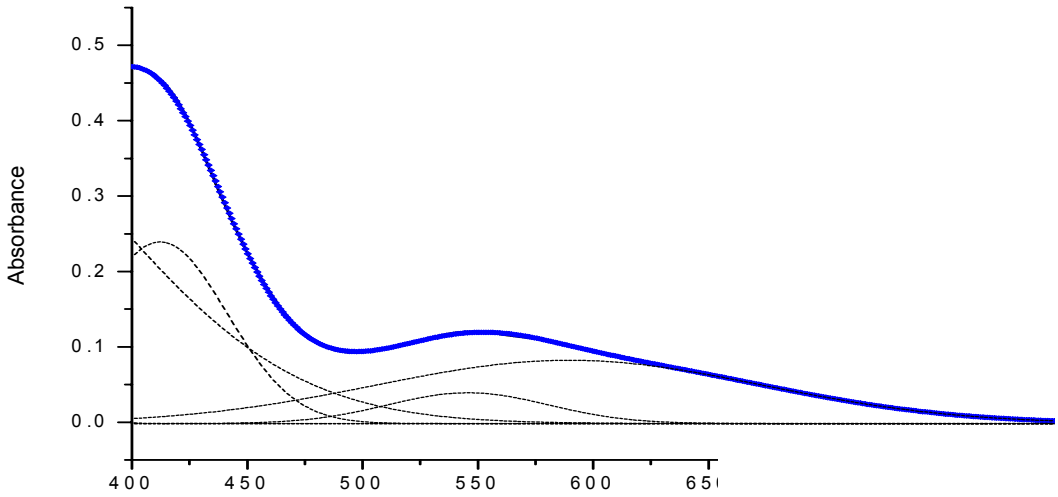

(a)

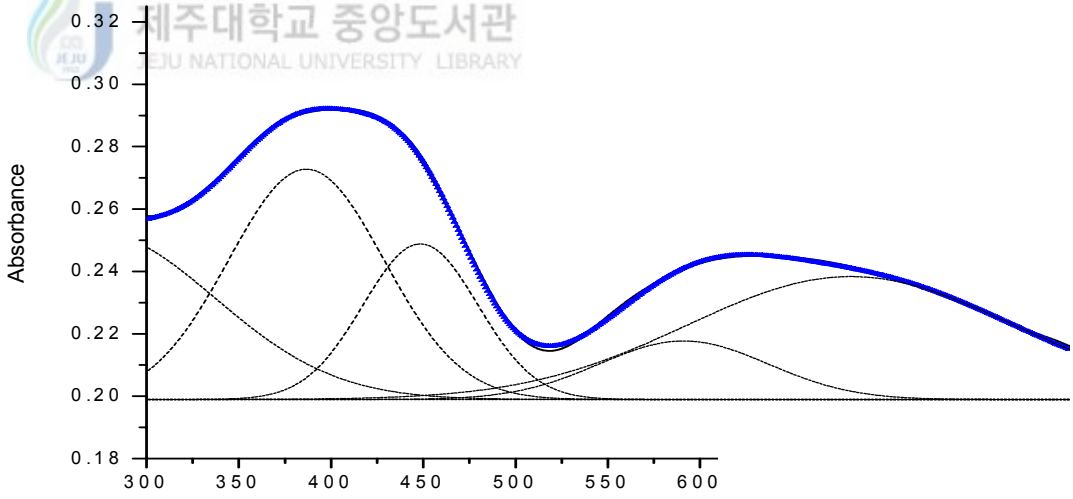

(b)

Fig. 26. Electronic absorption spectrum of $[Cu_2([20]\text{-DCHDC})I_2]$ in (a) DMSO (1.0×10^{-3}M) and (b) solid ($BaSO_4$).

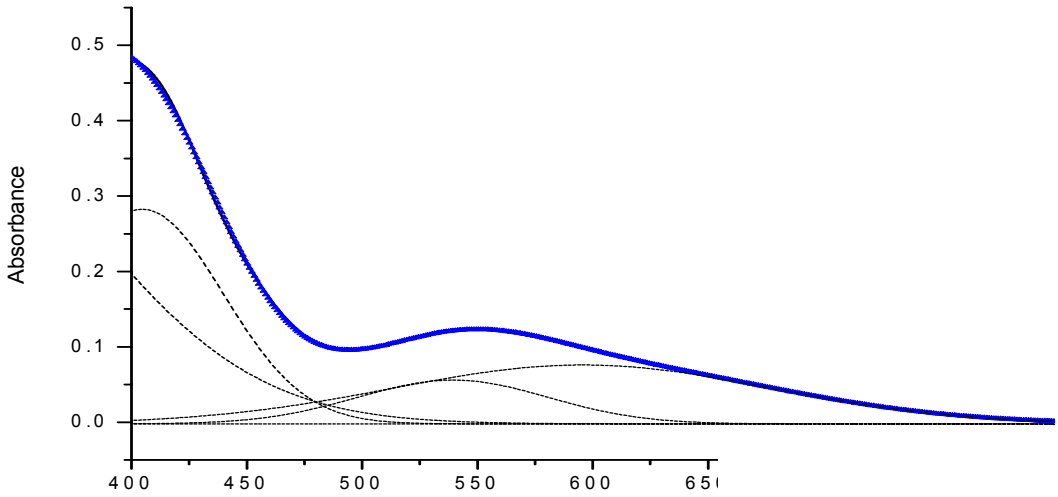

(a)

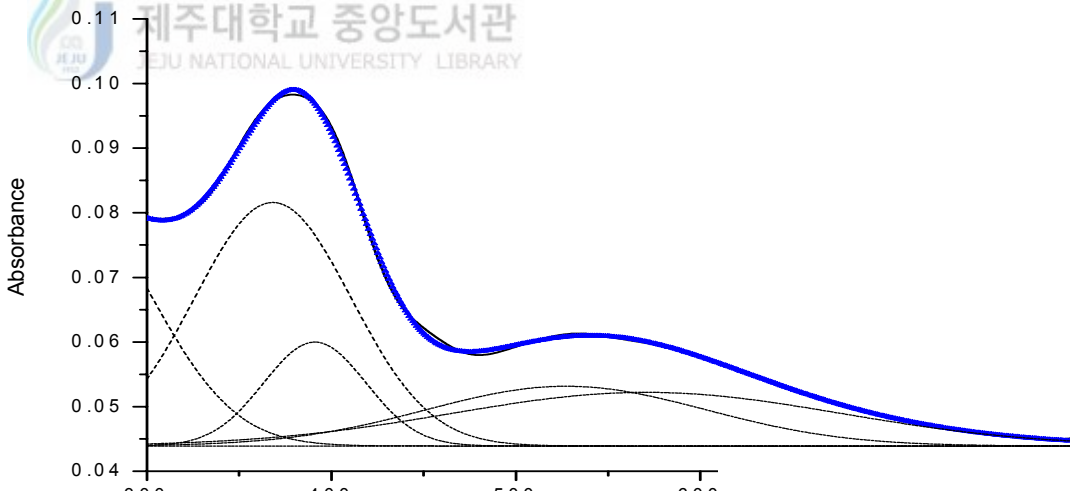

(b)

Fig. 27. Electronic absorption spectrum of $[Cu_2([20]\text{-DCHDC})(\mu\text{-}O_2ClO_2)_2] \cdot H_2O$ in (a) DMSO (1.0×10^{-3}M) and (b) solid ($BaSO_4$).

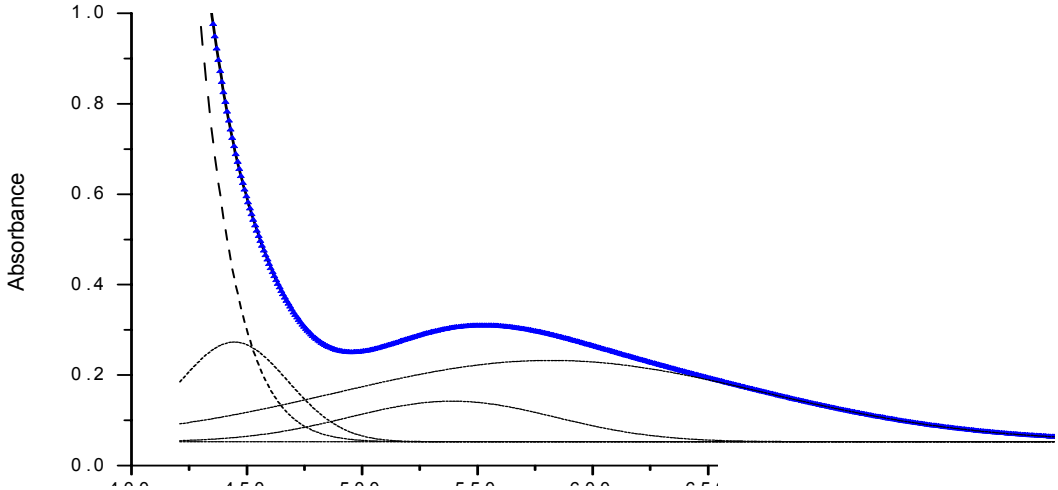

(a)

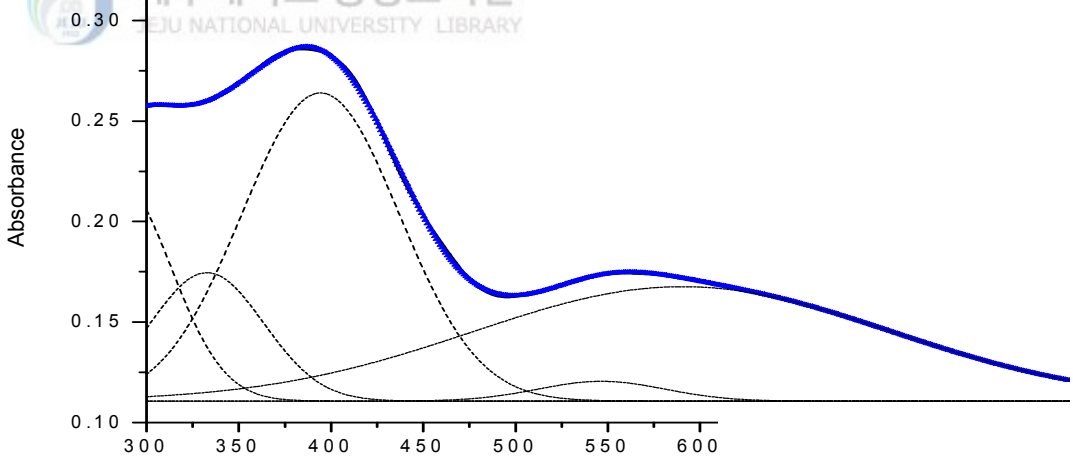

(b)

Fig. 28. Electronic absorption spectrum of $[Cu_2([20]\text{-DCHDC})(NCS)_2] \cdot H_2O$ in (a) DMSO (2.5×10^{-3}M) and (b) solid ($BaSO_4$).

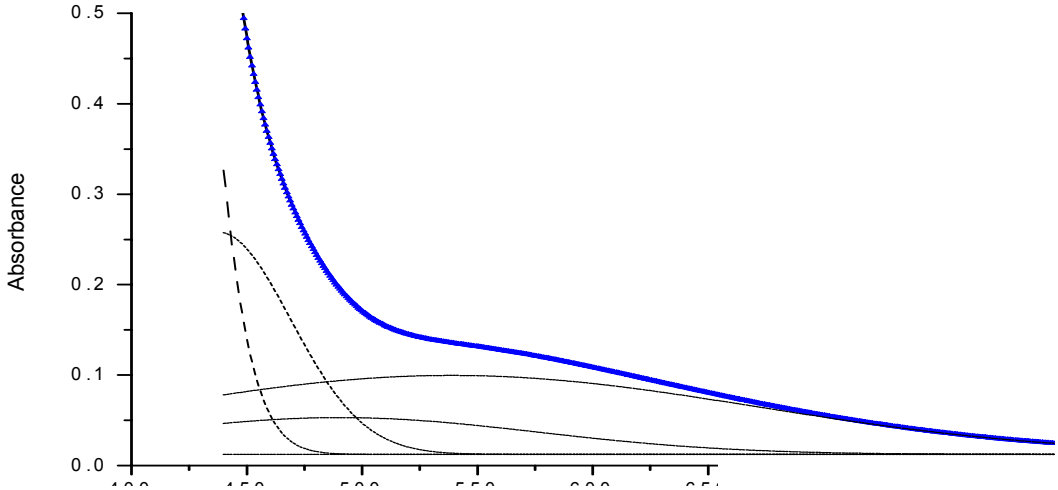

(a)

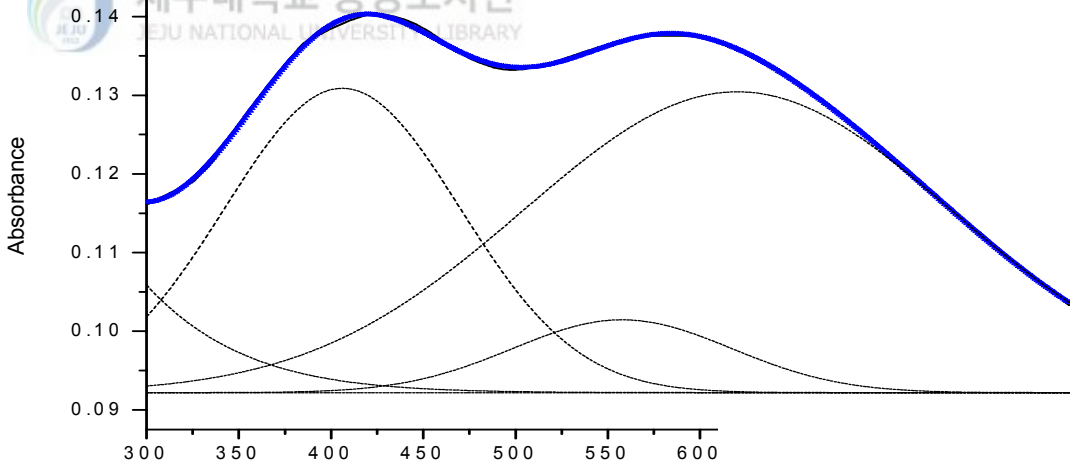

(b)

Fig. 29. Electronic absorption spectrum of $[Cu_2([20]\text{-DCHDC})(N_3)_2] \cdot 6H_2O$ in (a) DMSO (1.0×10^{-3}M) and (b) solid ($BaSO_4$).

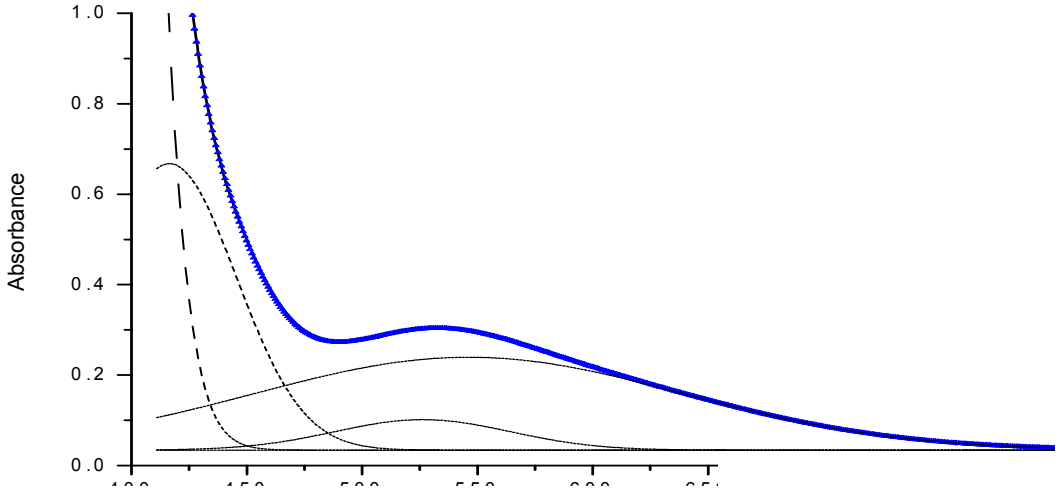

(a)

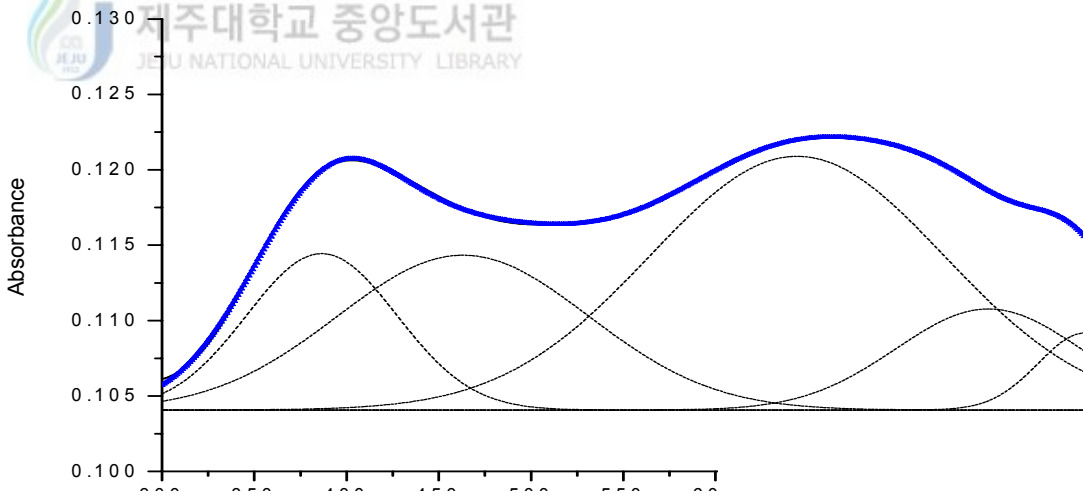

(b)

Fig. 30. Electronic absorption spectrum of $[Cu_2([20]\text{-}DCHDC)(\mu\text{-}O_2N)]NO_2 \cdot 6H_2O$ in (a) methanol (2.5×10^{-3}M) and (b) solid ($BaSO_4$).

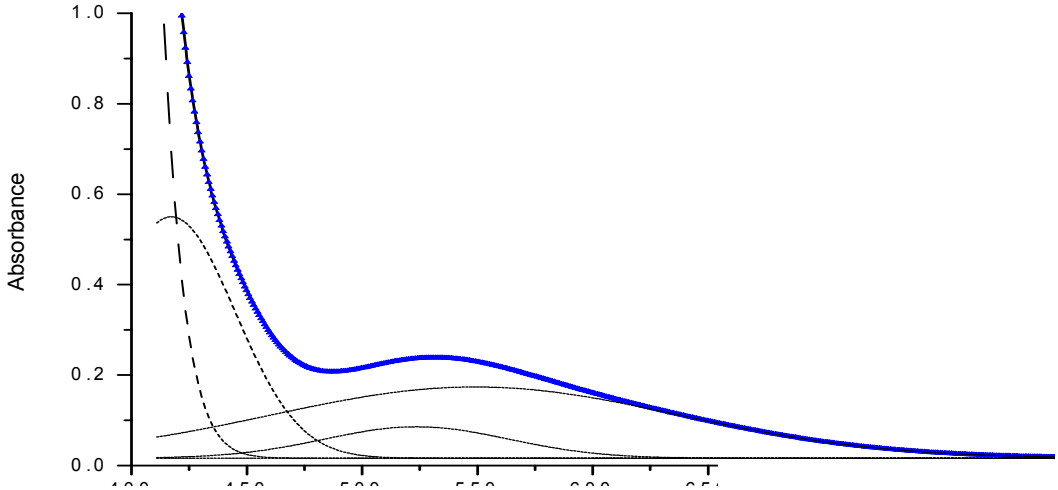

(a)

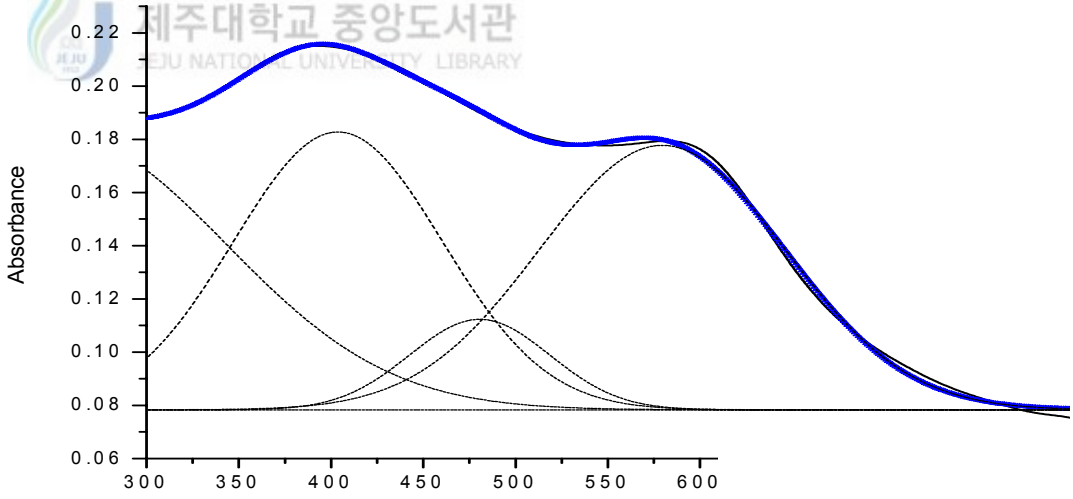

(b)

Fig. 31. Electronic absorption spectrum of $[Cu_2([20]\text{-}DCHDC)(\mu\text{-}O_2NO)]NO_3 \cdot 0.5H_2O$ in (a) methanol (2.5×10^{-3}M) and (b) solid ($BaSO_4$).

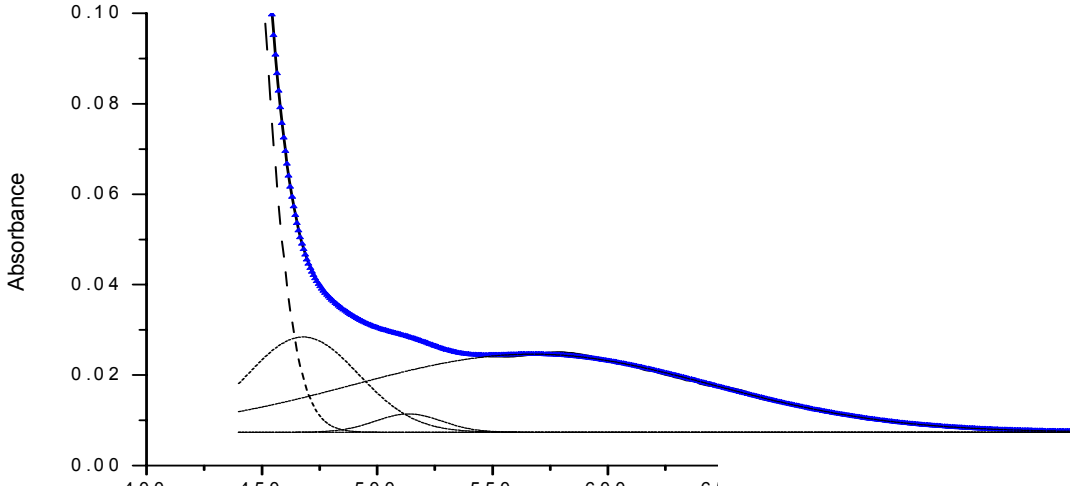

(a)

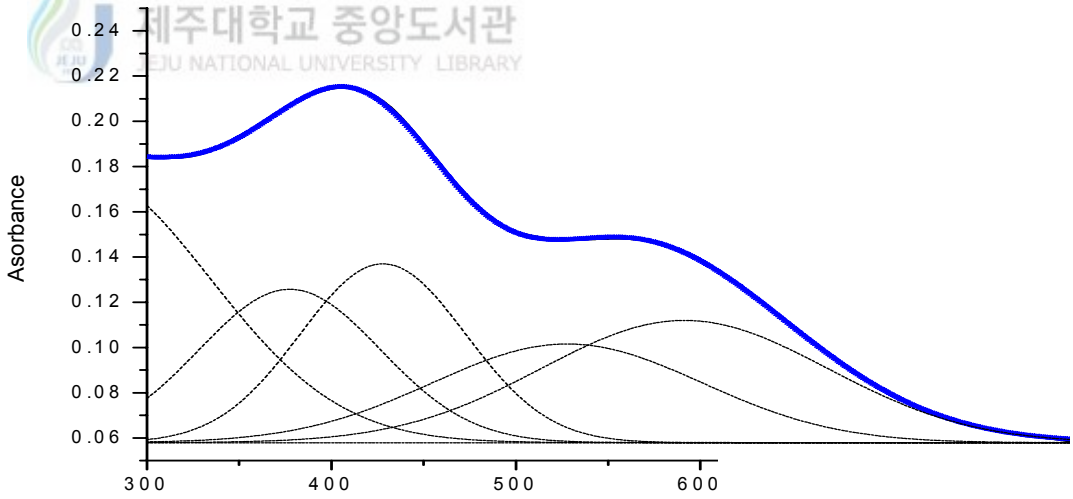

(b)

Fig. 32. Electronic absorption spectrum of $[Cu_2([20]\text{-}DCHDC)(\mu\text{-}S_2O_3)]$ in (a) DMSO (1.0×10^{-4}M) and (b) solid ($BaSO_4$).

5. Crystal Structures of the complexes.

1) $[Cu_2([20]\text{-DCHDC})Cl_2] \cdot 6H_2O$

Crystals of $[Cu_2([20]\text{-DCHDC})Cl_2] \cdot 6H_2O$ suitable for X-ray diffratration study were obtained by slow evaporation of water : methanol (1 : 1) solutions of the $[Cu_2([20]\text{-DCHDC})Cl_2] \cdot H_2O$ complex. Four formula units comprise the unit cell with quater of the binuclear complex in the asymmetric unit. An ORTEP drawing of asymmetric unit and core structure (top view) for the complex are given in Fig. 33 and 34, respectively.

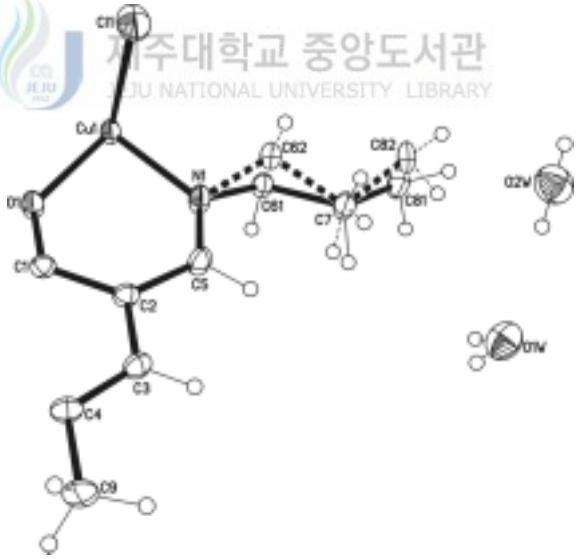

Fig. 33. Structural representation of asymmetric unit of $[Cu_2([20]\text{-DCHDC})Cl_2] \cdot 6H_2O$.

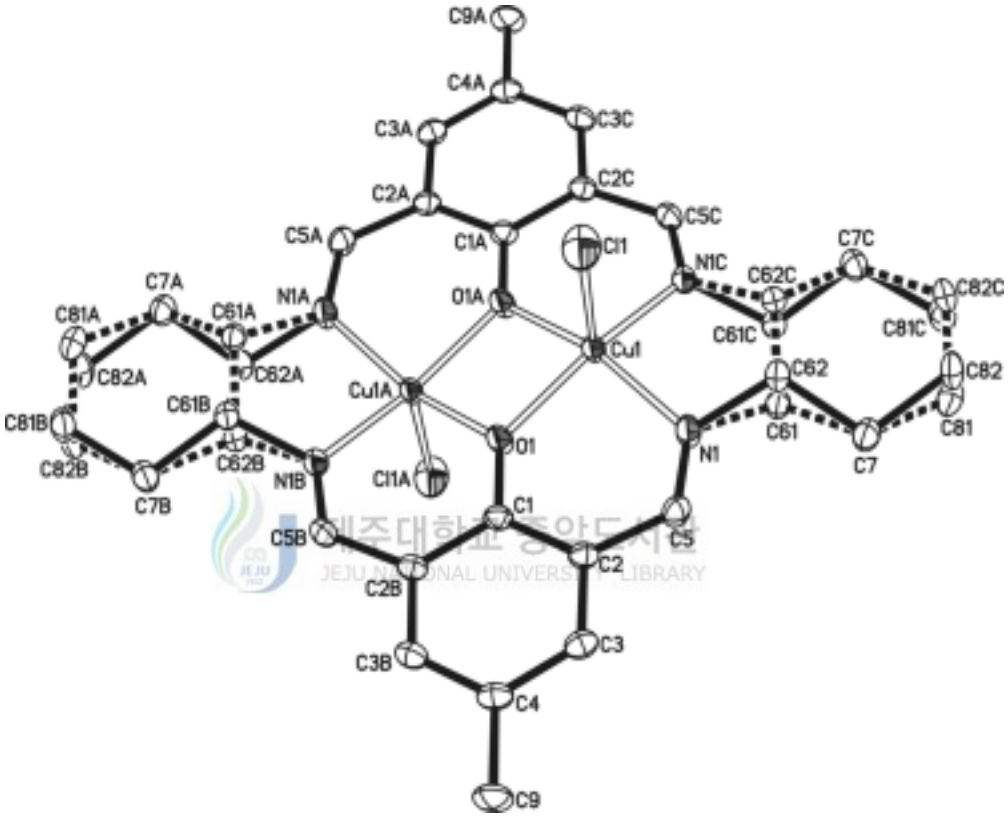

Fig. 34. An ORTEP view of core structure (top view) for the $[Cu_2([20]\text{-DCHDC})Cl_2] \cdot 6H_2O$ showing 30% probability thermal ellipsoids and labels for non-H atoms. Dotted lines represent the disordered parts, hydrogen atoms are omitted for clarity.

The relevant bond distances and angles are given in Table 21 and 22. The binuclear core structures are centrosymmetric with each copper(II) ion in the $N(imine)_2O_2$ sites being five-coordinate by square-pyramidal geometry of interactions with two nitrogen and two oxygen atoms of the binucleating ligand [20]-DCHDC and one chloride ligand at an apical site. The copper ions are 0.3625 Å displaced from the basal least-squares plane toward Cl^- ions. Two Cl^- ions attached to two central metal Cu are situated trans to each other with respect to the mean molecular plane ([A]).

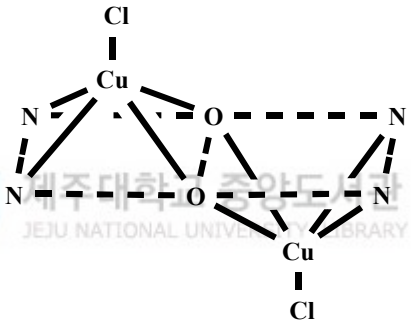

[A]

The interatomic Cu···Cu separation is 2.9707(7) Å. The in-plane Cu-to-donor distances range from 1.9136(17) Å to 1.9189(13) Å. The axial Cu-Cl bond distance (2.5215(9) A) is elongated owing to the Jahn-Teller effect of the d^9 electronic configuration.

The macrocyclic complex adopts a non-flat structure with two square-pyramidal copper centers bridged by the two phenoxide oxygen atoms, with quite large Cu-O-Cu angles (101.44(9)°) **([A])**.

In general, hydrogen bonding plays a principal role in the packing of the title compound. There are two types of H-bonds ; chloride ion - lattice water, and between lattice waters (Fig. 35 and Table 23).

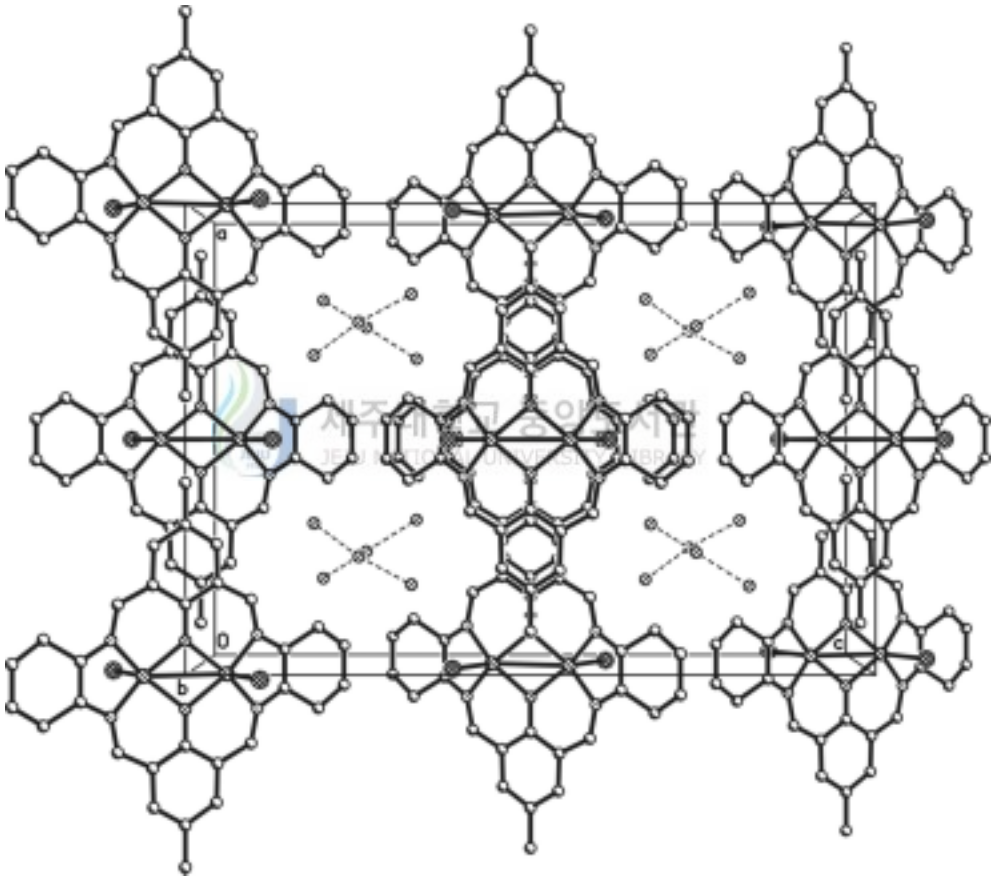

Fig. 35. The molecular packing diagram of $[Cu_2([20]\text{-}DCHDC)Cl_2] \cdot 6H_2O$. The hydrogen bonds between lattice waters are indicated by dotted lines.

Table 21. Bond lengths (Å) for $[Cu_2([20]\text{-}DCHDC)Cl_2] \cdot 6H_2O$

Cu(1)-N(1)	1.9136(17)	C(2)-C(3)	1.401(3)
Cu(1)-N(1)#1	1.9136(17)	C(2)-C(5)	1.466(3)
Cu(1)-O(1)#2	1.9189(13)	C(3)-C(4)	1.390(3)
Cu(1)-O(1)	1.9189(13)	C(4)-C(3)#3	1.390(3)
Cu(1)-Cl(1)	2.5215(9)	C(4)-C(9)	1.505(4)
Cu(1)-Cu(1)#2	2.9707(7)	C(61)-C(61)#1	1.413(9)
O(1)-C(1)	1.316(3)	C(61)-C(7)	1.498(5)
O(1)-Cu(1)#2	1.9189(13)	C(81)-C(81)#1	1.469(13)
N(1)-C(5)	1.286(3)	C(81)-C(7)	1.497(6)
N(1)-C(61)	1.499(5)	C(62)-C(62)#1	1.332(9)
N(1)-C(62)	1.514(5)	C(62)-C(7)	1.524(5)
C(1)-C(2)	1.425(2)	C(82)-C(82)#1	1.312(13)
C(1)-C(2)#3	1.425(2)	C(82)-C(7)	1.545(6)

Symmetry transformations used to generate equivalent atoms:
#1; -x+1, y, z #2; -x+1, -y, -z+1 #3; x, -y, -z+1

Table 22. Angles [°] for $[Cu_2([20]\text{-}DCHDC)Cl_2] \cdot 6H_2O$

N(1)-Cu(1)-N(1)#1	88.87(10)	O(1)-C(1)-C(2)#3	120.09(13)
N(1)-Cu(1)-O(1)#2	158.20(6)	C(2)-C(1)-C(2)#3	119.8(3)
N(1)#1-Cu(1)-O(1)#2	92.41(7)	C(3)-C(2)-C(1)	118.47(19)
N(1)-Cu(1)-O(1)	92.41(7)	C(3)-C(2)-C(5)	117.51(18)
N(1)#1-Cu(1)-O(1)	158.20(6)	C(1)-C(2)-C(5)	123.94(19)
O(1)#2-Cu(1)-O(1)	78.56(9)	C(4)-C(3)-C(2)	122.5(2)
N(1)-Cu(1)-Cl(1)	97.12(6)	C(3)#3-C(4)-C(3)	118.3(3)
N(1)#1-Cu(1)-Cl(1)	97.12(6)	C(3)#3-C(4)-C(9)	120.87(13)
O(1)#2-Cu(1)-Cl(1)	104.30(2)	C(3)-C(4)-C(9)	120.87(13)
O(1)-Cu(1)-Cl(1)	104.30(2)	N(1)-C(5)-C(2)	125.19(18)
N(1)-Cu(1)-Cu(1)#2	128.82(5)	C(61)#1-C(61)-C(7)	121.69(19)
N(1)#1-Cu(1)-Cu(1)#2	128.82(5)	C(61)#1-C(61)-N(1)	114.98(18)
O(1)#2-Cu(1)-Cu(1)#2	39.28(5)	C(7)-C(61)-N(1)	116.1(3)
O(1)-Cu(1)-Cu(1)#2	39.28(5)	C(81)#1-C(81)-C(7)	120.5(2)
Cl(1)-Cu(1)-Cu(1)#2	108.60(3)	C(62)#1-C(62)-N(1)	116.43(18)
C(1)-O(1)-Cu(1)#2	129.28(5)	C(62)#1-C(62)-C(7)	122.89(18)
C(1)-O(1)-Cu(1)	129.28(5)	N(1)-C(62)-C(7)	113.7(3)
Cu(1)#2-O(1)-Cu(1)	101.44(9)	C(82)#1-C(82)-C(7)	122.8(2)
C(5)-N(1)-C(61)	122.4(2)	C(81)-C(7)-C(61)	112.1(3)
C(5)-N(1)-C(62)	126.5(2)	C(81)-C(7)-C(62)	116.6(3)
C(61)-N(1)-C(62)	27.10(19)	C(61)-C(7)-C(62)	27.01(19)
C(5)-N(1)-Cu(1)	125.87(14)	C(81)-C(7)-C(82)	23.3(2)
C(61)-N(1)-Cu(1)	110.39(19)	C(61)-C(7)-C(82)	115.5(3)
C(62)-N(1)-Cu(1)	105.7(2)	C(62)-C(7)-C(82)	108.3(3)
O(1)-C(1)-C(2)	120.09(13)		

Symmetry transformations used to generate equivalent atoms:

#1 -x+1,y,z #2 -x+1,-y,-z+1 #3 x,-y,-z+1

Table 23. Selected bond lengths (Å) and angles(°) for hydrogen bond of $[Cu_2([20]\text{-}DCHDC)Cl_2] \cdot 6H_2O$

D-H···A	d(D-H)	d(H···A)	<DHA	d(D···A)
lattice water - chloride ion				
O2W-H2WA···Cl1 [x, y+1/2, -z+3/2]	0.841	2.600	171.15	3.433
between lattice waters				
O2W-H2WB···O1W	0.836	2.119	163.98	2.932
O1W-H1WA···O2W [x, y+1/2, -z+3/2]	0.861	2.072	156.03	2.880
O1W-H1WB···O2W [-x+3/2, y, -z+3/2]	0.856	2.115	159.47	2.932

2) $[Cu_2([20]\text{-DCHDC})Br_2] \cdot 6H_2O$

Suitable crystals of $[Cu_2([20]\text{-DCHDC})(Br)_2] \cdot 6H_2O$ were obtained by slow evaporation of methanol solutions of $[Cu_2([20]\text{-DCHDC})(Br)_2] \cdot 0.5H_2O$ complex at atmospheric pressure. Four formula units comprise the unit cell with quater of the binuclear complex in the asymmetric unit. An ORTEP drawing of asymmetric unit and core structure (top view) for the complex are given in Fig. 36 and 37, respectively.

Fig. 36. Structural representation of asymmetric unit of $[Cu_2([20]\text{-DCHDC})Br_2] \cdot 6H_2O$. open lines represent the disorder parts.

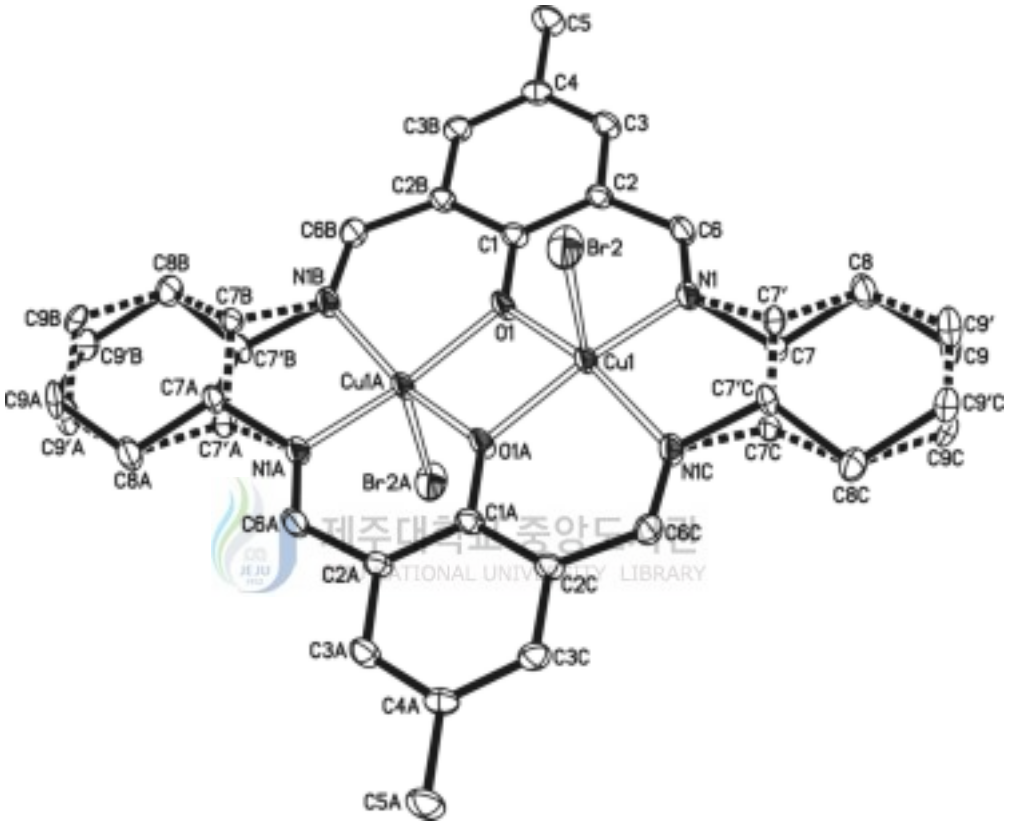

Fig. 37. An ORTEP view of core structure (top view) for the $[Cu_2([20]\text{-DCHDC})Br_2] \cdot 6H_2O$ showing 30% probability thermal ellipsoids and labels for non-H atoms.

The relevant bond distances and angles are given in Table 24 and 25. The binuclear core structures are centrosymmetric with each copper(II) ion in the $N(imine)_2O_2$ sites being five-coordinate by square-pyramidal geometry of interactions with two nitrogen and two oxygen atoms of the binucleating ligand [20]-DCHDC and one bromide ligand at an apical site. The copper ions are 0.3284 Å displaced from the basal least-squares plane toward Br^- ions. Two Br^- ions attached to two central metal Cu are situated trans to each other with respect to the mean molecular plane ([B]).

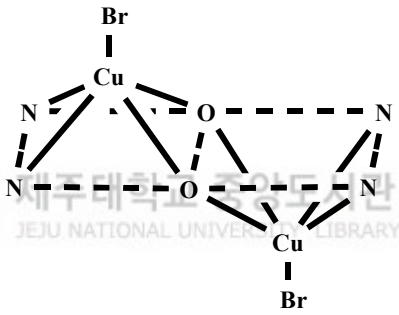

[B]

The interatomic Cu···Cu separation is 2.9549(8) Å. The in-plane Cu-to-donor distances range from 1.9138(14) Å to 1.904(2) Å. The axial Cu-Br bond distance (2.6821(6) Å) is elongated owing to the Jahn-Teller effect of the d^9 electronic configuration.

The macrocyclic complex adopts a non-flat structure with two square-pyramidal copper centers bridged by the two phenoxide oxygen atoms, with quite large Cu-O-Cu angles (101.07(10)°) **([B])**.

In general, hydrogen bonding plays a principal role in the packing of the title compound. There are two types of H-bonds ; bromide ion - lattice water, and between lattice waters (Fig. 38 and Table 26).

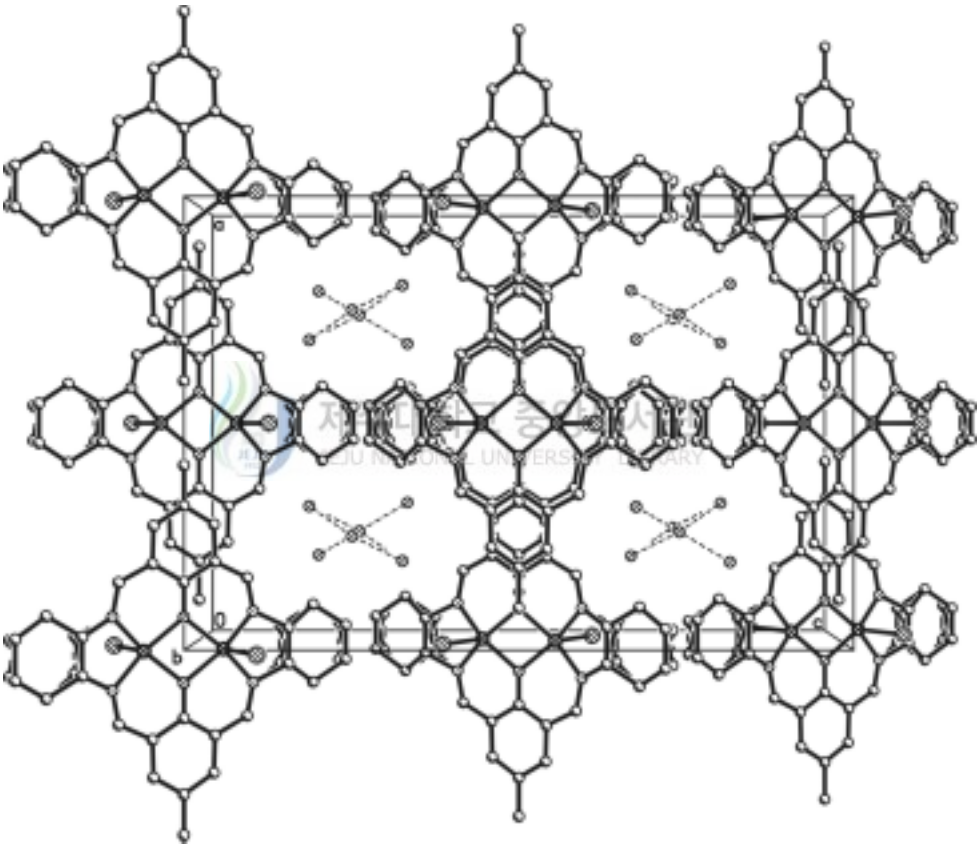

Fig. 38. The molecular packing diagram of $[Cu_2([20]\text{-DCHDC})Br_2] \cdot 6H_2O$. The hydrogen bonds between lattice waters are indicated by dotted lines.

Table 24. Bond lengths (Å) for $[Cu_2([20]\text{-}DCHDC)Br_2] \cdot 6H_2O$

Cu(1)-N(1)#1	1.904(2)	C(2)-C(3)	1.400(3)
Cu(1)-N(1)	1.904(2)	C(2)-C(6)	1.467(3)
Cu(1)-O(1)	1.9138(14)	C(3)-C(4)	1.388(3)
Cu(1)-O(1)#2	1.9138(14)	C(4)-C(3)#3	1.388(3)
Cu(1)-Br(2)	2.6821(6)	C(4)-C(5)	1.505(4)
Cu(1)-Cu(1)#2	2.9549(8)	C(7)-C(7)#1	1.413(10)
O(1)-C(1)	1.311(4)	C(7)-C(8)	1.498(5)
O(1)-Cu(1)#2	1.9138(14)	C(7')-C(7')#1	1.366(11)
N(1)-C(6)	1.283(3)	C(7')-C(8)	1.501(6)
N(1)-C(7)	1.497(6)	C(8)-C(9)	1.487(9)
N(1)-C(7')	1.512(5)	C(8)-C(9')	1.530(9)
C(1)-C(2)	1.424(3)	C(9)-C(9)#1	1.479(17)
C(1)-C(2)#3	1.424(3)	C(9')-C(9')#1	1.317(18)

Symmetry transformations used to generate equivalent atoms:

#1 -x+1,y,z #2 -x+1,-y,-z+1 #3 x,-y,-z+1

Table 25. Angles [°] for $[Cu_2([20]\text{-}DCHDC)Br_2] \cdot 6H_2O$

N(1)#1-Cu(1)-N(1)	89.30(12)	O(1)-C(1)-C(2)#3	120.21(14)
N(1)#1-Cu(1)-O(1)	160.64(7)	C(2)-C(1)-C(2)#3	119.6(3)
N(1)-Cu(1)-O(1)	92.87(8)	C(3)-C(2)-C(1)	118.6(2)
N(1)#1-Cu(1)-O(1)#2	92.87(8)	C(3)-C(2)-C(6)	117.7(2)
N(1)-Cu(1)-O(1)#2	160.64(7)	C(1)-C(2)-C(6)	123.8(2)
O(1)-Cu(1)-O(1)#2	78.93(10)	C(4)-C(3)-C(2)	122.6(2)
N(1)#1-Cu(1)-Br(2)	96.28(7)	C(3)-C(4)-C(3)#3	118.1(3)
N(1)-Cu(1)-Br(2)	96.28(7)	C(3)-C(4)-C(5)	120.96(15)
O(1)-Cu(1)-Br(2)	102.59(2)	C(3)#3-C(4)-C(5)	120.96(15)
O(1)#2-Cu(1)-Br(2)	102.59(2)	N(1)-C(6)-C(2)	125.5(2)
N(1)#1-Cu(1)-Cu(1)#2	130.05(6)	C(7)#1-C(7)-N(1)	115.0(2)
N(1)-Cu(1)-Cu(1)#2	130.05(6)	C(7)#1-C(7)-C(8)	121.5(2)
O(1)-Cu(1)-Cu(1)#2	39.47(5)	N(1)-C(7)-C(8)	116.2(4)
O(1)#2-Cu(1)-Cu(1)#2	39.47(5)	C(7')#1-C(7')-C(8)	122.4(2)
Br(2)-Cu(1)-Cu(1)#2	106.40(2)	C(7')#1-C(7')-N(1)	115.7(2)
C(1)-O(1)-Cu(1)	129.47(5)	C(8)-C(7')-N(1)	115.1(4)
C(1)-O(1)-Cu(1)#2	129.47(5)	C(9)-C(8)-C(7)	113.0(4)
Cu(1)-O(1)-Cu(1)#2	101.07(10)	C(9)-C(8)-C(7')	117.2(4)
C(6)-N(1)-C(7)	122.8(3)	C(7)-C(8)-C(7')	26.9(2)
C(6)-N(1)-C(7')	125.8(3)	C(9)-C(8)-C(9')	22.0(3)
C(7)-N(1)-C(7')	26.8(2)	C(7)-C(8)-C(9')	115.7(4)
C(6)-N(1)-Cu(1)	125.76(17)	C(7')-C(8)-C(9')	108.9(4)
C(7)-N(1)-Cu(1)	110.2(2)	C(9)#1-C(9)-C(8)	120.2(3)
C(7')-N(1)-Cu(1)	106.4(2)	C(9')#1-C(9')-C(8)	122.8(3)
O(1)-C(1)-C(2)	120.21(14)		

Symmetry transformations used to generate equivalent atoms:

#1 -x+1,y,z #2 -x+1,-y,-z+1 #3 x,-y,-z+1

Table 26. Selected bond lengths (Å) and angles(°) for hydrogen bond of $[Cu_2([20]\text{-}DCHDC)Br_2] \cdot 6H_2O$

D-H···A	d(D-H)	d(H···A)	<DHA	d(D···A)
lattice water - bromide ion				
O2W-H2WA···Br2 [-x+1, -y, -z+1]	0.841	2.693	167.02	3.518
between lattice waters				
O2W-H2WB···O3W [-x+1/2, -y+1/2, -z+1]	0.848	2.171	140.68	2.877
O3W-H3WA···O2W [-x+1/2, -y+1/2, -z+1]	0.847	2.031	179.36	2.877
O3W-H3WB···O2W [-x+1/2, -y, z+1/2]	0.848	2.064	164.73	2.891

3) $[Cu_2([20]\text{-}DCHDC)(\mu\text{-}O_2ClO_2)_2] \cdot 1.6CH_3CN \cdot 0.4CH_3OH$

Suitable crystals of $[Cu_2([20]\text{-}DCHDC)(\mu\text{-}O_2ClO_2)_2] \cdot 1.6CH_3CN \cdot 0.4CH_3OH$ were obtained by slow evaporation of acetonitrile : methanol (1 : 1) solutions of $[Cu_2([20]\text{-}DCHDC)(ClO_4)_2] \cdot H_2O$ complex at atmospheric pressure. Unfortunately, refinement of structure was hampered due to rather inferior quality of diffraction data and severe disordering of the acetonitrile and methanol molecules. Nevertheless, the structural analysis has elucidated the geometric features and connectivities in the complex molecule. Two formula units comprise the unit cell with half of the binuclear complex in the asymmetric unit. An ORTEP drawing of asymmetric unit and core structure (top view) for the complex are given in Fig. 39 and 40, respectively.

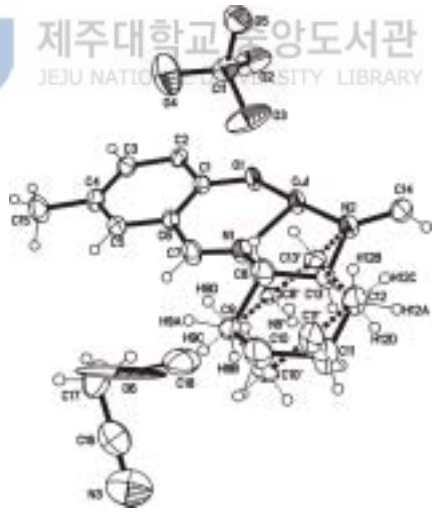

Fig. 39. Structural representation of asymmetric unit of $[Cu_2([20]\text{-}DCHDC)\text{-}(\mu\text{-}O_2ClO_2)_2] \cdot 1.6CH_3CN \cdot 0.4CH_3OH$. Dotted lines represent the disorder parts.

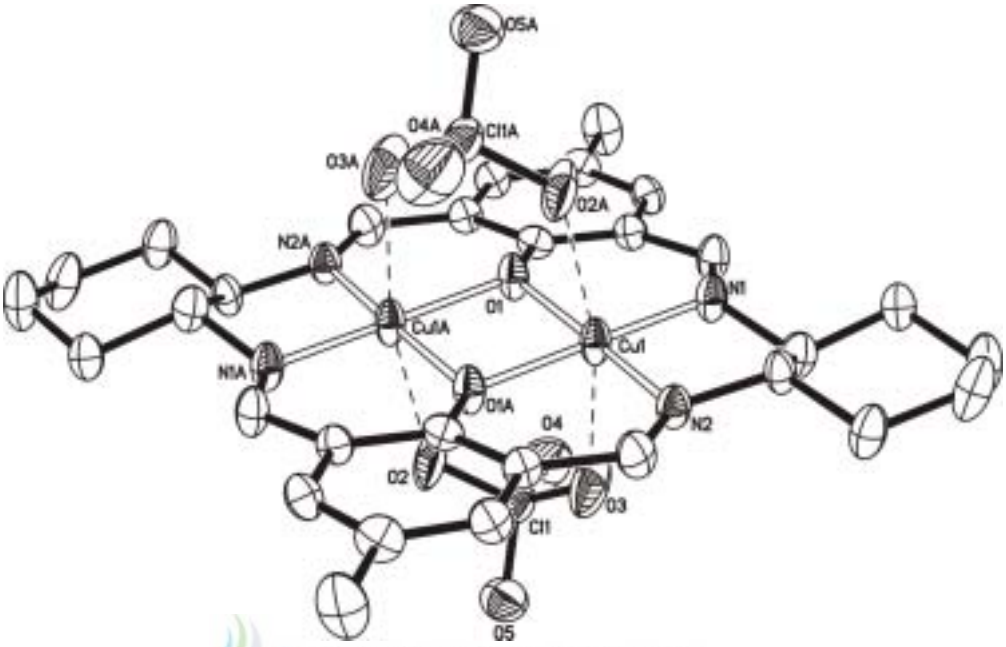

Fig. 40. An ORTEP view of core structure (top view) for the $[Cu_2([20]\text{-DCHDC})(\mu\text{-}O_2ClO_2)_2] \cdot 1.6CH_3CN \cdot 0.4CH_3OH$ showing 30% probability thermal ellipsoids and labels for non-H atoms. H-atoms and disorder parts are omitted for clarity.

The relevant bond distances and angles are given in Table 27 and 28. The binuclear core structures are centrosymmetric with each copper(II) ion in the $N(imine)_2O_2$ sites being six-coordinate by octahedral geometry of interactions with two nitrogen and two oxygen atoms of the binucleating ligand [20]-DCHDC and two oxygen atoms each from the bridging perchlorate ligands at an apical site ([C]).

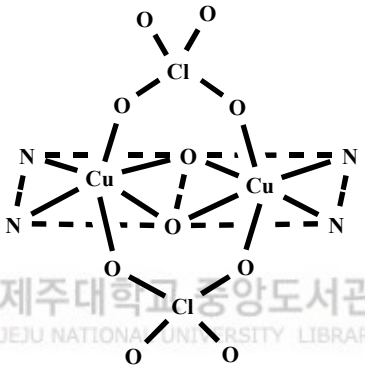

[C]

The macrocyclic complex adopts an essentially flat structure with the two octahedral copper centers bridged by the two phenoxide oxygen atoms, with quite large Cu-O-Cu angles (98.54(10)˚). Magnetostructural correlations in binuclear copper(II) complexes bridged equatorially by pairs of hydroxide groups show that the major factor controlling spin coupling between the *S*=1/2 metal centers is the Cu-O-Cu angle. The sum of angles at the phenoxide oxygens is almost exactly 360˚, indicating no square oxygen distortion. The sum of angles at the copper basal planes (CuN_2O_2) is almost

exactly 360°(360.28°), indicating no plane distortion.

The interatomic Cu···Cu separation is 2.8786(9) Å. The in-plane Cu-to-donor distances range from 1.886(3) Å to 1.900(2) Å. The Cu-O (perchlorate) bond distances are in the range of 2.586 and 2.660 Å. The bond angles N(2)-Cu-O(1),and O(2)-Cu-O(3A) are 174.46° and 168.15° , respectively. In this complex Cu-N (imines) and Cu-O (phenolic) distances are shorter than Cu-O (perchlorate) and the angle N(2)-Cu-O(1),and O(2)-Cu-O(3A) are smaller than the ideal value of 180°, indicating that the donor atoms are not able to achieve the axial positions of a perfect octahedron ; this is elongated owing to the Jahn-Teller effect and steric effect.

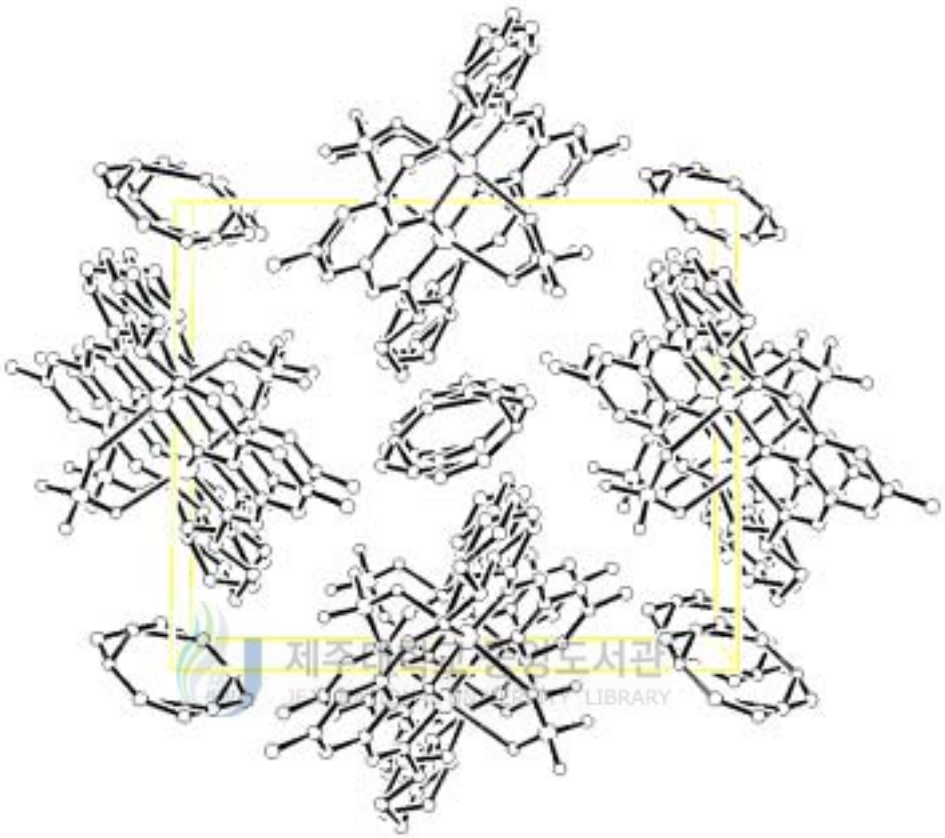

Fig. 41. The molecular packing diagram of $[Cu_2([20]\text{-}DCHDC)(\mu\text{-}O_2ClO_2)_2] \cdot 1.6CH_3CN \cdot 0.4CH_3OH$.

Table 27. Bond lengths (Å) for $[Cu_2([20]\text{-}DCHDC)(\mu\text{-}O_2ClO_2)_2]\cdot 1.6CH_3CN\cdot 0.4CH_3OH$

Cu(1)-N(2)	1.886(3)	C(8)-C(9)	1.552(10)
Cu(1)-N(1)	1.889(3)	C(8')-C(9)	1.495(9)
Cu(1)-O(1)#1	1.899(2)	C(8')-C(13')	1.581(13)
Cu(1)-O(1)	1.900(2)	C(9)-C(10)	1.52(2)
Cu(1)-Cu(1)#1	2.8786(9)	C(9)-C(10')	1.541(19)
O(1)-C(1)	1.323(4)	C(10)-C(11)	1.50(3)
O(1)-Cu(1)#1	1.899(2)	C(11)-C(12)	1.478(15)
Cu(1)#-O(2)	2.586(2)	C(10')-C(11')	1.54(2)
Cu(1)-O(3)	2.660(2)	C(11')-C(12)	1.575(13)
N(1)-C(7)	1.281(4)	C(12)-C(13)	1.503(11)
N(1)-C(8')	1.527(9)	C(12)-C(13')	1.522(12)
N(1)-C(8)	1.527(10)	C(14)-C(2)#1	1.463(5)
N(2)-C(14)	1.287(4)	Cl(1)-O(3)	1.423(3)
N(2)-C(13)	1.459(11)	Cl(1)-O(4)	1.425(3)
N(2)-C(13')	1.538(11)	Cl(1)-O(5)	1.435(3)
C(1)-C(2)	1.405(5)	Cl(1)-O(2)	1.441(3)
C(1)-C(6)	1.421(5)	N(3)-C(16)	1.143(8)
C(2)-C(3)	1.402(5)	N(3)-C(18)#2	1.38(2)
C(2)-C(14)#1	1.463(5)	C(16)-C(17)	1.360(10)
C(3)-C(4)	1.387(5)	C(16)-O(6)	1.73(3)
C(4)-C(5)	1.382(5)	O(6)-C(18)	1.59(5)
C(4)-C(15)	1.521(5)	C(18)-N(3)#2	1.38(2)
C(5)-C(6)	1.398(5)		
C(6)-C(7)	1.470(5)		
C(8)-C(13)	1.458(14)		

Symmetry transformations used to generate equivalent atoms:

#1 -x,-y+1,-z #2 -x+2,-y+1,-z+1

Table 28. Angles [°] for $[Cu_2([20]\text{-}DCHDC)(\mu\text{-}O_2ClO_2)_2]\cdot 1.6CH_3CN\cdot 0.4CH_3OH$

N(2)-Cu(1)-N(1)	90.11(12)	C(13)-C(8)-C(9)	114.8(8)
N(2)-Cu(1)-O(1)#1	94.55(11)	N(1)-C(8)-C(9)	111.5(7)
N(1)-Cu(1)-O(1)#1	173.85(12)	C(9)-C(8')-N(1)	114.8(6)
N(2)-Cu(1)-O(1)	174.46(12)	C(9)-C(8')-C(13')	109.2(6)
N(1)-Cu(1)-O(1)	94.16(11)	N(1)-C(8')-C(13')	103.4(6)
O(1)#1-Cu(1)-O(1)	81.46(10)	C(8')-C(9)-C(10)	115.0(9)
N(2)-Cu(1)-Cu(1)#1	135.17(9)	C(8')-C(9)-C(10')	110.3(8)
N(1)-Cu(1)-Cu(1)#1	134.72(9)	C(10)-C(9)-C(10')	23.3(6)
O(1)#1-Cu(1)-Cu(1)#1	40.74(7)	C(8')-C(9)-C(8)	28.0(4)
O(1)-Cu(1)-Cu(1)#1	40.71(7)	C(10)-C(9)-C(8)	108.0(9)
C(1)-O(1)-Cu(1)#1	128.6(2)	C(10')-C(9)-C(8)	115.5(8)
C(1)-O(1)-Cu(1)	129.4(2)	C(11)-C(10)-C(9)	116.3(13)
Cu(1)#1-O(1)-Cu(1)	98.54(10)	C(12)-C(11)-C(10)	113.8(12)
C(7)-N(1)-C(8')	125.8(4)	C(11')-C(10')-C(9)	109.0(10)
C(7)-N(1)-C(8)	125.3(5)	C(10')-C(11')-C(12)	110.6(10)
C(8')-N(1)-C(8)	28.1(4)	C(11)-C(12)-C(13)	113.5(7)
C(7)-N(1)-Cu(1)	125.2(3)	C(11)-C(12)-C(13')	116.6(7)
C(8')-N(1)-Cu(1)	108.4(4)	C(13)-C(12)-C(13')	25.6(4)
C(8)-N(1)-Cu(1)	105.7(4)	C(11)-C(12)-C(11')	26.0(6)
C(14)-N(2)-C(13)	124.6(5)	C(13)-C(12)-C(11')	115.7(7)
C(14)-N(2)-C(13')	126.8(5)	C(13')-C(12)-C(11')	106.6(7)
C(13)-N(2)-C(13')	25.7(4)	C(8)-C(13)-N(2)	108.9(8)
C(14)-N(2)-Cu(1)	124.5(3)	C(8)-C(13)-C(12)	113.0(8)
C(13)-N(2)-Cu(1)	108.6(4)	N(2)-C(13)-C(12)	118.8(7)

C(13')-N(2)-Cu(1)	107.8(4)	C(12)-C(13')-N(2)	112.9(7)
O(1)-C(1)-C(2)	119.9(3)	C(12)-C(13')-C(8')	109.3(7)
O(1)-C(1)-C(6)	119.2(3)	N(2)-C(13')-C(8')	104.1(7)
C(2)-C(1)-C(6)	120.9(3)	N(2)-C(14)-C(2)#1	126.0(3)
C(3)-C(2)-C(1)	117.7(3)	O(3)-Cl(1)-O(4)	109.8(2)
C(3)-C(2)-C(14)#1	117.6(3)	O(3)-Cl(1)-O(5)	109.6(2)
C(1)-C(2)-C(14)#1	124.7(3)	O(4)-Cl(1)-O(5)	108.7(2)
C(4)-C(3)-C(2)	122.9(3)	O(3)-Cl(1)-O(2)	110.05(18)
C(5)-C(4)-C(3)	118.0(3)	O(4)-Cl(1)-O(2)	109.7(2)
C(5)-C(4)-C(15)	121.1(4)	O(5)-Cl(1)-O(2)	109.04(19)
C(3)-C(4)-C(15)	121.0(3)	C(16)-N(3)-C(18)#2	130.2(11)
C(4)-C(5)-C(6)	122.7(4)	N(3)-C(16)-C(17)	179.5(8)
C(5)-C(6)-C(1)	117.8(3)	N(3)-C(16)-O(6)	148.7(17)
C(5)-C(6)-C(7)	117.3(3)	C(17)-C(16)-O(6)	31.2(17)
C(1)-C(6)-C(7)	124.8(3)	C(18)-O(6)-C(16)	121(3)
N(1)-C(7)-C(6)	125.4(3)	N(3)#2-C(18)-O(6)	138(2)
C(13)-C(8)-N(1)	109.0(7)		

Symmetry transformations used to generate equivalent atoms:

#1 -x,-y+1,-z #2 -x+2,-y+1,-z+1

4) $[Cu_2([20]\text{-}DCHDC)(N_3)_2] \cdot 2CH_3OH$

Suitable crystals of $[Cu_2([20]\text{-}DCHDC)(N_3)_2] \cdot 2CH_3OH$ were obtained by slow evaporation of methanol solutions of $[Cu_2([20]\text{-}DCHDC)(N_3)_2] \cdot 6H_2O$ complex at atmospheric pressure. Two formula units comprise the unit cell with half of the binuclear complex in the asymmetric unit. An ORTEP drawing of asymmetric unit and core structure (top view) for the complex are given in Fig. 42 and 43, respectively.

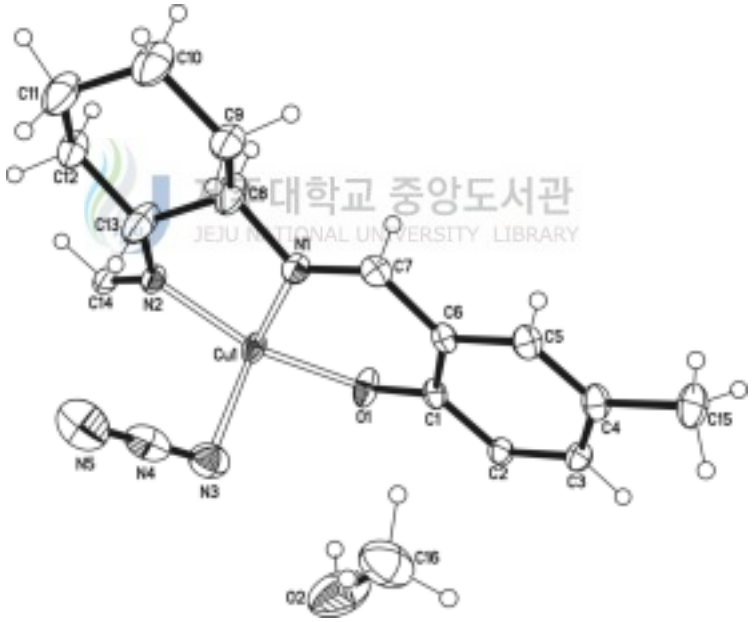

Fig. 42. Structural representation of asymmetric unit of $[Cu_2([20]\text{-}DCHDC)\text{-}(N_3)_2] \cdot 2CH_3OH$

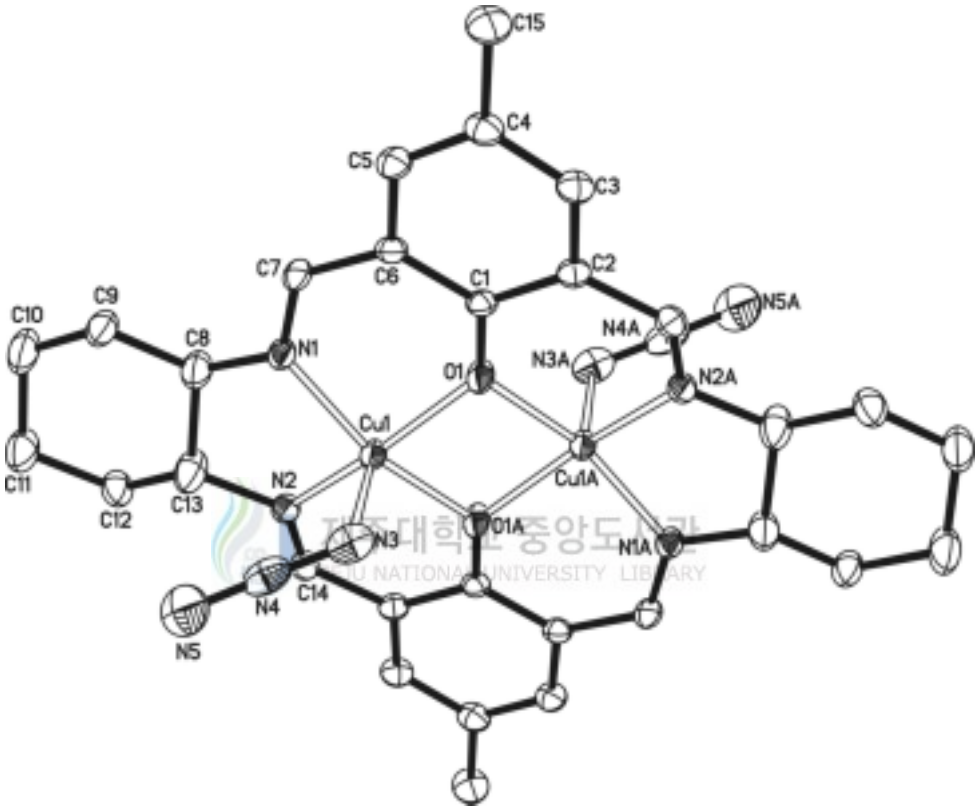

Fig. 43. An ORTEP view of core structure (top view) for the $[Cu_2([20]\text{-DCHDC})(N_3)_2]\cdot 2CH_3OH$ showing 30% probability thermal ellipsoids and labels for non-H atoms.

The relevant bond distances and angles are given in Table 29 and 30. The binuclear core structures are centrosymmetric with each copper(II) ion in the $N(imine)_2O_2$ sites being five-coordinate by square-pyramidal geometry of interactions with two nitrogen and two oxygen atoms of the binucleating ligand [20]-DCHDC and one nitrogen atom each from the azide ligands at an apical site. The copper ions are 0.3605 Å displaced from the basal least-squares plane toward N_3^- ions. Two N_3^- ions attached to two central metal Cu are situated trans to each other with respect to the mean molecular plane ([D]).

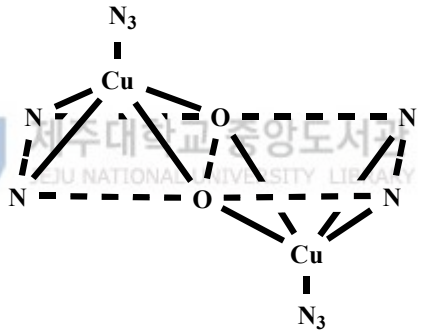

[D]

The interatomic Cu···Cu separation is 2.9608(8) Å. The in-plane Cu-to-donor distances range from 1.912(3) to 1.922(2) Å. The axial Cu-N3(azide) bond distance (2.257(3) Å) is elongated owing to the Jahn-Teller effect of the d^9 electronic configuration.

The macrocyclic complex adopts a non-flat structure with two square-pyramidal copper centers bridged by the two phenoxide oxygen atoms,

with quite large Cu-O-Cu angles (100.88(10)°) **([B])**.

In general, hydrogen bonding plays a principal role in the packing of the title compound. There are one type of H-bonds ; lattice methanol - azide ion (Fig. 44 snd Table 31).

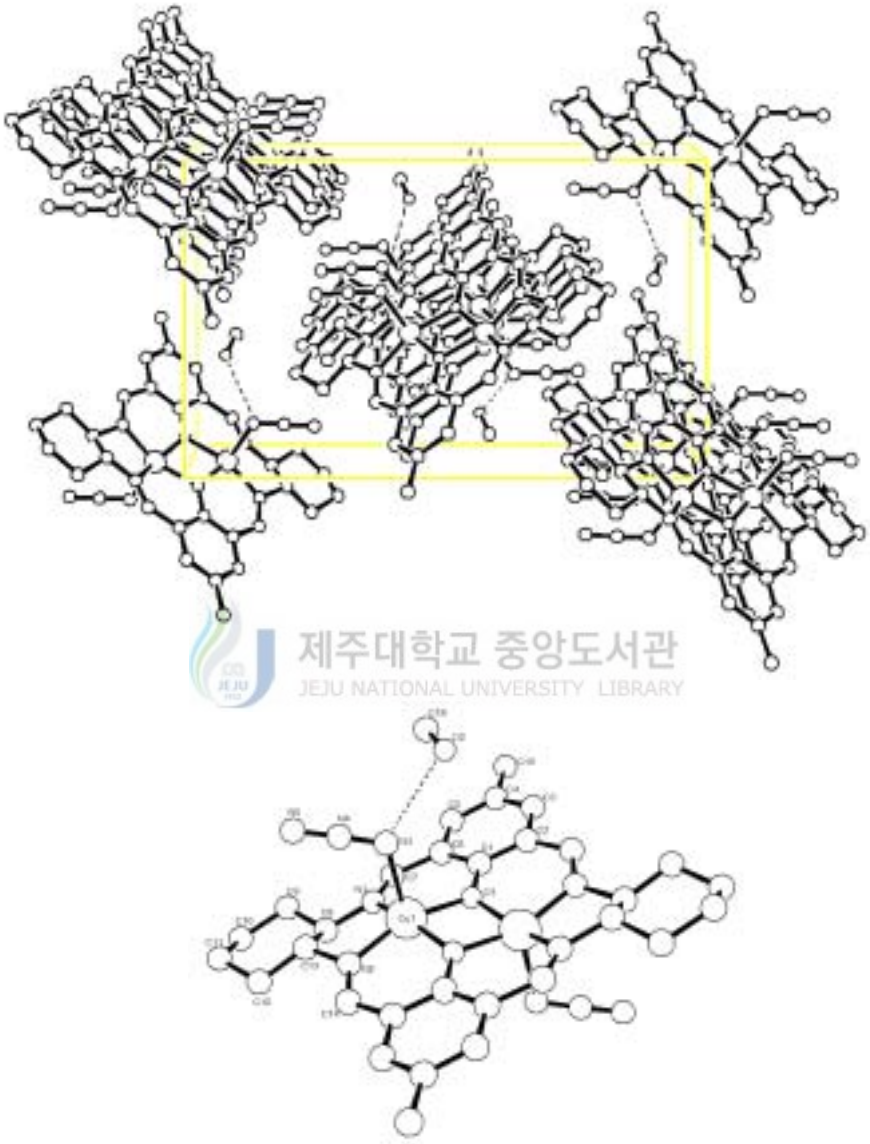

Fig. 44. The molecular packing diagram of $[Cu_2([20]\text{-DCHDC})(N_3)_2] \cdot 2CH_3OH$. Dotted lines represent hydrogen bond between azide and lattice methanol.

Table 29. Bond lengths (Å) for $[Cu_2([20]\text{-}DCHDC)(N_3)_2] \cdot 2CH_3OH$

Cu(1)-N(2)	1.912(3)	C(2)-C(3)	1.403(4)
Cu(1)-N(1)	1.918(3)	C(2)-C(14)#1	1.474(5)
Cu(1)-O(1)#1	1.918(2)	C(3)-C(4)	1.400(5)
Cu(1)-O(1)	1.922(2)	C(4)-C(5)	1.382(5)
Cu(1)-N(3)	2.257(3)	C(4)-C(15)	1.523(4)
Cu(1)-Cu(1)#1	2.9608(8)	C(5)-C(6)	1.403(4)
O(1)-C(1)	1.321(4)	C(6)-C(7)	1.471(4)
O(1)-Cu(1)#1	1.918(2)	C(8)-C(9)	1.495(5)
N(1)-C(7)	1.292(4)	C(8)-C(13)	1.505(5)
N(1)-C(8)	1.483(4)	C(9)-C(10)	1.524(5)
N(2)-C(14)	1.280(4)	C(10)-C(11)	1.495(6)
N(2)-C(13)	1.481(5)	C(11)-C(12)	1.517(5)
N(3)-N(4)	1.191(5)	C(12)-C(13)	1.498(5)
N(4)-N(5)	1.164(5)	C(14)-C(2)#1	1.474(5)
C(1)-C(2)	1.417(4)	O(2)-C(16)	1.378(6)
C(1)-C(6)	1.423(4)		

Symmetry transformations used to generate equivalent atoms: #1 -x+1,-y+1,-z+1

Table 30. Angles [°] for $[Cu_2([20]\text{-}DCHDC)(N_3)_2]\cdot 2CH_3OH$

N(2)-Cu(1)-N(1)	88.84(12)	O(1)-C(1)-C(2)	120.0(3)
N(2)-Cu(1)-O(1)#1	92.90(11)	O(1)-C(1)-C(6)	119.6(3)
N(1)-Cu(1)-O(1)#1	160.60(12)	C(2)-C(1)-C(6)	120.4(3)
N(2)-Cu(1)-O(1)	158.31(12)	C(3)-C(2)-C(1)	118.3(3)
N(1)-Cu(1)-O(1)	92.27(11)	C(3)-C(2)-C(14)#1	117.5(3)
O(1)#1-Cu(1)-O(1)	79.12(10)	C(1)-C(2)-C(14)#1	124.2(3)
N(2)-Cu(1)-N(3)	103.31(13)	C(4)-C(3)-C(2)	122.2(3)
N(1)-Cu(1)-N(3)	97.67(12)	C(5)-C(4)-C(3)	118.2(3)
O(1)#1-Cu(1)-N(3)	100.71(12)	C(5)-C(4)-C(15)	121.7(3)
O(1)-Cu(1)-N(3)	98.01(12)	C(3)-C(4)-C(15)	120.1(3)
N(2)-Cu(1)-Cu(1)#1	129.50(9)	C(4)-C(5)-C(6)	122.8(3)
N(1)-Cu(1)-Cu(1)#1	129.56(9)	C(5)-C(6)-C(1)	118.1(3)
O(1)#1-Cu(1)-Cu(1)#1	39.61(7)	C(5)-C(6)-C(7)	118.0(3)
O(1)-Cu(1)-Cu(1)#1	39.51(7)	C(1)-C(6)-C(7)	123.8(3)
N(3)-Cu(1)-Cu(1)#1	102.17(9)	N(1)-C(7)-C(6)	125.1(3)
C(1)-O(1)-Cu(1)#1	130.4(2)	N(1)-C(8)-C(9)	117.0(3)
C(1)-O(1)-Cu(1)	127.5(2)	N(1)-C(8)-C(13)	110.1(3)
Cu(1)#1-O(1)-Cu(1)	100.88(10)	C(9)-C(8)-C(13)	113.6(3)
C(7)-N(1)-C(8)	124.2(3)	C(8)-C(9)-C(10)	112.5(3)
C(7)-N(1)-Cu(1)	125.1(2)	C(11)-C(10)-C(9)	114.6(3)
C(8)-N(1)-Cu(1)	110.3(2)	C(10)-C(11)-C(12)	114.6(3)
C(14)-N(2)-C(13)	125.6(3)	C(13)-C(12)-C(11)	111.7(3)
C(14)-N(2)-Cu(1)	126.4(2)	N(2)-C(13)-C(12)	118.8(3)
C(13)-N(2)-Cu(1)	108.0(2)	N(2)-C(13)-C(8)	110.2(3)
N(4)-N(3)-Cu(1)	113.8(3)	C(12)-C(13)-C(8)	113.6(3)
N(5)-N(4)-N(3)	178.3(4)	N(2)-C(14)-C(2)#1	125.3(3)

Symmetry transformations used to generate equivalent atoms: #1 -x+1,-y+1,-z+1

Table 31. Selected bond lengths (Å) and angles(°) for hydrogen bond of $[Cu_2([20]\text{-DCHDC})(N_3)_2] \cdot 2CH_3OH$

D-H···A	d(D-H)	d(H···A)	<DHA	d(D···A)
lattice methanol - azide ion				
O2-H2···N3(azide)	0.839	2.306	124.23	2.864

IV. Conclusion

The reaction of 2,6-diformyl-*p*-cresol and trans-1,2-diaminocyclohexane in methanol in equimolar ratio using the high dilution technique affords a [3 + 3] Schiff-base macrocycle L_4 as yellow solid in high yield. The CHN, IR, NMR and FAB mass spectral data of the product do not agree with the expected a [2 + 2] Schiff-base macrocycle ligand L_3 (= H_2[20]-DCHDC) but match with the composition of [3 + 3] Schiff-base macrocycle L_4.

Binuclear Cu(II) complexe, $[Cu_2([20]\text{-DCHDC})Cl_2]\cdot H_2O$, with [2 + 2] symmetrical N_4O_2 compartmental macrocyclic ligand containing bridging phenolic oxygen atoms was synthesized by metal template condensation of 2,6-diformyl-*p*-cresol, trans-1,2-diaminocyclohexane, and $CuCl_2\cdot 2H_2O$. The reaction of $[Cu_2([20]\text{-DCHDC})Cl_2]\cdot H_2O$ with auxiliary ligands (La ; Br^-, I^-, ClO_4^-, SCN^-, N_3^-, NO_2^-, NO_3^-, and $S_2O_3^{2-}$) in aqueous solution formed a new 8 complexes; $[Cu_2([20]\text{-DCHDC})Br_2]\cdot 0.5H_2O$, $[Cu_2([20]\text{-DCHDC})I_2]$, $[Cu_2([20]\text{-DCHDC})(\mu\text{-}O_2ClO_2)_2]\cdot H_2O$, $[Cu_2([20]\text{-DCHDC})(NCS)_2]\cdot H_2O$, $[Cu_2\text{-}([20]\text{-DCHDC})(N_3)_2]\cdot 6H_2O$, $[Cu_2([20]\text{-DCHDC})(\mu\text{-}O_2N)]NO_2\cdot 6H_2O$, $[Cu_2([20]\text{-DCHDC})(\mu\text{-}O_2NO)]NO_3\cdot 0.5H_2O$, and $[Cu_2([20]\text{-DMTADO})(\mu\text{-}S_2O_3)]$, where [20]-DCHDC is the dianion of the binucleating macrocyclic ligand 14,29-dimethyl-3,10,18,25-tetraazapentacyclo-[25,3,1,$0^{4,9}$,$1^{12,16}$,$0^{19,24}$]ditriacontane-2,10,12,14,16(32),17,27(31),28,30-decane-31,32-diol.

X-ray crystals and molecular structures of $[Cu_2([20]\text{-DCHDC})Cl_2]\cdot 6H_2O$ **(1)**, $[Cu_2([20]\text{-DCHDC})Br_2]\cdot 6H_2O$ **(2)**, $[Cu_2([20]\text{-DCHDC})(\mu\text{-}O_2ClO_2)_2]\cdot 1.6CH_3CN\cdot 0.4CH_3OH$ **(3)**, and $[Cu_2([20]\text{-DCHDC})(N_3)_2]\cdot 2CH_3OH$ **(4)** have

been determined on a Bruker SMART-CCD diffractometer.

In **(1)** complex, a total 2047 reflections at the 2σ(*I*) significance were used to give final discrepancy indices of R_1 = 0.0317 and wR_2 = 0.0841. The complex crystallizes in the orthorhombic space group *Cmca* in a cell having the dimensions *a* = 16.8306(7) Å, *b* = 7.9928(3) Å, and *c* = 24.5686(10) Å. The calculated density is 1.585 g/cm^3. Four formula units comprise the unit cell with quater of the binuclear complex in the asymmetric unit. The binuclear core structures are centrosymmetric with each copper(II) ion in the N(imine)$_2$O$_2$ sites being five-coordinate by square-pyramidal geometry of interactions with two nitrogen and two oxygen atoms of the binucleating ligand [20]-DCHDC and one chloride ligand at an apical site. The interatomic Cu···Cu separation is 2.9707(7) Å. The copper ions are 0.3625 Å displaced from the basal least-squares plane toward Cl^- ions. Two Cl^- ions attached to two central metal Cu are situated trans to each other with respect to the mean molecular plane. The in-plane Cu-to-donor distances range from 1.9136(17) Å to 1.9189(13) Å. The axial Cu-Cl bond distance (2.5215(9) Å) is elongated owing to the Jahn-Teller effect of the d^9 electronic configuration. The macrocyclic complex adopts a non-flat structure with two square-pyramidal copper centers bridged by the two phenoxide oxygen atoms, with quite large Cu-O-Cu angles (101.44(9)°).

In **(2)** complex, a total 2130 reflections at the 2σ(*I*) significance were used to give final discrepancy indices of R_1 = 0.0305 and wR_2 = 0.0752. The complex crystallizes in the orthorhombic space group *Cmca* in a cell having the dimensions *a* = 116.8510(7) Å, *b* = 8.0835(3) Å, and *c* = 24.7963(11) Å. The calculated density is 1.726 g/cm^3. Four formula units comprise the

unit cell with quater of the binuclear complex in the asymmetric unit. The binuclear core structures are centrosymmetric with each copper(II) ion in the $N(imine)_2O_2$ sites being five-coordinate by square-pyramidal geometry of interactions with two nitrogen and two oxygen atoms of the binucleating ligand [20]-DCHDC and one bromide ligand at an apical site. The interatomic Cu···Cu separation is 2.9549(8) Å. The copper ions are 0.3284 Å displaced from the basal least-squares plane toward Br^- ions. Two Br^- ions attached to two central metal Cu are situated trans to each other with respect to the mean molecular plane. The in-plane Cu-to-donor distances range from 1.9138(14) Å to 1.904(2) Å. The axial Cu-Br bond distance (2.6821(6) Å) is elongated owing to the Jahn-Teller effect of the d^9 electronic configuration. The macrocyclic complex adopts a non-flat structure with two square-pyramidal copper centers bridged by the two phenoxide oxygen atoms, with quite large Cu-O-Cu angles (101.07(10)°).

In **(3)** complex, a total 4383 reflections at the $2\sigma(I)$ significance were used to give final discrepancy indices of R_1 = 0.0495 and wR_2 = 0.1043. The complex crystallizes in the monoclinic space group $P2_1/c$ in a cell having the dimensions a = 8.0773(6) Å, b = 16.7494(13) Å, c = 14.0614(11) Å and β = 100.447(2)°. The calculated density is 1.575 g/cm^3. Four formula units comprise the unit cell with half of the binuclear complex in the asymmetric unit. The binuclear core structures are centrosymmetric with each copper(II) ion in the $N(imine)_2O_2$ sites being six-coordinate by octahedral geometry of interactions with two nitrogen and two oxygen atoms of the binucleating ligand [20]-DCHDC and two oxygen atoms each from the bridging perchlorate ligands at an apical site. The macrocyclic complex adopts an

essentially flat structure with the two octahedral copper centers bridged by the two phenoxide oxygen atoms, with quite large Cu-O-Cu angles (98.54(10) °). The sum of angles at the phenoxide oxygens is almost exactly 360°, indicating no square oxygen distortion. The sum of angles at the copper basal planes (CuN_2O_2) is almost exactly 360°(360.28°), indicating no plane distortion. The interatomic Cu···Cu separation is 2.8786(9) Å. The in-plane Cu-to-donor distances range from 1.886(3) Å to 1.900(2) Å. The Cu-O (perchlorate) bond distances are in the range of 2.586 and 2.660 Å. The bond angles N(2)-Cu-O(1),and O(2)-Cu-O(3A) are 174.46° and 168.15° , respectively. In this complex Cu-N (imines) and Cu-O (phenolic) distances are shorter than Cu-O (perchlorate) and the angle N(2)-Cu-O(1),and O(2)-Cu-O(3A) are smaller than the ideal value of 180°, indicating that the donor atoms are not able to achieve the axial positions of a perfect octahedron ; this is elongated owing to the Jahn-Teller effect and steric effect.

In **(4)** complex, a total 3813 reflections at the $2\sigma(I)$ significance were used to give final discrepancy indices of R_1 = 0.0549 and wR_2 = 0.1217. The complex crystallizes in the monoclinic space group $P2_1/c$ in a cell having the dimensions a = 6.9849(5) Å, b = 19.6663(13) Å, c = 12.0317(8) Å, and β = 97.1770(10)°. The calculated density is 1.535 g/cm^3. Four formula units comprise the unit cell with half of the binuclear complex in the asymmetric unit. The binuclear core structures are centrosymmetric with each copper(II) ion in the $N(imine)_2O_2$ sites being five-coordinate by square-pyramidal geometry of interactions with two nitrogen and two oxygen atoms of the binucleating ligand [20]-DCHDC and one nitrogen atom each from the azide

ligands at an apical site. The copper ions are 0.3605 Å displaced from the basal least-squares plane toward N_3^- ions. Two N_3^- ions attached to two central metal Cu are situated trans to each other with respect to the mean molecular plane. The interatomic Cu···Cu separation is 2.9608(8) Å. The in-plane Cu-to-donor distances range from 1.912(3) to 1.922(2) Å. The axial Cu-N3(azide) bond distance (2.257(3) Å) is elongated owing to the Jahn-Teller effect of the d^9 electronic configuration. The macrocyclic complex adopts a non-flat structure with two square-pyramidal copper centers bridged by the two phenoxide oxygen atoms, with quite large Cu-O-Cu angles (100.88(10)°).

The strong four IR bands at 1148, 1121, 1109, and 1085 cm^{-1} in $[Cu_2([20]\text{-DCHDC})(\mu\text{-}O_2ClO_2)_2] \cdot H_2O$ complex are attributed to a bridging bidentate ligand Cu-O-ClO_2-O-Cu. The absorption vibrations due to the N-coordinated bonded NCS^- in $[Cu_2([20]\text{-DCHDC})(NCS)_2] \cdot H_2O$ appear 2067 and 894 cm^{-1}. The absorption peak at 2034 cm^{-1} in the $[Cu_2([20]\text{-DCHDC}))(N_3)_2] \cdot 6H_2O$ is assigned to the asymmetric stretching mode of coordinated azide. The symmetric stretching frequency of coordinated azide is observed at 1321 cm^{-1}. The strong absorption peaks at 1446 and 1205 cm^{-1} in the $[Cu_2([20]\text{-DCHDC})(\mu\text{-ONO})]NO_2 \cdot H_2O$ are assigned to a bridging bidentate ligand Cu-ONO-Cu. The absorption bands of bidentate coordinate nitrate occurring in the IR spectra of $[Cu_2([20]\text{-DCHDC})(\mu\text{-}O_2NO)]\text{-}NO_3 \cdot 0.5H_2O$ in the 1454, 1339 and 1043 cm^{-1} regions are assignable to the ν(N=O) (ν_1), $\nu_a(NO_2)$ (ν_5) and $\nu_s(NO_2)$ (ν_2) vibrations, respectively. The absorption peaks at 1236-1198 and 1022-1005 cm^{-1} in the $[Cu_2([20]\text{-DCHDC})\text{-}(\mu\text{-}S_2O_3)]$ are assigned to the asymmetric and symmetric stretching mode of

bridging coordinate $S_2O_3^{2-}$, respectively. A weak bands at near 503 cm^{-1} region associated with the Cu-N(macrocycle) vibration.

The $[Cu_2([20]\text{-DCHDC})]^+$ species of these complexes are well observed in the FAB mass spectra at m/z 608 region. α-Cleavage peaks of one cyclohexane from the $[Cu_2([20]\text{-DCHDC})]^+$ ion in the formation of the fragment $[Cu_2(L_{ac})]^+$ are observed at m/z 526 region. Removal peaks of one copper ion from the $[Cu_2([20]\text{-DCHDC})]^+$ ion in the formation of the fragment $[Cu([20]\text{-DCHDC})]^+$ is observed at m/z 545. The FAB mass spectra of all the complexes contain peaks corresponding to the $[(H_2[20]\text{-DCHDC})]^+$ fragment ion at m/z 489 region. This indicates that the species $[Cu_2([20]\text{-DCHDC})]^+$ undergoes demetallation to give the tetraazadioxa macrocycle H_2[20]-DCHDC under FAB conditions. These peaks are associated with peaks of mass one or two greater or less, which are attributed to protonated /deprotonated forms.

The one *d-d* band of title complexes observed at 17,271 ~ 18,868 cm^{-1} can be related to the spin-allowed transition, $^2E_g \rightarrow {}^2T_{2g}$. The two peak positions calculated at 16,778 - 17,793 and 18,349 - 20,408 cm^{-1} can be assigned to the $^2B_{1g} \rightarrow {}^2B_{2g}$ and $^2B_{1g} \rightarrow {}^2E_g$, respectively. The $^2B_{1g} \rightarrow {}^2A_{1g}$ transition bands have expected at much lower energy. The 21,368 - 24,752 cm^{-1} bands are clearly associated with ligand to metal charge transfer transitions.

References

[1] B. Dietrich, P. Viout, and J. -M. Lehn, *Macrocyclic Chemistry*, VCH Verlagsgesellschaft, Weinheim, **1993**.

[2] J. -M. Lehn, *Supramolecular Chemistry*, VCH Verlagsgesellschaft, Weinheim, **1995**.

[3] E. C. Constable, *Metals and Ligand Reactivity*, VCH Verlagsgesellschaft, Weinheim, 1996.

[4] J. R. Fredericks and A. D. Hamilton, in: A. D. Hamilton (Ed.), *Supramolecular Control of Structure and Reactivity*, Wiley, Chichester, *1996*, Chapter 1.

[5] J. W. Steed and J. L. Atwood, *Supramolecular Chemistry*, Wiley, Chichester, 2000.

[6] J. -C. G. Bünzli and C. Piguet, *Chem. Rev.* 102 (**2002**), 1897.

[7] N. Sabbatini, M. Guargigli, I. Manet, R. Ungaro, A. Casnati, R. Ziessel, G. Ulrich, Z. Asfari, and J. -M. Lehn, *Pure Appl. Chem.* 67 (**1995**), 135.

[8] M. P. Oude Wolbers, F. C. J. M. van Veggel, B. H. M. Snellick-Ruël, J. W. Hofstraat, F. A. J. Guerts, and D. N. Reinhoudt, *J. Am. Chem. Soc.* 119 (**1997**), 138.

[9] J. Huskens, J. A. Peters, and H. Van Bekkum, *Inorg. Chem.* 34 (**1995**), 1756.

[10] D. Parker and J. A. G. Williams, *J. Chem. Soc., Dalton Trans.* (**1996**), 3613.

[11] S. E. Matthews, C. W. Pouton, and M. D. Threadgill, *Adv. Drug*

Delivery Rev. 18 (**1996**), 219.

[12] D. Parker, *Coord. Chem. Rev.* 205 (**2000**), 109.

[13] D. Parker, R. S. Dickins, H. Purschmann, C. Crossland, and J. A. K. Howard, *Chem. Rev.* 102 (**2002**) 1977.

[14] Y. Bretonniere, M. Mazzanti, R. Wietzke, and J. Pécaut, *Chem. Commun.* (**2000**), 1543.

[15] J. -C. G. Bünzli, N. André, M. Elhabiri, G. Muller, and C. Piguet, *J. Alloys Compd.* 303-304 (**2000**), 66.

[16] C. Piguet, C. Edder, H. Nozary, F. Renaud, S. Rigault, J. -C. G. Bünzli, *J. Alloys Compd*. 303-304 (**2000**), 94.

[17] T. Gunnlaugsson, D. A. Mac Dónaill, and D. Parker, *J. Am. Chem. Soc.* 123 (**2001**), 12866.

[18] C. M. Rudzinski, A. M. Young, and D. G. Nocera, *J. Am. Chem. Soc.* 124 (**2002**), 1723.

[19] Y. Bretonnière, M. J. Cann, D. Parker, and R. Slater, *Chem. Commun.* (**2002**), 1930.

[20] P. Atkinson, Y. Bretonniere, and D. Parker, *Chem. Commun.* (**2004**), 438.

[21] D. Parker, *Chem. Soc. Rev*. 33 (**2004**), 156.

[22] É. Tóth, L. Helm, and A. E. Merbach, in: J. A. McCleverty and T. J. Meyer (Eds.), *Comprehensive Coordination Chemistry II*, vol. 9, Elsevier, **2004**, Chapter 19.

[23] (a) R. B. Lauffer, *Chem. Rev.* 87 (**1987**), 901, (b) P. Caravan, J. J. Ellison, T. J. McMurry, and R. B. Lauffer, *Chem. Rev.* 99 (**1999**), 2293.

[24] S. Zhang, K. Wu, and A. D. Sherry, *Angew. Chem. Int. Ed.* 38 (**1999**),

3192.

[25] V. Comblin, D. Gilsoul, M. Hermann, V. Humblet, V. Jacques, M. Mesbahi, C. Sauvage, and J. F. Desreux, *Coord. Chem. Rev.* 185-186 (**1999**), 451.

[26] J. P. André, É. Tóth, H. Fischer, A. Seelig, H. R. Mäcke, and A. E. Merbach, *Chem. Eur. J.* 5 (**1999**), 2977.

[27] M. Woods, S. Aime, M. Botta, J. A. K. Howard, J. M. Moloney, M. Navet, D. Parker, M. Port, O. Rousseaux, *J. Am. Chem. Soc.* 122 (**2000**), 9781.

[28] M. Botta, *Eur. J. Inorg. Chem.* (**2000**), 399.

[29] F. A. Dunand, R. S. Dickins, D. Parker, and A. Merbach, *Chem. Eur. J.* 7 (**2001**), 5160.

[30] S. Aime, D. D. Castelli, F. Fedeli, and E. Terreno, *J. Am. Chem. Soc.* 124 (**2002**), 9364.

[31] W. Li, G. Parigi, M. Fragai, C. Luchinat, and T. J. Meade, *Inorg. Chem.* 41 (**2002**), 4018.

[32] M. Woods, Z. Kovacs, S. Zhang, and A. D. Sherry, *Angew. Chem. Int. Ed.* 42 (**2003**), 5889.

[33] S. Zhang, R. Trokowski, and A. D. Sherry, *J. Am. Chem. Soc.* 125 (**2003**), 15288.

[34] F. Yerly, A. Borel, L. Helm, and A. E. Merbach, *Chem. Eur. J.* 9 (**2003**), 5468.

[35] L. V. Elst, M. Port, I. Raynal, C. Simonot, and R. N. Muller, *Eur. J. Inorg. Chem.* (**2003**), 2495.

[36] K. Kimpe, T. N. Parac-Vogt, S. Laurent, C. Piérart, L. V. Elst, R. N.

Muller, and K. Binnemans, *Eur. J. Inorg. Chem.* (**2003**), 3021.

[37] S. Jurisson, D. Berning, W. Jia, and D. Ma, *Chem. Rev.* 93 (**1993**), 1137.

[38] Y. H. Jang, M. Blanco, S. Dasgupta, D. A. Keire, J. E. Shively, and W. A. Goddard III, *J. Am. Chem. Soc.* 121 (**1999**), 6142.

[39] H. Ali and J. E. Van Lier, *Chem. Rev.* 99 (**1999**), 2379.

[40] D. A. Keire, Y. H. Jang, L. Li, S. Dasgupta, W. A. Goddard III, and J. E. Shively, *Inorg. Chem.* 40 (**2001**), 4310.

[41] J. L. Sessler, T. D. Mody, G. W. Hemmi, V. Lynch, S. W. Young, and R. A. Miller, *J. Am. Chem. Soc.* 115 (**1993**), 10368.

[42] S. W. A. Bligh, N. Choi, C. F. G. C. Geraldes, S. Knoke, M. Mc-Partlin, M. J. Sanganee, and T. M. Woodroffe, *J. Chem. Soc., Dalton Trans.* (**1997**), 4119.

[43] L. Thunus and R. Lejeune, *Coord. Chem. Rev.* 184 (**1999**), 125.

[44] K. Wang, R. Li, Y. Cheng, and B. Zhu, *Coord. Chem. Rev.* 190-192 (**1999**), 297.

[45] D. Kong, L. Meng, L. Song, and Y. Xie, *Transition Met. Chem.* 24 (**1999**), 553.

[46] J. L. Sessler and R. A. Miller, *Biochem. Pharmacol.* 59 (**2000**), 733.

[47] L. A. D. Williams, R. C. Howell, R. Young, I. and A. Kahwa, *Comp. Biochem. Physiol. Part C: Toxicol. Pharmacol.* 128 (**2001**), 119.

[48] M. Woods, Z. Kovacs, and A. D. Sherry, *J. Supramolecular Chem.* 2 (**2002**), 1.

[49] R. W. Hay and N. Govan, *J. Chem. Soc., Chem. Commun.* (**1990**), 714.

[50] J. R. Morrow, L. A. Buttery, V. M. Shelton, and K. A. Berback, *J. Am.*

Chem. Soc. 114 (**1992**), 1903.

[51] N. Hayashi, N. Takeda, T. Shiiba, M. Yashiro, K. Watanabe, and M. Komiyama, *Inorg. Chem.* 32 (**1993**), 5889.

[52] J. K. Bashkin and L. A. Jenkins, *Comments Inorg. Chem.* 16 (**1994**), 77.

[53] B. K. Takasaki and J. Chin, *J. Am. Chem. Soc.* 116 (**1994**), 1121.

[54] K. Matsumura, M. Endo, and M. Komiyama, *J. Chem. Soc., Chem. Commun.* (**1994**), 2019.

[55] D. Magda, R. A. Miller, J. L. Sessler, and B. L. Iverson, *J. Am. Chem. Soc.* 116 (**1994**), 7439.

[56] K. G. Ragunathan and H. -J. Schneider, *Angew. Chem. Int. Ed.* 35 (**1996**), 1219.

[57] R. Häner and J. Hall, *Antisense Nucl. Acid Drug Dev.* 7 (**1997**), 423.

[58] B. F. Baker, H. Khalili, N. Wei, and J. R. Morrow, *J. Am. Chem. Soc.* 119 (**1997**), 8749.

[59] P. E. Jurek and A. E. Martell, *Chem. Commun.* (**1999**), 1609.

[60] B. F. Baker, S. S. Lot, J. Kringel, S. Cheng-Flournoy, P. Villiet, H. M. Sasmor, A. M. Siwkowski, L. L. Chappell, and J. R. Morrow, *Nucl. Acids Res.* 27 (**1999**), 1547.

[61] D. M. Epstein, L. L. Chappell, H. Khalili, R. M. Supkowski, W. DeW. Horrocks Jr., and J. R. Morrow, *Inorg. Chem.* 39 (**2000**), 2130.

[62] S. J. Franklin, *Curr. Opin. Chem. Biol.* 5 (**2001**), 201.

[63] S. W. A. Bligh, N. Choi, E. G. Evagorou, M. McPartlin, and K. N. White, *J. Chem. Soc., Dalton Trans.* (**2001**), 3169.

[64] C. Liu, M. Wang, T. Zhang, and H. Sun, *Coord. Chem. Rev.* 248

(**2004**), 147.

[65] C. H. Evans, in: E. Frieden (Ed.), *Biochemistry of Lanthanides*, Plenum Press, New York, **1990**, Chapter 9.

[66] J. -C. G. Bünzli, in: K. A. Gschneidner Jr., and L. Eyring (Eds.), *Handbook on the Physics and Chemistry of Rare Earths*, vol. 9, Elsevier, Amsterdam, **1987**, Chapter 60.

[67] M. F. Tweedle, in: J. -C. G. Bünzli and G. R. Choppin (Eds.), *Lanthanide Probes in Life, Chemical and Earth Sciences*, Elsevier, Amsterdam, **1989**, Chapter 5.

[68] H. Tsukube and S. Shinoda, *Chem. Rev.* 102 (**2002**), 2389.

[69] P. H. Brown, A. H. Rathjen, R. D. Graham, and D. E. Tribe, in: K. A. Gschneidner Jr. and L. Eyring (Eds.), *Handbook on Physics and Chemistry of Rare Earths*, vol. 13, Elsevier Science Publishers, Amsterdam, **1990**, Chapter 92.

[70] J. R. Duffield, D. M. Taylor, and D. R. Williams, in: K. A. Gschneidner Jr., L. Eyring, G. R. Choppin, and G. H. Lander (Eds.), *Handbook on Physics and Chemistry of Rare Earths*, vol. 18, Elsevier Science Publishers, Amsterdam, **1994**, Chapter 129.

[71] J. M. Harrowfield, M. I. Ogden, R. Richmond, and A. H. White, *J. Chem. Soc., Dalton Trans.* (**1991**), 2153.

[72] S. Aime, M. Botta, M. Fasano, and E. Terreno, *Chem. Soc. Rev.* 27 (**1998**), 19.

[73] W. A. Volkert and T. J. Hoffman, *Chem. Rev.* 99 (**1999**), 2269.

[74] M. J. Heeg and S. S. Jurisson, *Acc. Chem. Res.* 32 (**1999**), 1053.

[75] (a) D. E. Fenton and P. A. Vigato, *Chem. Soc. Rev.* 17 (**1988**), 69; (b)

S. R. Collinson and D. E. Fenton, *Coord. Chem. Rev.* 148 (**1996**), 19; (c) H. Ōkawa, H. Furutachi, and D. E. Fenton, *Coord. Chem. Rev.* 174 (**1998**), 51.

[76] L. M. J. Vallarino, in: K. A. Gschneidner Jr. and L. Eyring (Eds.), *Handbook on the Physics and Chemistry of Rare Earths*, vol. 15, Elsevier, Amsterdam, **1991**, Chapter 104.

[77] V. Alexander, *Chem. Rev.* 95 (**1995**), 273.

[78] R. Hernández-Molina and A. Mederos, in: J. A. McCleverty and T. J. Meyer (Eds.), *Comprehensive Coordination Chemistry II*, vol. 1, Elsevier, **2004**, Chapter 19.

[79] N. F. Curtis, in: J. A. McCleverty and T. J. Meyer (Eds.), *Comprehensive Coordination Chemistry II*, vol. 1, Elsevier, **2004**, Chapter 20.

[80] (a) S. Brooker, *Coord. Chem. Rev.* 222 (**2001**), 33; (b) S. Brooker, *Eur. J. Inorg. Chem.* (**2002**), 2535.

[81] (a) D. H. Bush, A. L. Vance and A. G. Kolochinksii, in: J. -M. Lehn (Ed.), *Comprehensive Supramolecular Chemistry*, vol. 9, Pergamon Press, **1996**, Chapter 1; (b) N. V. Gerbeleu, V. B. Arion and J. Burges, *Template Synthesis of Macrocyclic Compounds*, Wiley-VCH, Weinheim, **1999**.

[82] S. M. Nelson, C. V. Knox, M. McCann, and M. G. B. Drew, J. *Chem. Soc., Dalton Trans.* (**1981**), 1659.

[83] W. Radecka-Paryzek, *Inorg. Chim. Acta* 35 (**1979**), 349.

[84] W. Radecka-Paryzek, M. Kaczmarek, V. Patroniak, and I. Pospieszna -Markiewicz, *J. Alloys Compd.* 323-324 (**2001**) 173.

[85] V. Patroniak and W. Radecka-Paryzek, *Mater. Sci. Eng. C* 18 (**2001**), 113.

[86] W. Radecka-Paryzek, M. Kaczmarek, I. Pospieszna-Markiewicz, *Pol. J. Chem.* 76 (**2002**), 679.

[87] W. Radecka-Paryzek, M. Kaczmarek, V. Patroniak, and I. Pospieszna -Markiewicz, *Inorg. Chem. Commun.* 6 (**2003**), 26.

[88] M. Kaczmarek, I. Pospieszna-Markiewicz, and W. Radecka-Paryzek, *J. Inclusion Phenom. Macrocyclic Chem.* 49 (**2004**) 115.

[89] I. Pospieszna-Markiewicz and W. Radecka-Paryzek, *J. Alloys Compd.* 374 (**2004**), 254.

[90] N. H. Pilkington and R. Robson, *Aust. J. Chem.* 23 (**1970**), 2225.

[91] H. Ōkawa, S. Kida, *Bull. Chem. Soc. Jpn.* 45 (**1972**), 1759.

[92] B. F. Hoskins, R. Robson, and G. A. Williams, *Inorg. Chim. Acta* 16 (1976) 121.

[93] L. K. Thompson, S. K. Mandal, S. T. Tandon, J. N. Bridson, and M. K. Park, *Inorg. Chem.* 35 (**1996**), 3117.

[94] A. Asokan, B. Varghese, A. Caneschi, and P. T. Manoharan, *Inorg. Chem.* 37 (**1998**), 228.

[95] H. Wada, K. Motoda, M. Ohba, H. Sakiyama, N. Matsumoto, and H. Ōkawa, *Bull. Chem. Soc. Jpn.* 68 (**1995**), 1105.

[96] H. -R. Chang, S. K. Larsen, P. D. W. Boyd, C. G. Pierpont, and D. N. Hendrickson, *J. Am. Chem. Soc.* 110 (**1988**), 4565.

[97] R. R. Gagne, C. L. Spiro, T. J. Smith, C. A. Hamann, W. R. Thies, and A. K. Shiemke, *J. Am. Chem. Soc.* 103 (**1981**), 4073.

[98] S. K. Dutta, J. Ensling, R. Werner, U. Flörke, W. Haase, P. Gütlich,

and K. Nag, *Angew. Chem. Int. Ed.* 36 (**1997**), 152.

[99] A. Asokan, B. Varghese, A. Caneschi, and P. T. Manoharan, *Inorg. Chem.* 37 (**1998**), 228.

[100] A. J. Atkins, A. J. Blake, and M. Schröder, *J. Chem. Soc., Chem. Commun.* (**1993**) 353.

[101] A. J. Atkins, D. Black, A. J. Blake, A. Marin-Becerra, L. Ruiz-Ramirez, and M. Schröder, *J. Chem. Soc., Chem. Commun.* (**1996**) 457.

[102] A. J. Atkins, D. Black, R. L. Finn, A. Marin-Becerra, A. J. Blake, L. Ruiz-Ramirez, W. -S. Li, and M. Schröder, *Dalton Trans.* (**2003**), 1730.

[103] D. Black, A. J. Blake, R. L. Finn, L. F. Lindoy, A. Nezhadali, G. Rougnaghi, P. A. Tasker, and M. Schröder, *Chem. Commun.* (**2002**) 340.

[104] M. Yonemura, Y. Matsumura, H. Furutachi, M. Ohba, H. Ōkawa, and D. E. Fenton, *Inorg. Chem.* 36 (**1997**), 2711.

[105] S. Kita, H. Furutachi, and H. Ōkawa, *Inorg. Chem.* 38 (**1999**), 4038.

[106] M. Yonemura, N. Usuki, Y. Nakamura, M. Ohba, and H. Ōkawa, *J. Chem. Soc., Dalton Trans.* (**2000**), 3624.

[107] M. Yonemura, K. Arimura, K. Inoue, N. Usuki, M. Ohba, and H. Ōkawa, *Inorg. Chem.* 41 (**2002**), 582.

[108] M. Tadakoro, H. Ōkawa, N. Matsumoto, M. Koikawa, and S. Kida, *J. Chem. Soc., Dalton Trans.* (**1991**) 1657.

[109] P. Starynowicz and J. Lisowski, *Chem. Commun.* (**1999**) 769.

[110] B. Dutta, B. Adhikary, P. Bag, U. Flörke, and K. Nag, *J. Chem. Soc., Dalton Trans.* (**2002**) 2760.

[111] J. Lisowski, *Inorg. Chim. Acta* 285 (**1999**) 233.

[112] S. Kobayashi, T. Hamada, S. Nagayama, and K. Manabe, *Org. Lett.* 3 (**2001**), 165.

[113] T. Hamada, K. Manabe, S. Ishikawa, S. Nagayama, M. Shiro, and S. Kobayashi, *J. Am. Chem. Soc.* 125 (**2003**), 2989.

[114] S. W. A. Bligh, N. Choi, W. J. Cummins, E. G. Evagorou, J. D. Kelly, and M. McPartlin, *J. Chem. Soc., Dalton Trans.* (**1994**), 3369.

[115] J. Lisowski and P. Starynowicz*, Polyhedron* 19 (**2000**) 465-469.

[116] T. Tsubomura, K. Yasaku, T. Sato, and M. Morita, *Inorg. Chem.* 31 (**1992**), 447.

[117] D. D. Perrin and W. L. F. Armarego, *Purification of Laboratory Chemicals, Pergamon,* 3rd edn., **1988**.

[118] T. Shozo, *Bull. Chem. Soc. Jpn*. 57 (**1984**), 2683.

[119] J. C. Byun, Y. C. Park, and C. H. Han, *J. Kor. Chem. Soc.* 43/3 (**1999**), 267.

[120] G. M. Sheldrick, *SADABS*. University of Göttingen, Germeny, *1999*

[121] Bruker, *SAINTPLUS NT Version 5.0. Software Reference Manual Bruker AXS: Madison*, Wisconsin, **1998**.

[122] Bruker, *SHELXTL NT Version 5.16. Program for Solution and Refinement of Crystal Structures Bruker AXS*: Madison, Wisconsin, **1998**.

[123] L. A. Kahwa, J. Selbin, T. C. Y. Hsieh and R. A. Laine, *Inorg. Chim. Acta* 118 (**1986**), 179.

[124] D. Suresh Kumar and V. Alexander, *Inorg. Chim. Acta* 238(**1995**), 63.

[125] G. Socrates, *Infrared and Raman Charateristic Group Frequencies*. 3rd edn., Wiley, New York, **2001**, p. 299.

[126] G. Socrates, *Infrared and Raman Charateristic Group Frequencies*. 3rd

edn., Wiley, New York, **2001**, p. 320.

[127] G. Socrates, *Infrared and Raman Charateristic Group Frequencies*. 3rd edn., Wiley, New York, **2001**, p. 321.

[128] G. Socrates, *Infrared and Raman Charateristic Group Frequencies*. 3rd edn., Wiley, New York, **2001**, p. 317.

[129] P. Guerriero, U. Casellato, S. Tamburini, P. A. Vigato and R. Graziani, *Inorg. Chim. Acta* 129 (**1987**), 127.

[130] G. K. Druschel, R. J. Hamers, and J. F. Banfield, *Geochimica et Cosmochimica Acta* 67/23 (**2003)**, 4457.

[131] D. Sutton, *Electronic Spectra of Transition Metal Complexes*, McGraw -Hill, London, **1968**.

초 록

메탄올 용액 하에서 2,6-diformyl-*p*-cresol와 *trans*-1,2-diaminocyclohexane의 축합반응은 [2 + 2] N_4O_2 거대고리 리간드 {H_2[20]-DCHDC; 14,29-dimethyl-3,10,18,25-tetraazapentacyclo-[25,3,1,$0^{4,9}$,$1^{12,16}$,$0^{19,24}$]ditriacontane-2,10,12,14,16(32),17,27(31),28,30-decane-31,32-diol} 형태가 아닌 [3 + 3] N_6O_3 거대고리 리간드가 합성되었다. 그러나, Cu(II) 금속을 주형으로 한 이들의 축합반응은 두개의 Cu(II) 금속이 페놀의 산소 원자에 의해 다리 결합을 하고 있는 [2 + 2] 20-원 N_4O_2 칸막이형 거대고리 착물인 [Cu_2([20]-DCHDC)Cl_2]·H_2O 이 합성되었다. [Cu_2([20]-DCHDC)Cl_2]·H_2O을 수용액 하에서 L_a (Br^-, I^-, ClO_4^-, SCN^-, N_3^-, NO_2^-, NO_3^-, $S_2O_3^{2-}$)와 반응시켜 새로운 Cu(II) 이핵 착물 8개를 합성하였다. 이들 착물들은 원소분석, 전기전도도, UV/Vis, IR 분광법, 질량 분석법 및 X-ray 결정분석법 등을 이용하여 특성 및 구조적 성질을 확인·고찰하였다. 이 착물들의 결정구조 분석 결과, 이들 착물들의 중심금속은 2가지 형태의 구조 환경을 갖고 있었다 ; (1) 사각-피리미드 구조 (square-pyramidal geometry) ; [Cu_2([20]-DCHDC)Cl_2]·$6H_2O$, [Cu_2([20]-DCHDC)Br_2]·$6H_2O$, [Cu_2([20]-DCHDC)(N_3)$_2$]·$2CH_3OH$, (2) 팔면체 구조 (octahedral geometry) ; [Cu_2([20]-DCHDC)(μ-O_2ClO_2)$_2$]·$1.6CH_3CN$·$0.4CH_3OH$. 사각-피라미드 구조 착물들의 두 Cu(II) 간 거리는 2.95 - 2.97 Å 정도였지만, 팔면체 착물은 2.88 Å 정도로 다소 짧았다. 또한 사각-피라미드 구조 착물들의 Cu(II) 중심 금속들은 축상 보조 리간드 쪽으로 0.3284 - 0.3625 Å 정도 떨어져 있다.